All Printed Organic Electrochemical Transistors

CHEN YINGJUN

School of Electrical & Electronic Engineering

A thesis submitted to the Nanyang Technological University
in partial fulfilment of the requirement for the degree of
Master of Engineering

2022

Statement of Originality

I hereby certify that the work embodied in this thesis is the result of original research, is free of plagiarised materials, and has not been submitted for a higher degree to any other University or Institution.

21/10/22
. . . . . .
Date

. . . . . .
Chen Yingjun

Supervisor Declaration Statement

I have reviewed the content and presentation style of this thesis and declare it is free of plagiarism and of sufficient grammatical clarity to be examined. To the best of my knowledge, the research and writing are those of the candidate except as acknowledged in the Author Attribution Statement. I confirm that the investigations were conducted in accord with the ethics policies and integrity standards of Nanyang Technological University and that the research data are presented honestly and without prejudice.

21/10/22

. . . . . .

Date

. . . . . .

Assoc. Prof. Leong Wei Lin

Authorship Attribution Statement

This thesis **does not** contain any materials from papers published in peer-reviewed journals or from papers accepted at conferences in which I am listed as an author.

21/10/22
. . . . . .
Date

. . . . . .
Chen Yingjun

Acknowledgements

First of all, I want to express my sincere gratitude to my supervisor Prof. Leong Wei Lin for the her support and encouragement for my wonderful M.Eng journey. It's her immense knowledge, patience, and energy, gave me the confidence and inspired me to start my research life and keep going.

I also appreciate my mentors, Dr. Cindy Tang, who always be my guidance when I need help both in experiments and life. Thanks to her for reading though my thesis drafts, providing her useful advice in building systematic work and improving the quality of writing.

Thanks to my tutors Dr. Wu Xihu, Dr. Chen Shuai and Dr. Akshay Moudgil. Special thanks to Dr. Wu Xihu for teaching me how to do screen printing and inspiring me with his wonderful ideas. I am so lucky to have our group members to work and play together. Thanks to our amazing group, I benefited from professional and technical knowledge shared and a free study atmosphere.

I also like to thank my partner – screen printer, for overcoming many difficulties with me. Thanks to our lab NML, providing nice and spacious space for me to study and work. Thanks to our lab manager Mr. Chua Tong Sun in arranging all the chemicals and equipment and keep NML a safe and tidy place. Thanks to myself for hardworking.

Finally, I would like to thank my best family for always supporting me and telling me that I am the best one since last century. Thanks to my mom for bringing me to this beautiful world. Thanks to my friends who always by my side and keeps from feeling lonely when studying far away from home.

Fyodor Dostoevsky said, building a tower is not for reaching the sky, but to bring the unknown to the ground. I will continue this wonderful trip for picking the unknown star. Please bless me!

Table of Contents

Summary

The Human Machine Interface (HMI) is a bridge that allows humans to interact with computers in novel ways. It enables connection and exchange of information between different things including the physical objectors and the human body. To fabricate soft interfaces for flexible sensing applications, printed electronics technology, which enables large scale fabrication at a low cost is widely used. In the area of printed electronics, the focused research and work have been done on transistors based on flexible substrates and organic semiconductor materials for applications in multiple sensing and logic units. Especially, the organic electrochemical transistors (OECTs) which have a low operating voltage (<1V) and high transconductance (gm) (typically >50 μS), has gained substantial attentions in recent years.

In this work, the printing parameters of OECTs which constitute various layers (semiconducting channel, conducting electrodes and insulating layers) were optimized and deposited on the flexible substrate. The OECT array has been printed successfully with high uniformity and close channel dimension as designed.

To overcome the limitations of OECT devices imposed by liquid electrolytes, alternative solid electrolytes based on various polymer matrixes with addictive ions were tested. The device performance of solid OECT in both steady state and transient state is measured and compared. The screen printable PSSNa(sodium-4-styrene sulfonate)-blended electrolyte has the best performance with high on/off ratio(1×10^4), low threshold voltage(1.2V), fast transient response(69ms for switching off and 480ms for switching on).

To further improve the transient performance of solid OECTs, the design of gate electrode was also optimized. The non-faradaic and faradaic mode of OECT gating are discussed and compared. Device with top gate structure performs better than side gate since the distance between channel and gate electrode decreased and hence reduce the time constants of ionic circuit and leads to the fast transient response(1.9ms for switching off and 28ms for switching on) which is comparable and even fast than the reported screen printed OECT in literature. The device also show good bending stability which provide a potential in wearable electronics applications.

For the future scope, the different device structure and functional electrolytes can be improved to break though the printing resolution limit.

List of Figures

List of Tables

1. Introduction

This chapter describes the motivation and background for this research project. The significance of the development of novel materials and devices for soft human machine interface is emphasized. The reasons for the choice of printing technique for fabrication are briefly discussed. This work aims to develop and improve the capabilities of the screen printing technology for the production of flexible and printable devices including Organic Electrochemical Transistors (OECTs). Various novel electrolyte materials and printing methods of the OECTs are developed and optimized. The transient response performance of the OECTs is improved by using different gate structures and materials. A printed transistor array is also demonstrated in this thesis.

1.1 Research Motivation

The Human Machine Interface (HMI) is a bridge that allows humans to interact with computers in novel ways. It enables connection and exchange of information between different things including the physical objectors and the human body. For signal processing and exchange, machines need to be connected with the biological interface and sense various physical stimuli from humans including temperature [1,2], humidity [3–5], pressure [6–11], touch and proximity [12–14], etc. Hence, flexible and bio-compatible sensors for soft and compliant interfaces are needed to be developed and improved.

Traditional silicon-based transistors are incompatible for flexible sensing applications due to the materials' physical property limitations and high-temperature fabrication process: Silicon wafers are limited by the bulky and rigid material factors. In addition, the manufacture of silicon based integrated circuit usually relies on vacuum deposition, which makes high production expensive and challenging. Hence, transistors based on flexible substrates and organic semiconductors have attracted much attention in recent years.

To fabricate soft interfaces for flexible sensing applications, printed electronics technology is often used. They are applicable to many areas including wearable electronics, health monitoring, large-scale sensing, flexible displays, soft robotics, and so on (Figure 1). Compared to the traditional fabrication methods, printing enables large scale fabrication of tiny and flexible transistors and sensors at a low cost.

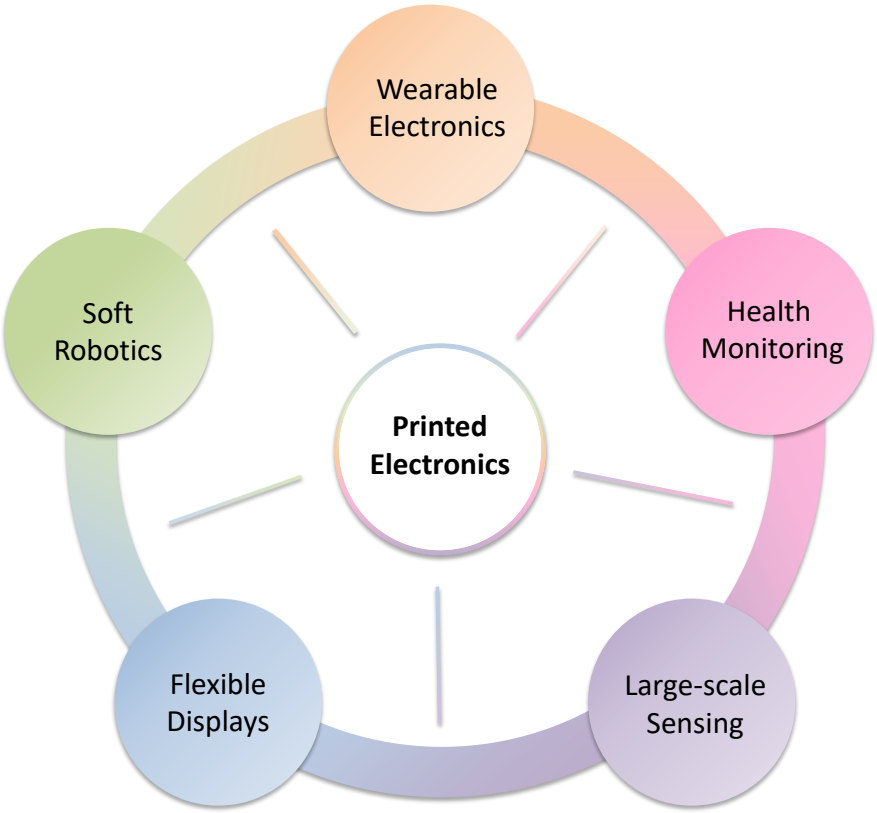

Figure 1.1 Printed electronics in various application areas

In printed electronics, the focused research and work have been done on transistors based on flexible substrates and organic semiconductor materials. Compared to other organic semiconductor-based transistors like organic field-effect transistors (OFETs), the organic electrochemical transistors (OECTs) have a low operating voltage (<1V) and high transconductance (g_m) (typically >50 μS) due to the high capacitance between the electrolyte and organic semiconductor interface [15] and the coupling between ionic and electronic charges[16]. Owing to this high performance, OECTs are widely used in flexible electronics and multiple sensing.

To this end, many researchers have fabricated OECTs by different printing methods[17–20]. However, these 'printed' OECTs have certain shortcomings and limitations, such as (1) the printed OECTs suffer from a slow transient response (commonly around tens of milliseconds), mainly constrained by the printing resolution and channel thickness. (2) The commonly used electrolytes for OECTs are in a liquid state which is not printable, and its concentration may vary over time as it evaporates. (3) Many solid-state electrolytes for OECTs contain incompatible solvents that will destroy the printing equipment or dry too quickly before the

completion of the printing process. (4) Some printing techniques depend on the needle/nozzle movement and lead to slow printing speed and poor printing uniformity.

Among the printing techniques, screen printing has been mostly employed to solve some of these challenges. Different from digital printing methods like inkjet printing and direct ink writing (DIW), customized screen masks are needed for screen printing. Screen printing offers advantages of large-scale fabrication, high printing productivity, good printing uniformity, and various choices of printable pastes and inks.

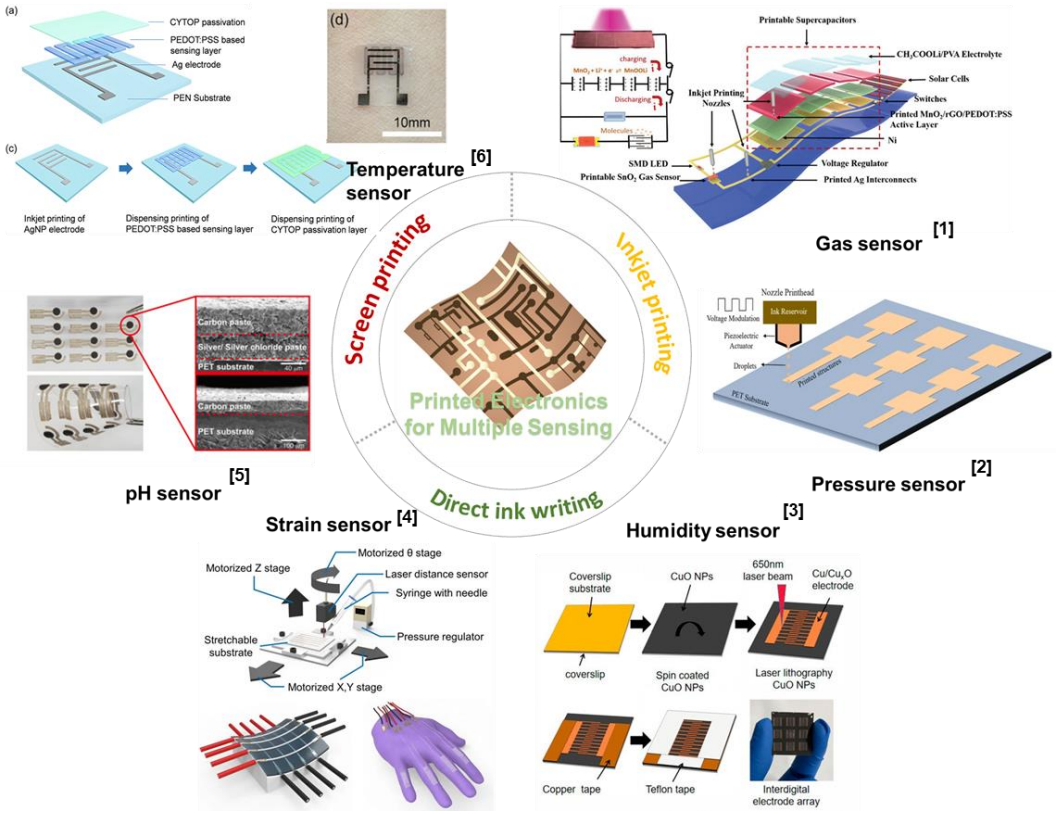

Figure 1.2 Printed electronics for multiple sensing

Generally, commercially-available conductive pastes including silver, carbon and PEDOT: PSS (Poly (3,4-ethylenedioxythiophene) polystyrene sulfonate) have been widely used for screen printing onto flexible substrates while non-commercial electrolytes for OECTs are rarely printed by screen printing. Furthermore, for OECTs, the most commonly used gate is Ag/AgCl pellet. However, Ag/AgCl pellets can only be used with liquid electrolytes and are not compatible with solid electrolytes. Commercially-available Ag/AgCl paste has been screen-printed and used as side gates for OECT. Although top-gate OECTs are generally have better transient response compared to its side-gate counterpart, top gates from Ag/AgCl paste

has however not been patterned before on solid electrolytes possibly due to its non-orthogonal solubility with previously reported solid electrolytes. This thesis would address this gap and demonstrate an all- printed OECT array with a top Ag/AgCl gate electrode that is compatible with a water-based solid electrolyte. The devices reported here can achieve a transient response of 1.9ms (switching off) and 28ms (switching on) which, to the best of our knowledge, is the fastest screen-printed OECT reported.

1.2 Objective and Scope

1.2.1 Objective

- To develop the screen-printing processes of source-drain electrodes, channel, gate electrodes and solid electrolyte for OECTs.
- To determine the effect of different electrolytes, gate structures, and materials on the performance of OECTs.
- To design and fabricate all printed OECTs with fast operation speed.

1.2.2 Scope

- Development and optimization of the screen-printing processes for different layers of OECTs (silver electrode, carbon electrode, PEDOT: PSS channel, and insulating layer) by varying the printing parameters, including the printing pressure, printing gap, and the number of printing layers. The trade-off between pattern resolution and uniformity will be considered.
- Electrical characterizations of all printed OECTs, including their transfer and output curves, transient response, and long-term stability with different electrolytes.
- Compare different OECTs gate electrode materials, structures, and their effects on the OECT performance.
- Demonstrate small performance variability for an all-printed OECT array.

1.3 Major contribution of thesis

1.3.1 Problem statement

(a) The commonly used electrolytes for OECTs are in a liquid state which is not printable and easy to evaporate, while many solid-state electrolytes contain solvents that are incompatible and will destroy the stencil mask used in screen printing or dry too quickly before the printing process is done. Therefore, development of solid electrolytes is needed to fabricate all screen-printed OECTs with good performance and long-term stability.

(b) Owing to the limitation of resolution for the printing method, the channel size of printed OECTs is larger than traditional methods such as by photolithography; Hence, reported printed OECTs do not show good transient response performance. However, improvement can be done for other components like electrolytes and gate structure to enhance the switching performance and make the printed OECTs more universal for fast circuit operation.

1.3.2 Outcome and novelty

This thesis features the development and optimization of a screen-printed OECT array on flexible substrates. A water-based solid electrolyte, with cross-orthogonality to subsequent top gate electrode, has been formulated and successfully printed. Furthermore, a patterned gate printed with Ag/AgCl paste on top of the solid electrolyte is demonstrated. The fabricated OECT array reported here can achieve a transient response of 1.9ms (switching off) and 28ms (switching on) which, to the best of our knowledge, is the fastest screen-printed OECT reported.

1.4 Organization of thesis

Chapter 1 yields a research motivation and background for the project and sketches the major contribution of this work.

Chapter 2 summarizes the literature focusing on improvement for performance of printed OECTs. Different printing technologies and materials are discussed and compared in this chapter.

Chapter 3 lists the experimental materials, the details of printing procedure and principles of characterization and measurement methods are discussed.

Chapter 4 describes the development and optimization of screen printing technology for the OECT array.

Chapter 5 discusses the effect of different electrolytes on all printed OECTs' electrical performance in various aspects.

Chapter 6 discusses the effect of different gate materials and gate structures on all printed OECTs' electrical performance in various aspects.

Chapter 7 concludes the work and provides recommendation for future work.

2. Literature Review

This chapter introduces the prior development of various printed electronic devices in flexible sensing field. The development in printed electronics and different printing methods including inkjet printing, direct ink writing, and screen printing are compared in diverse aspects ranging from printing speed, printing resolution, and printing uniformity. The various screen-printing parameters that influence the printed pattern quality such as printing pressure, printing gap, and printing velocity of screen-printing technology will be discussed. The working mechanism and diverse materials and device structure used in the Organic Electrochemical Transistor are introduced. The limitation of the reported printed Organic Electrochemical Transistor such as slow transient response and incompatible electrolytes will be emphasized towards the end of this chapter.

2.1 Flexible sensing and printed electronics

As introduced in the previous chapter, the flexible Human Machine Interface (HMI) that enables connections and exchanges of information between machines and the human body is needed. To this end, flexible electronic devices are rapidly developing due to their compatibility with a soft interface including the human body and biological environment. Various types of flexible electronic devices including temperature sensors[1,2], humidity sensors[3–5], pressure sensors[6–11], displays[21–23], and energy harvesting devices[24,25] have been developed and are used to collect the physical information related to the human body and convert it to electrical signals. Based on the natural environment, the flexible sensors can work in diverse conditions including water-soluble ability, stretchability, and biological compatibility. Besides, they could also be self-powered and self-healable without additional assistance (Figure 2.1).

Figure 2.1 Flexible electronics in various applications[26].

The traditional fabrication methods based on silicon wafers such as etching, sputtering, and lithography are not suitable for fabricating the soft interface for flexible sensing applications. On the one hand, silicon wafers are constrained to the rigid and bulky form factors. On the other hand, these silicon-based fabrication processes rely heavily on high-temperature and clean room conditions, which makes high volume production expensive and challenging.

Hence, to fabricate the soft interface for flexible sensing applications, more recent attention has focused on the development and optimization of various printing methods [27,28]. Also, there are several research on printing technologies that pay particular attention to printable materials[29–31] .

However, over the past years, most research on printed devices remains on the lab scale owing to undesirable printing uniformity and repeatability. The large-scale printed device production is still under-explored. To this end, flexible and printable devices with low power consumption, desirable compatibility, and long-term stability, are in urgent demand for applications in wireless communications, multifunctional sensors, healthcare monitoring, etc.

2.2 Printing methods for flexible electronics

The concept of printed electronics starting from screen printing in the industry has been rapidly adopted in a range of fields such as multiple sensors[32,33], flexible display[21,34,35], solar cell[28,36], and integrated system[37]. Advanced printing methods - digital printing, including inkjet printing, 3D printing, and direct ink writing have been developed for various applications. Recent studies also focus on the process optimization of printing to enable high-resolution printing. There are also other studies that focus on optimizing ink formulation to provide alternative printable materials for diverse devices and applications. For example, liquid metal has been demonstrated to print on an uneven surface as a keypad [38] and self-powered skin[39]. Other organic semiconductors can also be printed as active layer in OLED[40] array and electrochromic device[41].

Here, three different printing methods including inkjet printing, direct ink writing, and screen printing will be introduced and compared in detail to determine its suitability for various applications (See Figure 1.2).

2.3 Inkjet Printing

Inkjet printing is a robust non-contact printing technology for direct deposition of conductive/functional inks on various substrates. The customized patterns can be printed by patterning solution-based functional materials by the movement of nozzles and cartridges. Therefore, inkjet printing is a mask-free fabrication process. It can simplify the fabrication

process and reduce the cost, and inkjet printing has higher adaptability for real-time design and fabrication of electronic devices, including sensors[20], solar cells[36,42], supercapacitors[43], and so on.

The working mechanism is different for different inkjet printers which can be simply divided into two type: continuous inkjet (CIJ) printing method and drop-on-demand (DOD) printing methods[31]. For CIJ printing, continuous flow of drops can be formed when the pressure is applied, it will split into a stream of drops subsequently owing to the surface tension as shown in Figure 2.1 (a). After passing through the electrostatic field, some drops will be charged and then deposited on the substrate. At the same time, the remaining uncharged droplets are collected for rework. During the DOD printing, discrete ink drops are extruded only when needed. Depends on the different drop-control mechanism, DOD can be divided into thermal and piezoelectric types. For the piezoelectric DOD printing, an electrical stimulus is applied to the active piezoelectric part, resulting changed reservoir shape, as shown in Figure 2.1 (b). During the piezoelectric inkjet printing, both volume and velocity of droplet rise with an increasing applied electrical field[44]. While for a thermal DOD printing, the ink is heated to create air bubbles in the reservoir. The collapsed bubbles can push ink drops from print head to substrate (Figure 2.1(c). Compared to CIJ printing, smaller drops can be formed and achieve high resolutions in DOD printing. Among the two different mechanisms of DOD inkjet printing, the piezoelectric one is more popular as it can be used to process a wide variety of organic and inorganic materials[45,46].

Furthermore, the inkjet printing quality is also significantly depends on ink formulation, wettability of substrate and ink, and various post treatment processes.

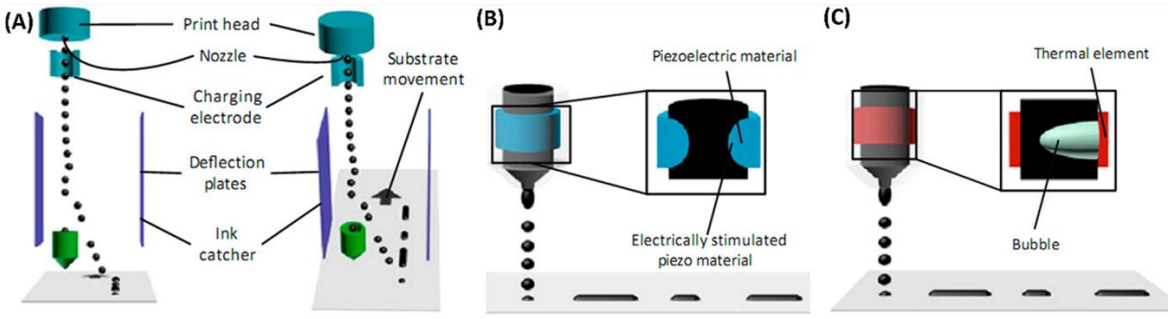

Figure 2.1 Mechanisms of (A) CIJ inkjet printing, (B) piezoelectric DOD inkjet printing, and (C) thermal DOD inkjet printing processes[43].

Due to the excellent control of the ink droplets, inkjet printing is a popular method for forming high-resolution patterns. Moreover, many commercial inkjet printers are usually integrated with substrate heating capabilities. This simplifies the alignment process because post-annealing treatment can be performed without removing the substrates. Hence, the next layer can be printed without further alignment. Given these advantages, inkjet printing has become a widely used printing method and can also be combined with other printing methods for high-resolution and small-area layer printing.

However, compared to other printing methods, inkjet printing has a relatively strict requirement for ink viscosity. The rheological properties of the ink need to be tuned and adjusted according to the desired requirements of inkjet printing systems[47]. The inkjet nozzle is easily blocked if the high viscosity ink is used for printing. Among all the different considerations for inkjet printing, ink formula is the most crucial issue and particular care should be taken on the aspect of ink development process. Selecting suitable materials and developing printable ink is important in the inkjet printing process. This issue is not a challenging process, but it can have a vital effect on the resulting pattern and device performance. Many elements are involved with ink formulation, including the material selection, geometry, and the mixture process. As a result, each of these components affects the performance, flexibility, and manufacturability of printed devices[20].

On the flip side, inkjet printing is limited to large-scale production due to its slow printing speed and poor uniformity. Although solution-based ink offers the advantage of high printing resolution, the transient variation of this kind of ink involved some uncontrollable and time-consuming physical phenomena. These issues include the drop molding, extrusion, recoiling, as well as free flight of the spherical drops, which will be affected by environmental conditions. Hence, it also results in poor printing uniformity, especially for large-scale production[44].

2.4 Direct Ink Writing

Direct ink writing (DIW) is an extrusion additive manufacturing technique that enable the production of 3D structures at the microscale[48]. As with inkjet printing and other digital printing technology, direct ink writing does not require the pre-fabrication of printing pattern masks. Instead, the customized pattern can be designed simply using software and sent directly

to the printer, which can simply deposit the filament or droplet row by row and yield the 2D or 3D pattern.

Distinct from other additive manufacturing techniques like inkjet printing, direct ink writing allows the use of a wide materials and viscosity range. A simple and low-cost nozzle is used in the DIW system, unlike inkjet printing where the cartridges can be rather expensive and fragile.

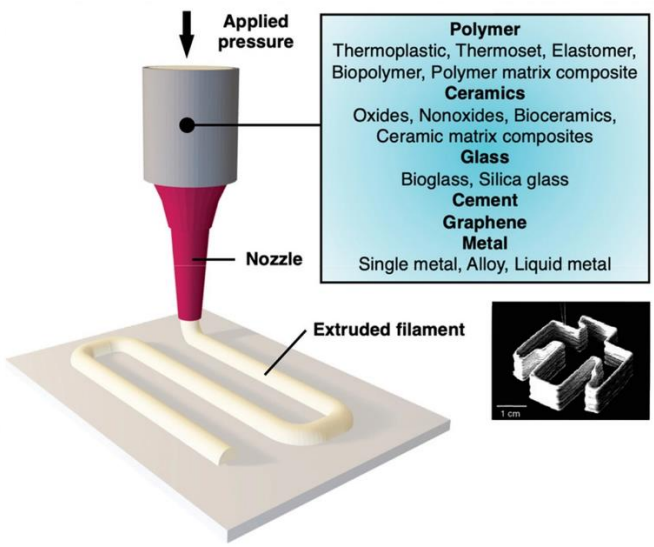

Figure 2.2 Schematic process illustration of direct ink writing[48].

The working mechanism of direct ink writing is demonstrated in Figure 2.2. The printing process of the DIW can be divided into 4 stages: 1) immediate pattern design via the software, 2) precise 3D movement of the DIW nozzle, 3) extraction of functional ink or paste, and 4) post-treatment.

To define if the ink or paste is printable for direct ink writing, the key point is whether the ink can be forced out to form the continuous filament under the applied pressure via the nozzle. In general, the printable ink with viscosity ranging from 10^2 and 10^6 mPa·s and a shear rate of 0.1 s^{-1} is needed to ensure the DIW printability. Unlike inkjet printing which has a high requirement of the ink formula and development, the key factors of direct ink writing are the nozzle size and applied pressure: different nozzle sizes will define the printing resolution and the applied pressure depends on the viscosity of paste and ink.

Compared to other printing electronics technologies, the DIW printing method has advantages on the wide selection of materials, a small number of raw ink or paste materials, as well as the feasibility for multi-material printing[30]. Hence, direct ink writing is suitable for laboratory-

scale manufacture using different componence concentrations, advanced functional ink, and device structure. Therefore, the DIW has attracted much attention from researchers in recent years, and the direct ink writing printing device can be used in different application scenarios, including energy harvesting [25,49,50], tactile sensing[51], super capacitance[52], etc.

On the other hand, during the printing process, there is a trade-off between achieving a uniform pattern under high applied pressure and thin thickness under low applied pressure. Moreover, the nozzles used in DIW are typically larger than 100μm which limits the achievable resolution. Besides, the extraction of filament is not always continuous even when constant pressure is applied. The print-out of certain materials will be affected by various parameters including the ink extrusion, the printing height (the gap between nozzle and substrate), properties of ink, surface condition of the substrate, and the printing speed. Commonly, good printing uniformity highly depends on the slow printing speed, which constrained the direct ink writing from large-scale printing production.

2.5 Screen Printing

Screen printing is a traditional method with a long history compared to the previous digital printing methods. It has been widely used in industry for the printed circuit board since the middle of the last century owing to its ability to fabricate a big batch of large-scale devices or circuits simultaneously. The most significant difference between screen printing and digital printing is the requirement of a screen mask. The screen-printing mask can be made of different materials, including stainless steel, nylon, and polyester.

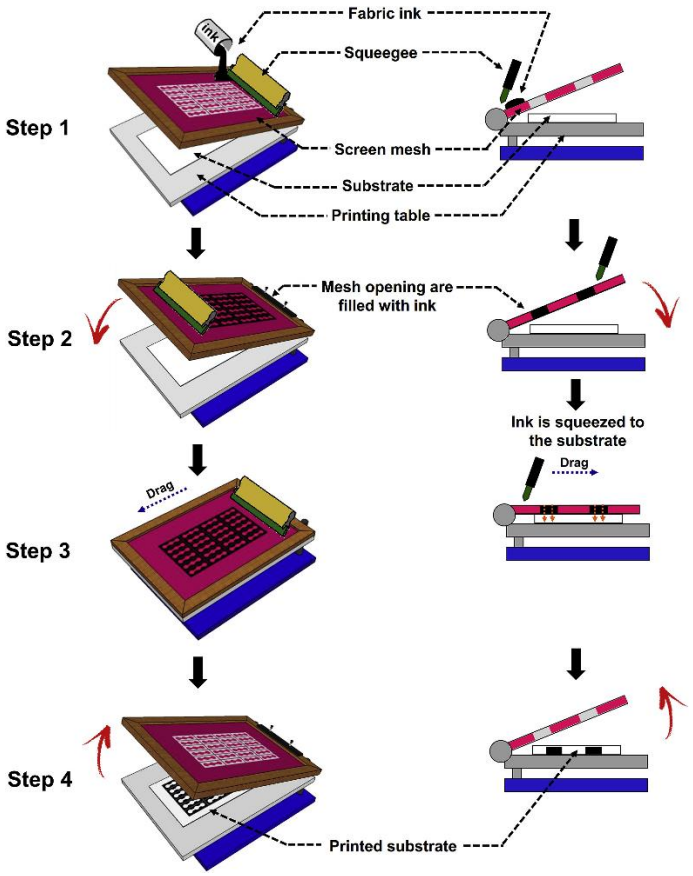

Figure 2.3 Schematic of the screen-printing process[53].

An illustration of the screen-printing process is shown in Figure 2.3. Screen-printing is carried out by using the basic principle that the mesh of the screen-printing mask is 'transparent' to the paste, and the mesh of the non-graphic part is impermeable. Before printing, the paste is first added to one end of the screen-printing mask. Controlled pressure is applied by the squeegee and moved across the mask pattern to transfer thus transferring the paste through the opened area on the masks onto the substrate During the screen printing process, a certain pressues is applied on squeegee to ensure the squeegee is in contact with the mask and substrate. A certain gap is existed between mask and substrate to generate a force on the squeegee through mask tension. Because of this reaction force, the mask and the substrate are only in line contact which move with the movement of squeegees, while the remain part of the screen mask is separated with the substrate. The paste and the screen are separated when the height of the substrate is reduced, which ensures the accuracy of printed pattern and avoids paste smudging on the substrate. When the squeegee scrapes the whole layout and lifts, the mask is also lifted, and the paste is gently scraped back to the original position to form the printed pattern. The effect of

these printing parameters on printing quality such as printing pressure, printing velocity, and printing gap will be further discussed in section 2.5.2.

Screen printing has two superiorities when compared with other mask-based printing technologies including gravure or flexographic printing[54]. First, the masks materials for screen printing can be polyester, silk, and stainless-steel mesh, which are much cheaper compared to the engraved metal masks in gravure printing[55]. Second, the alignment process can be easily completed before screen printing process owing to the semi-transparent and flat screen printing mask. On the other hand, the gravure printing and flexographic printing have either the roll-state mask or the substrate, leading to challenging alignment process in both directions. Therefore, the accurate and simplified alignment process of screen printing makes it compatible for the high volume production of large-scale and multilayer devices.

Nowadays, screen-printing is regarded as a developed printing method in the industry because of its flexibility in printing different patterns and its high repeatability. In recent years many researchers have used it to deposit the paste on flexible substrates to get large-scale flexible electronics for matrix sensing[56], transistor arrays[41,57], and displays[58,59] on flexible[41,60] and stretchable or uneven substrate[35,53].

2.5.1 Screen printing mask

For the traditional mask-based printing technology – stencil printing, thixotropic fluid materials such as solder paste, carbon paste, and other high viscosity paste are difficult to be printed out. Thixotropic fluids are materials that have a time-dependent shear-thinning viscosity, i.e. the viscosity of paste decreases with time at high shear rates and increases with time when shear rates are low or zero[29,61]. With the movement of squeegee, the paste viscosity decreases. This thixotropic property facilitates the paste with high viscosity to fill in the opening area on the screen printing mask. However, for stencil printing, when the substrate will only be separated from the mask when the paste is in solid or static state, in the opening area. Hence, paste of high viscosity will remain in the mask instead of transferring to the substrate, leads to poor printing quality and low printing uniformity [27]. This will lead to incomplete printed patterns, especially for fine patterns. Obtaining accurate formation of printed patterns by screen printing is becoming challenging owing to the higher integrated level of electronics. Non-contact screen printing with high resolution helps to address this issue. For screen printing, thixotropic fluid will first remain in the screen due to the density mesh area. With the movement of squeegee,

paste viscosity is reduced and more paste can be transfer to the substrate; while the paste obtain the solid state and maintains the shape of opening area when the squeegee is moving away [27].

One key factor of screen-printed pattern quality is the printing resolution, which is depends on various printing factors including the printing equipment and printing parameter. The properties of the screen mask such as the tensile strength, opening rate, emulsion thickness, mesh count, bias angle, screen tensile level[62], and area size are important factors.

Among all the mask properties, the mesh count is a key factor that determines the attainable resolution. In screen printing, the amount of paste that can transfer to the substrate via the opening area is affected by the deformation of the mask. The high tensile strength leads to severe mask deformation and further results in high dimensional accuracy. Thus, mesh strength is also an most important aspect of printing. The discharged ink volume, which depends on the screen mesh opening rate and bias angle, will also affect the printed pattern quality (Figure 2.4). When the opening rate is too high it often causes bleeding, and the printed pattern edge will not be as sharp as expected.

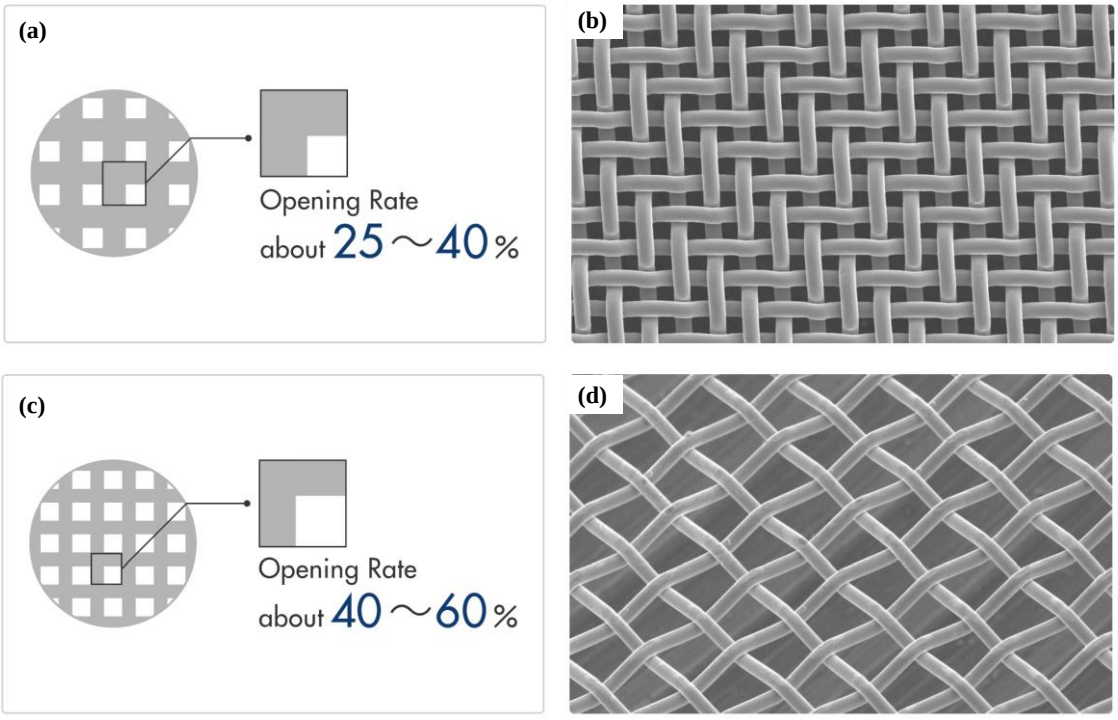

Figure 2.4 Screen-printing mask with different opening rate and bias angle. (a) opening rate and (b) SEM photo of screen mask with 0° bias angle. (c) opening rate and (d) SEM photo of screen mask with 45° bias angle[63].

2.5.2 Screen printing parameters

As discussed in the previous section, for the screen-printing process, the crucial printing parameters are defined as follow (Figure 2. 5): 1) the paste or ink will first be dispensed onto the screen mask, and a printing pressure will be applied on the squeegee, 2) setting the printing gap between the screen mask and substrate, 3) setting printing velocity which determines the moving velocity of the squeegee, 4) the number of printing layer will be further defined by the squeegee moving cycles.

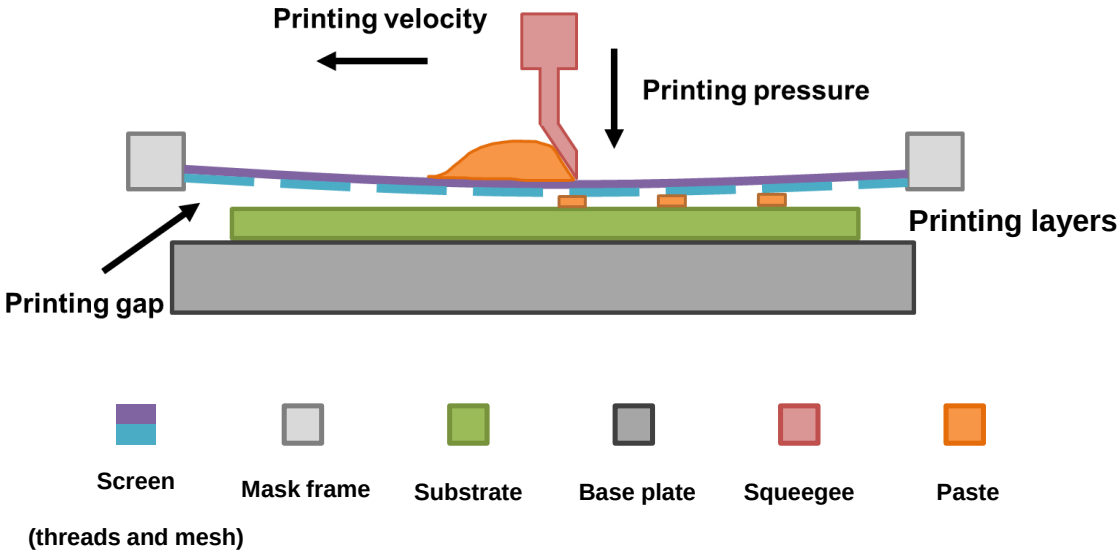

Figure 2.5 Crucial screen-printing parameters

According to the above printing process, three crucial factors will influence the printed pattern thickness: print speed, the print gap between mask and substrate, and the print pressure applied by squeegee. *Wan et al* have figured out the effect of the printing process and materials viscosity on printed film thickness and accuracy.[45] Figure 2.6 shows different parameters considered to obtain the expected thickness. When the print speed decreases, the film thickness will also reduce. The printed pattern thickness can be defined by the amount of ink and paste can transfer from the printing mask to substrate via the designed opening area. This amount is strongly depending on the deformation of the mask. Severe deformation can be form when the squeegee moves at a higher speed, leading to larger amount of paste going through the opening area and be deposited to the substrate, further leading to high thickness. Besides, the thickness can also be significantly influenced by the print gap, which is determined by the distance between the substrate and mask. When the printing gap rise from 2 mm to 4 mm as Figure 2.6(b) shows, the film thickness increased. Another crucial printing parameter is the print pressure. The film thickness increase firstly then decrease as printing pressure increases (Figure

2.6(c)). The mask may not attach to the substrate when low pressure is applied on the squeegee, resulting little amount of paste that can be deposited. In contrast, the screen mesh is in much more severe deformation, the valid opening area of screen mesh decreases. The high pressure will suppress the transfer of the paste from the mask to the substrate, and further reduce the film thickness. Hence, the trade-off between these three print parameters should be considered to obtain the proper thickness for the design during the setting of the screen-printing process.

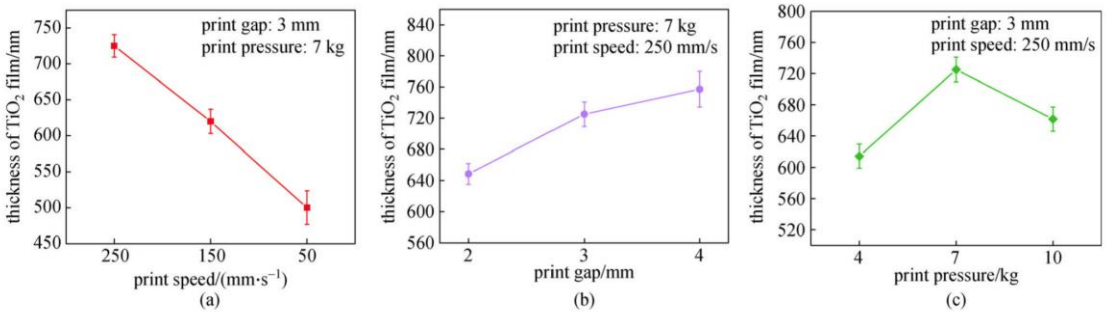

Figure 2.6 Effect of printing parameters (a) print speed, (b) print gap, and (c) print pressure on the film thickness during screen printing process[28].

Furthermore, this paper also investigated the accuracy and resolution of TiO_2 patterned. The printing accuracy may vary for pastes with different solid content and viscosity, as shown in Figure 2.7. The target position can be formed later by etching the layer in Figure 2.7(b). These results demonstrated rough edge issue of the TiO_2 pattern. In addition, the length of printed pattern and edge accuracy are also investigated (Figures 2.7(c) and (d)). These results indicate that the poor printing quality is not only caused by the diffusion of the paste but also by the limited resolution accuracy of the printer. Therefore, besides screen printing parameter and screen printer, the viscosity and property of different ink or paste will also affect the printing result. Tuning the printing parameters for different paste is crucial for the screen-printing process.

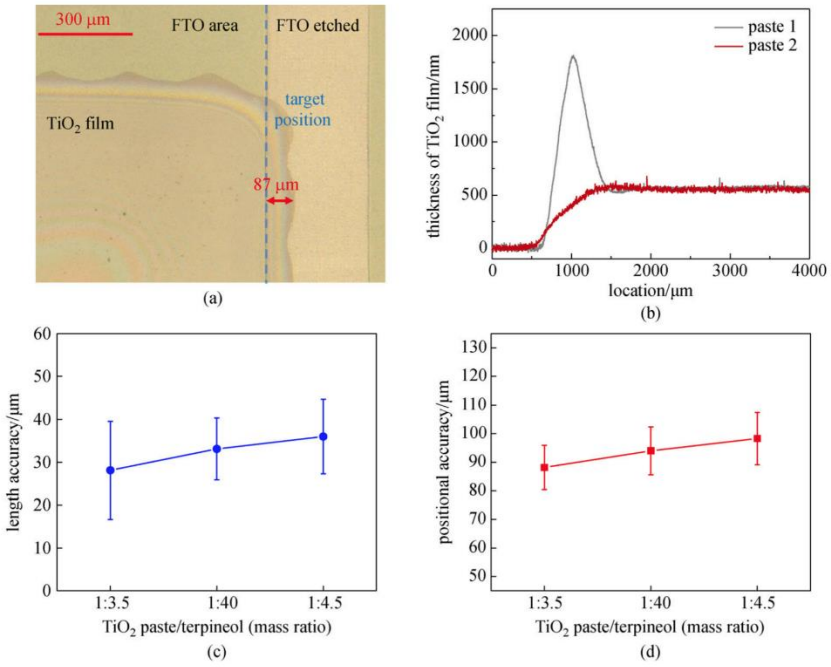

Figure 2.7 (a) Position accuracy for printed TiO_2 pattern; (b) Microscope image of the edge of printed TiO_2 films;(c) Length accuracy of printed TiO_2 pattern; (d) Edge effect of the printed TiO_2 pattern [28].

According to the effects of various printing parameters, the effect of printing pressure, printing velocity, and printing gap on printed pattern thickness and accuracy can be demonstrated in Figure 2.8, Compared to the optimal settings, high printing pressure, and velocity will increase the printing thickness, and the low printing gap will lead to paste diffusion and finally resulted in the poor printing resolution.

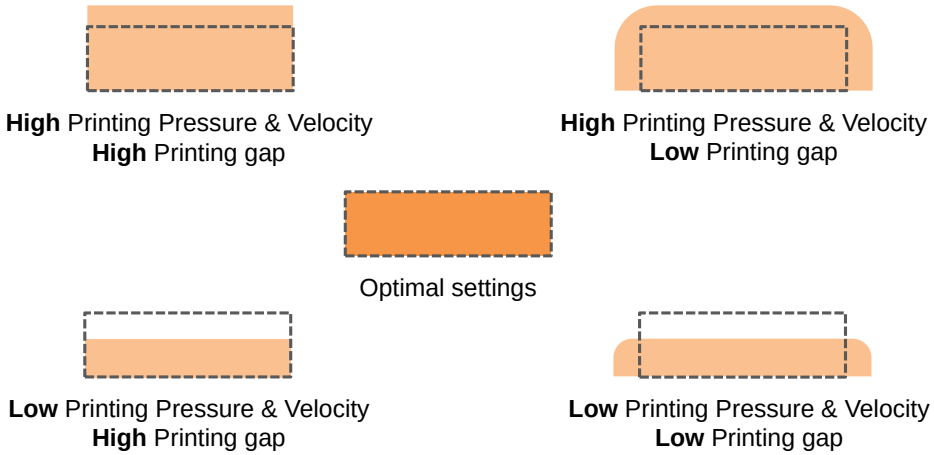

Figure 2.8 Effects of printing pressure, velocity and gap on printed film thickness and accuracy.

2.5.3 Screen printing materials

Screen printing also provide a wide range of printable materials. The acceptable ink viscosity for screen printing is from 10^{-1} to 10^{2}. The commercial screen printable materials including conductive ink, dielectric ink, active materials, packaging materials, and electrolytes can be easily obtained by some company (Dupont, Dycotech, etc.). Besides, some screen printable paste for certain application have been fabricated by researchers at lab-scale. With the new screen printable paste, people can achieve the stretchable and wearable devices[64,65], highly conductive 2D-materials[66], multi-color displays[22,35,67], and high efficiency solar cell[68] by screen printing.

2.6 Comparison of different printing methods

The requirement of materials viscosities varies for different printing methods, as shown in Figure 2.9. For example, direct writing has a wide printable viscosity range from 10^{-3} Pa·s to 1 Pa·s, while inkjet printing and screen printing have different printable viscosity requirements due to the different ink deposition mechanisms. Hence, these printing methods have their corresponding applications and can also be combined with some specific applications including displays[35,60], logic circuit[34,69,70] and multiple sensors[11,14,24].

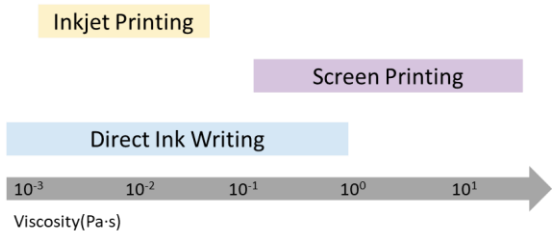

Figure 2.9 The printable ink viscosity for different printing methods.

In addition to the difference in requirements on the printable ink viscosities, these three printing methods also vary in other aspects. Different printing methods have been used for different applications based on their properties. For the digital printing method like inkjet printing and direct ink writing, the distinctive advance is the free-mask printing, while the limitation of digital printing is the small printing area. For the mask-based printing method including screen printing and blade coating, on the one hand, the pre-fabrication of the mask increases the

fabrication period, on the other hand, the large-scale mask and fast printing process will also reduce the printing process once the mask is fabricated.

Screen printing enables large-scale production with high printing uniformity with the combination of all printing parameters. This in in contrast to inkjet printing and direct ink writing which are incompatible with large-scale production due to the volatile and time-consuming printing process. Table 2.1 summarizes the comparison of three different printing methods.

Table 2.1 Comparison of three different printing methods

Characteristic	**Inkjet printing**	**Direct ink writing**	**Screen printing**
Ink viscosity	low	moderate	high
Mask pre-fabrication	No need	No need	Need
instant design	Possible	Possible	Not possible
Multiple layer alignment	Difficult	Difficult	Easy
Printing speed	Slow	Slow	Fast
Printing uniformity	Low	Low	High
Printing resolution	High (~10μm)	Low (~100 μm)	From 10 μm~100 μm (Depends on the mask mesh count)

Printing scale	Small	Small	Large
Equipment life	Short	Long	Long

2.7 Organic electrochemical transistor (OECTs)

In the soft HMI and flexible sensing fields, traditional silicon-based transistors are not compatible due to the high-temperature fabrication process and materials limitations. For example, silicon wafers are limited by the rigid and bulky materials. Besides, the production of integrated circuit based silicon wafers relies strongly on vacuum deposition, which makes high volume fabrication challenging and expensive.

Owing to the growing requirement for connection between the soft human body and rigid machine terminal, transistors based on flexible substrates and organic semiconductors have attracted much attention in recent years. Advancements in materials have promoted flexible electronics that can function well even when they are bent or stretched[71,72]. Recent studies on the large-scale flexible logic circuit based on organic transistors[41] also provide the possibility to connect the flexible sensor with a rigid machine interface.

2.7.1 Working mechanism of Organic Electrochemical Transistor

Organic electrochemical transistors (OECTs) are a type of electrolyte-gated organic transistors. In OECTs, the electrolyte acts as the dielectric layer between the gate and channel. Electrochemical reactions and ion injection occur within the *entire* volume of the channel with an applied gate that can tune the conductivity of organic semiconductor channels and then switch the transistor between on/off states. The working mechanism of OECTs is demonstrated in Figure 2.10.

Like other transistors, OECTs have three terminals, source(S), drain (D), and Gate (G). A fine and thin organic semiconductor layer forming the transistor channel by connecting the source and drain, the gate is then connected to the channel with the channel by the special electrolyte layer.

The distribution of cation and anion in the electrolyte-channel interface can be controlled by the applied gate voltage V_g. For instance, when a positive V_g is applied, cations in electrolyte can be pushed to get into the channel surface and then the whole channel bulk, doping or de-

doping the organic semiconductor by changing the concentration of charge carrier in channel. Therefore, the conductivity of the channel and the drain current can be modulated by the injection of cations from the electrolyte to the channel.

There are also two operation modes in OECTs, dividing by the different initial charge carrier density: depletion mode and accumulation mode. For OECTs operating in the depletion mode, the channel is initially doped and the OECT is on when V_g=0. The injection of cations or anion from electrolyte to channel result in a de-doping organic semiconductor, and further leads to decreased charge carrier density and current between source and drain. If the applied gate voltage is large enough, the transistor will be switched from on to off.

In contrast, for the accumulation mode, the channel of OECT is initially de-doped with low charge carriers density and the OECT is off when V_g=0. Applying a gate potential will again force cations or anions into the transistor channel, doping the semiconductor material and increasing its conductivity to switch off.

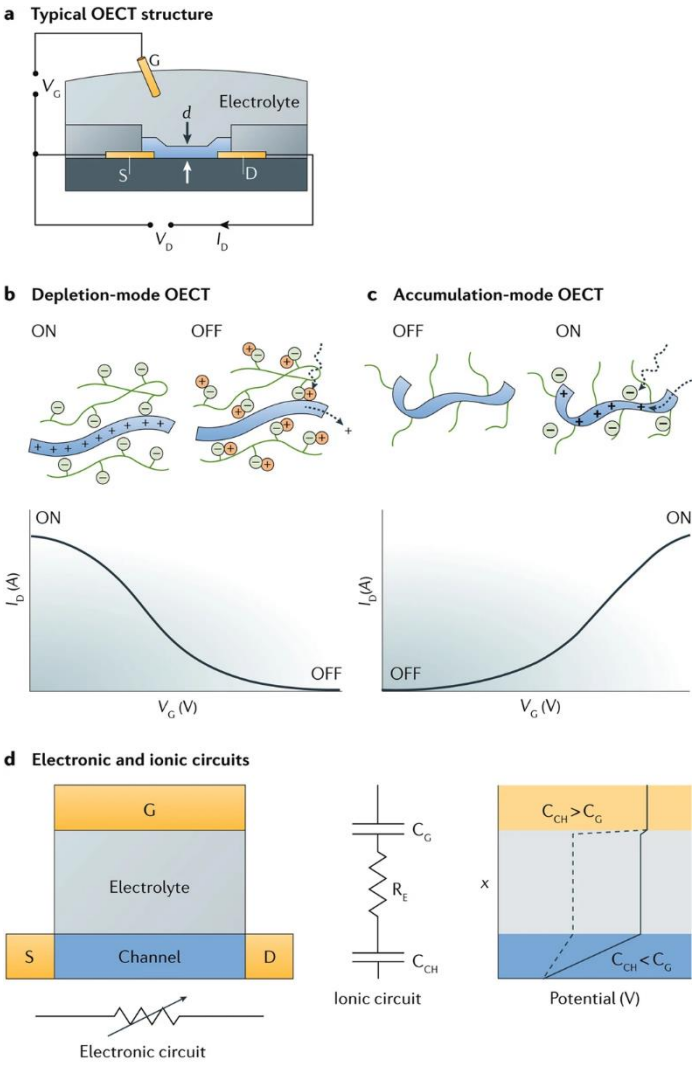

Figure 2.10 The device physics and working mechanism of organic electrochemical transistors [16].

The semiconducting poly(3,4-ethylenedioxythiophene) (PEDOT) is a p-type doped (also known as oxidized) polymer. This type of semiconductor enable the major mobile carries - holes hop from one chain to another chain, froming a current caused by holes when applying a voltage on drain electrode. The OECTs based on PEDOT: PSS channel, work in depletion mode. When there is no gate potential (V_g=0), a drain current flows between drain to source. When a positive potential is applied to the gate electrode (V_g>0), the cations in the electrolyte will be push into the PEDOT:PSS channel and the channel is de-doped (Fig. 2.12 (b)). This is an equivalent process as implanting donors in p-type silicon in traditional semiconductor technology. The hole density thus the conductivity of PEDOT: PSS channel is decreases, resulting in the drop in the magnitude of drain current. Consequently, the transistor will switch to off state.

Compared to OFETs, OECTs have a low operating voltage (<1V) and high transconductance (g_m) (typically >50 μS) due to the high capacitance between the electrolyte and organic semiconductor interface[15] and the coupling between ionic and electronic charges[16]. Owing to this high performance, OECTs are widely used in flexible electronics such as neuromorphic applications[73,74] and various sensing applications, including ion detectors[75,76] and biosensors[77].

Flexible OECTs and OECT-based sensors are often fabricated with organic materials that were made into conductive inks and pastes. These organic materials and the flexible substrates (e.g., plastic films such as polyimide (PI), polyethylene terephthalate (PET), polyethylene naphthalate (PEN), etc.) that they are fabricated on are typically unable to withstand high-temperature processing of more than 200-250°C. Some researchers have fabricated flexible electronic devices by traditional fabrication methods, including photolithography and spray coating[78–80]. But they may not be suitable for large-scale devices due to the high cost and materials waste. To solve these problems, combining different deposition methods such as spin coating and drop-casting is a possible choice. However, these composite fabrication processes are usually complicated and time-consuming.

Fabrication of OECTs is in the research and development stage, and the devices are still individual and isolated. However, there is an urgent need to develop scalable printing methods for large-scale integrated organic circuits such as OECT arrays in an active-matrix configuration for different practical applications like display back panels, sensor arrays, and data-storage devices.

2.7.2 Printed Organic Electrochemical Transistor

Printed circuit based on the organic electrochemical transistor has attracted much attention in recent years due to their flexibility, low power consumption, and good biocompatibility. Researchers have successfully printed the large-scale OECT-based circuit for flexible sensing or logic function[41,70] using the commercial screen printable paste or ink. Marzieh[70] et al. have developed an OECT-based inverter with low power and can function well when operated at 10Hz. Although it is already fast to operate compared to other printed OECT-based inverters, it is still slow compared to other types of printed OFET-based inverters. For the reported screen printed OECTs, commonly, the fastest switching time from off to on is around tens of milliseconds, while the fastest switching time from on to off is around hundreds of milliseconds [81,82]. The switching time of tens of milliseconds has been reached by many studies by reducing

channel dimensions(width of 150 µm and length of 100 µm), which is very close to the highest resolution limitation of screen printing with a 400 mesh count mask (~120 µm). Besides, the fine channel dimension will also lead to a reduction in ON current. Therefore, for the current OECT-based circuits, limited by the printing resolution and thickness, it is difficult to get the screen-printed OECT with a high operating frequency by simply reducing the channel dimension.

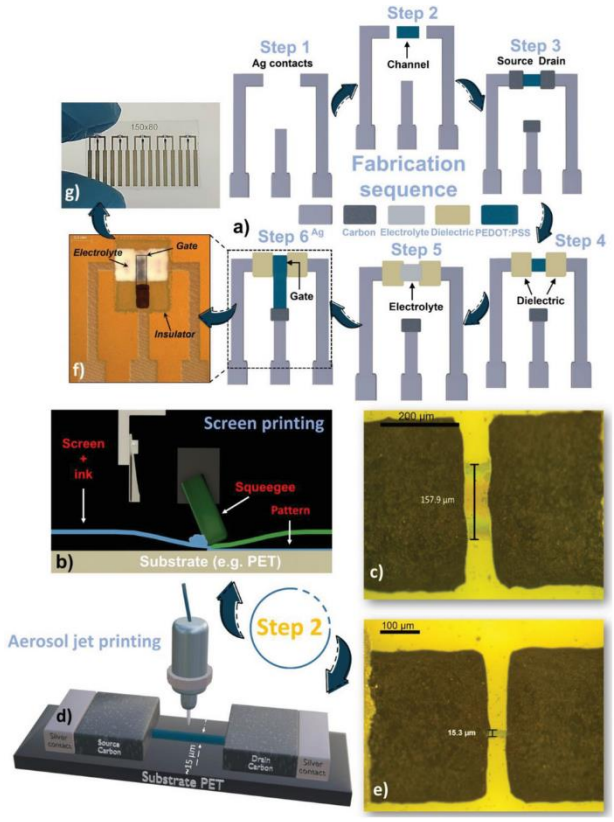

Figure 2.11 The fabrication sequence and the different layers by screen printing and aerosol printing[83].

To solve this problem, Anatolii[83] et al. combined screen printing and aerosol jet printing to obtain small and thin channel dimensions shown in Figure 2.11. All the layers are printed by screen printing except PEDOT: PSS channels which are formed by both screen printing and aerosol jet printing for comparison. The aerosol jet printing was employed to give even smaller channel dimensions. For the OECT with screen-printed PEDOT:PSS, the channel dimension has a limitation of around 150µm. For the aerosol jet printed channel, the channel volume was reduced from 7080 μm^3 to 300 μm^3, and leading to significantly faster switching time of around 4ms compared to 32 ms for the screen-printed OECT.

Another solution for slow switching is to change the gate structure or materials. According to the Bernards model[84], the properties of the gate (including gate materials and gate dimension) will affect device performance in both steady-state and switching process, including the threshold voltage and the transient performance. Ag/AgCl is typically used in OECTs-based biosensing applications for liquid or gel state electrolytes. Compared to the printed gate which is often made by carbon paste in the side gate structure, the Ag/AgCl pellet top gate is more efficient for channel control. Hence, some researchers use the Ag/AgCl pellet as the gate to drive their printed OECTs[19]. However, Ag/AgCl pellets cannot be used with printed all-solid-state OECTs.

In summary, to obtain fast-switching screen printed OECTs, various methods including reducing the channel volume by other printing methods or using the external gate were investigated. However, they are short-term solutions for the screen-printing situation. Besides the channel and gate, the electrolytes also play an essential role in improving the device's performance. Various electrolytes and printed top gate structures may be another solution for the enhancement of transient response.

Hence, to shorten the transient response time of screen-printed OECTs, other components that will affect the channel modulation process such as electrolyte and gate needs to be improved.

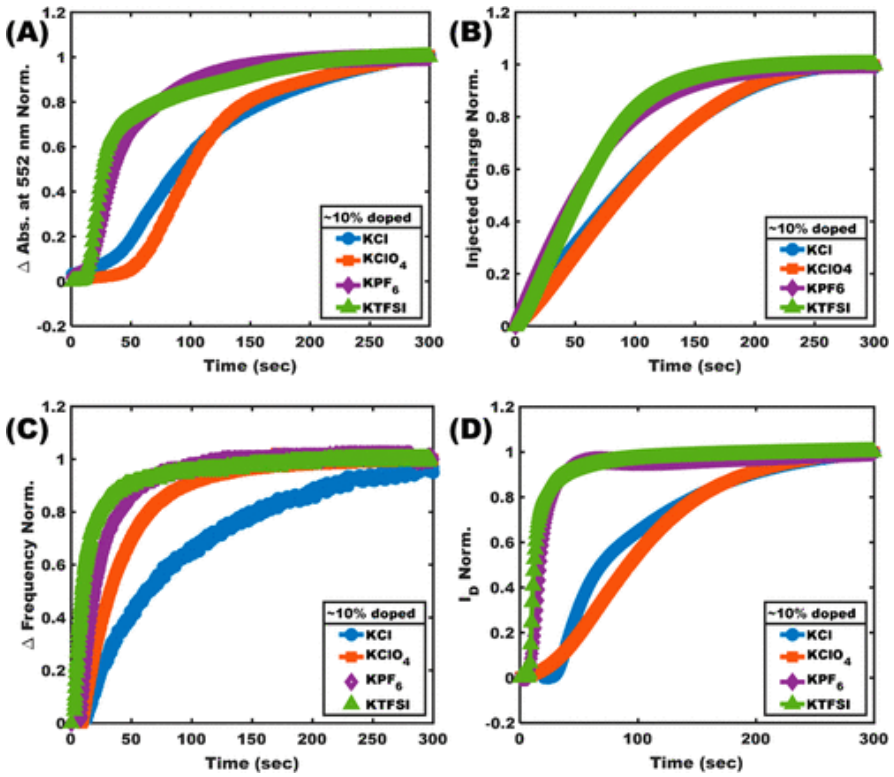

Figure 2.12 Doping kinetics of PEDOT:PSS-based OECTs with different ions in electrolyte. [85].

According to the working mechanism of OECTs, the channel conductivity is modulated by the injection and extraction of ions from an electrolyte when the gate potential is applied. Previous studies have proved that the response speed of PEDOT:PSS-based OECT can be enhanced by blending the channel with ionic liquid to change the film morphology[80,86]. On the other hand, studies focusing on an electrolyte with other semiconductor indicates that a larger crystallographic radius and minimally hydrated anion in electrolyte display increased transconductance, lower threshold voltages, and greater transistor currents but slower response times[85,87](as demonstrated in Figure 2.12).

Besides, the electrolyte's operating condition and electrolyte-swollen state also show significant differences in its morphology, and crystal lattice spacings, which will further govern transport relevant for electrochemical devices[80]. Hence, the ion nature and distribution in electrolytes and channels can be tuned to improve the transient response. In this project, the different electrolytes with various types of anions will be deposited on the PEDOT:PSS channel by different printing methods to speed up the switching.

Another component that will affect the transient response time of OECT is gate influence. Previous research has established the simulation modes to understand the steady state and transient behavior of OECTs[78,84,88]. In total, the modes of OECTs can be divided into two types, capacitive mode[78,89,90] and faradaic mode[91,92]. Figure 2.13 demonstrates the working mechanism of the capacitive mode (non-faradaic mode) and faradaic mode. At a metal/electrolyte interface, the channel modulation is dominated by capacitive processes. This non-faradaic mode works by storing charge at a double layer capacitor formed in gate-electrolyte interface. In the contrast, at a conducting polymer/electrolyte interface, the channel modulation is dominated by faradaic processes. The more efficient gating can be achieved by faradaic mode transferring electrons to redox-active solutes in the electrolyte.

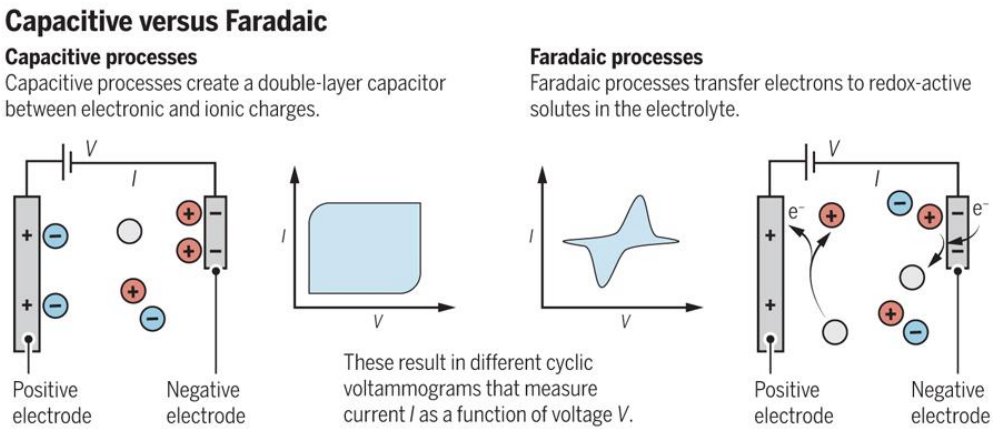

Figure 2.13 Working mechanism of capacitive and faradaic mode.[93]

For the non-faradaic gate, the channel and gate electrode can be regarded as two capacitors in series. The transient response of the device strongly depends on the large potential drop in electrolyte.[78,90] While for the faradaic mode, the channel modulation is achieved via reactions that happened in the electrolyte/gate interface, it will result in electron transfer near the gate area. The faradaic mode leads to negligible voltage to drop through the electrolyte/gate interface and most of the applied potential will drop across the channel bulk, resulting in more effective channel modulation compared to the capacitive mode.

With this understanding of different gating modes at hand, OECTs performance can be promoted or suppressed by changing the gate materials from metal to conducting polymers and electrochemical electrodes such as Ag/AgCl reference electrodes. Engineering electron transfer to solutes throughout the bulk of the semiconductor channel can be useful to obtain a higher on/off ratio, lower threshold voltage, and faster transient response.

2.8 Summary

The Human Machine Interface (HMI) is a bridge that allows humans to interact with computers in novel ways. It enables connection and exchange of information between different things including the physical objectors and the human body. Hence, the flexible and bio-compatible sensors for soft and compliant interfaces are needed to be developed and improved. To achieve the flexible interface, the printed electronics can help with the fabrication of these devices. The OECT can work under a low operating voltage (<1V) and achieve high transconductance (gm)

(typically >50 μS). Owing to this high performance, OECTs are widely used in flexible electronics. There are 3 main technologies for printing the OECTs, including inkjet printing, direct ink writing, and screen printing, among them, screen printing can achieve high volume fabrication with proper resolution at a low cost. Screen printing has been used for patterning various materials and flexible electronic devices.

3. Methodology

In this chapter, materials used to fabricate the screen-printed OECT array is introduced. The screen-printing sequence and post-treatment process are explained. Equipment for screen-printing and device measurement is illustrated. Device characterization methods and detailed parameters is demonstrated.

3.1 Materials

The silver ink (Ag 5000 DuPont) is used for printing the electrodes. Carbon ink (7102 DuPont) is used for source/drain contacts to reduce the reduction front effect. PEDOT:PSS (Clevios SV3 Heraeus), serves as the electrochemically active transistor channel, and the UV cured insulating ink (5018 DuPont) is used as an insulator to limit the overlapping area between the gate electrolyte to source and drain electrodes. The screen printable Ag/AgCl paste (Creative materials 124-36) is employed as gate materials.

The aqueous sodium chloride (NaCl) electrolyte is prepared with concentration of 0.1M. The poly(vinylidene fluoride-co-hexafluoropropylene) (PVDF-HFP) (Sigma Aldrich, average M_w~400k) based solid electrolyte is prepared by blending PVDF-HFP: acetone: ionic liquid (either 1-ethyl-3-methylimidazolium tetrafluoroborate (EMIM:BF_4) (Sigma Aldrich) or 1-ethyl-3-methylimidazolium bis (trifluoromethanesulfonic)imide (EMIM:TFSI) (Sigma Aldrich)) at a weight ratio of 1:7:4. The printable poly(vinyl alcohol) (PVA) (Sigma Aldrich, M_w~70,000)-based electrolyte are prepared by blending PVA: water: NaCl at a weight ratio of 10:40:1. The printable poly(2-acrylamido-2-methyl-1-propanesulfonic acid) (PAAMPSA) (Sigma Aldrich, M_w~1M) based electrolyte is prepared by blending PAAMPSA: water: NaCl at a weight ratio of 10:40:1. The screen printable poly(sodium 4-styrene sulfonate) (PSSNa) blend electrolyte is prepared by blending PSSNa (M_w~ 70kDa): PSSNa (M_w~1M Da): water: D-sorbitol (Sigma Alrich): glycerol (Sigma Aldrich) at a weight ratio of 3:1:4:1:1.

3.2 Sheet resistance measurement

The sheet resistance were measured at room temperature by 4-point probe system(Ossila T2001A3). Due to the small printing area, the final results were obtained after applying appropriate geometrical correction factor. Later the conductivity is calculated with the film sheet resistance and thickness.

3.3 Thickness characterization

The thickness of screen printed films can be simply characterized by exposing the cross sections of printed films to the microscope(Olympus Microscope BX53M). The thickness were obtained using the measurement tool in microscope software.

3.4 Devices fabrication

All materials, except the electrolyte layer, were screen-printed with a flatbed sheet-fed screen printer (DEK Horizon 03iX) on polyethylene terephthalate (PET) and Polyimide (PI) substrates. The configuration of screen printing equipment is demonstrated in Figure 3.1. Before the typical screen printing process, the substrate is firstly rise to the printing height, then printing paste is dispensed on the mask manually. After proceed to printing, the mask is loaded and locked, camera will move to the position of fiducials for alignment check, and the certain pressure will be applied on the squeegee. After the calibration of pressure, squeegees will move as print carriage moves and deposit the paste on the substrate via the opening area on screen mask.

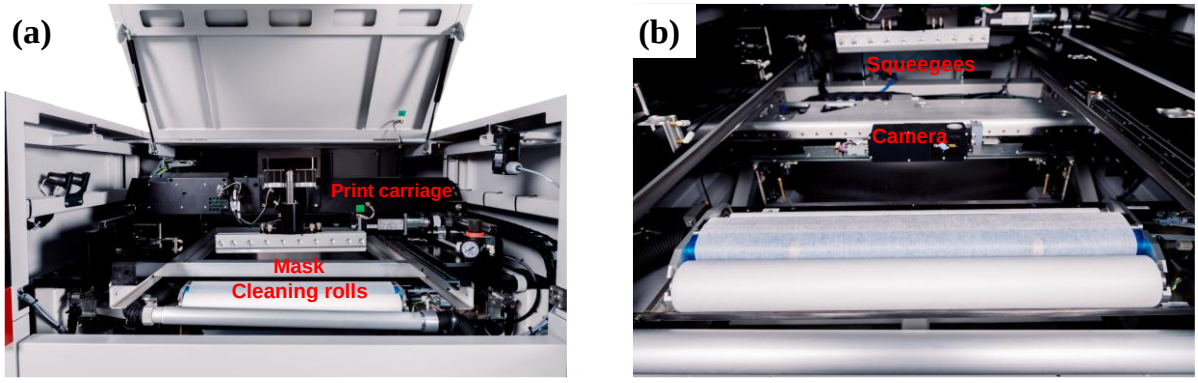

Figure 3.1 Internal structure of screen printer. (a) Internal structure with the loaded mask. (b) Internal structure without loaded mask to show the exposed camera for alignment.

In this work, the silver layer is first printed on the substrate as electrodes and annealed at 120°C for 5mins. A PEDOT:PSS channel pattern is then deposited between the silver electrodes and annealed at 90°C for 5mins to form the channel, followed by the carbon electrodes, which were annealed at 90°C for 10mins, achieving an active channel area of 400 × 800 μm^2. The insulator is then printed and UV-cured for 2 minutes. The electrolytes are then deposited by different printing methods including spin coating, blade coating and screen printing. Finally, Ag/AgCl paste was printed.

3.5 Characterization of OECTs

The transfer characteristics and the transient response of OECTs were measured under room temperature in the dark using a precision source/measure unit (Keysight B2912A) and a probe station (Karl Suss PM5). The channel length and width of the OECT is 400 μm and 800 μm,

respectively. During the transfer characteristics measurement, the source is connected to the ground and the applied drain bias is -0.5V. During transient response measurement, the gate voltage is scanned from -0.5V to +1V or 0V to +1V.

3.6Cyclic voltammetry measurements

The cyclic voltammetry (CV) was carried out under 2-terminal mode. The counter electrode and reference electrode are shorted and connected to the blade-coated PEDOT: PSS film deposited on a patterned silver electrode with an area of 5mm × 10mm. The working electrode is connected to different gates in each CV scan. The CV scan is carried out under a scan rate of 0.025 V/s and scan step of 2mV. All the gate materials including carbon, PEDOT: PSS, and Ag/AgCl are blade-coated onto a patterned silver electrode with an area of 5mm × 10mm. Finally, the electrolyte is coated over both the working and counter electrodes.

3.7 Electrochemical Impedance Spectroscopy measurement

The electrochemical impedance spectroscopy measurement is hired to test the ion conductivity of electrolyte. During the measurement, the two stainless steel flakes are connected together thought the electrolyte to be measured. The scan frequency is from 10^5 Hz to 0.1 Hz. The resistance of electrolyte film is extracted from the impedence under highest frequency.

4. Investigation of printing parameters for Screen-Printed OECTs

In this chapter, the initial setup for screen printing of different functional paste was developed and optimized. The device structure, multiple layers, and printing sequence of all-printed OECT array have been designed and aligned on the screen mask. The effect of various printing parameters on different printed pattern quality has been discussed. Customized printing parameters for different layers including silver electrodes, PEDOT: PSS channel, carbon electrodes, and insulator have been optimized with the combination of key printing parameters including printing pressure, printing velocity, printing gap, and the number of printing layers. All-printed large-scale transistor array containing 10 OECTs has been fabricated with high uniformity.

4.1Screen Printing process

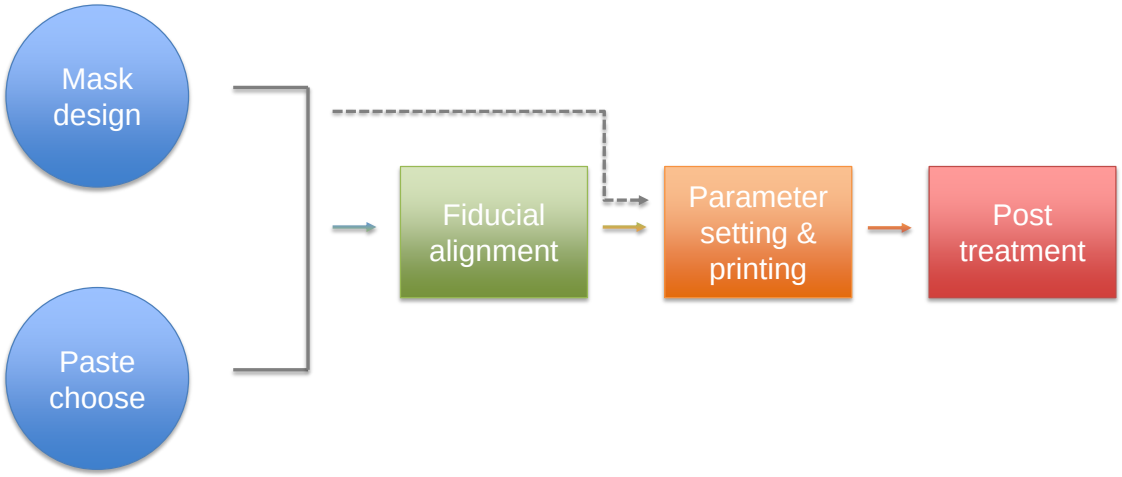

Figure 4.1 Block diagram of screen-printing process

The screen printing process contains five basic blocks as demonstrated in Figure 4.1 – mask design, choice of paste, fiducial alignment, parameter setting and printing, and the post-treatment. The dash line in Figure 4.1 represents the printing process of first layer on a blank substrate – no fiducial alignment is needed.

The screen printing system (Figure4.2(a)) typically consists of squeegees (Figure 4.2(b)), mask, camera for alignment, and a board loading system to load the substrate into the screen printer (Figure 4.2(c)). The screen printed pattern on PI substrate is shown in Figure 4.2(d). A pair of squeegees will move towards the printing direction with set pressure from 0~20kg. A screen mask can be made of different materials including stainless steel, silk and polyester. The paste will be deposited on the substrate with specific pattern design depending on the mask. A board loading system is used to load the substrate into the screen printer before printing and unload the substrate after printing. The system contains a vacuum setup which holds the flexible substrate fixed on a board. The camera system enables the fiducial identification and alignment for printing multiple layers on the same substrate. Various parameters including the hardness and angle of squeegees, mesh number, mesh material, emulsion thickness of the mask, viscosity and surface tension of the paste will affect the printing resolution, thickness, and uniformity[94].

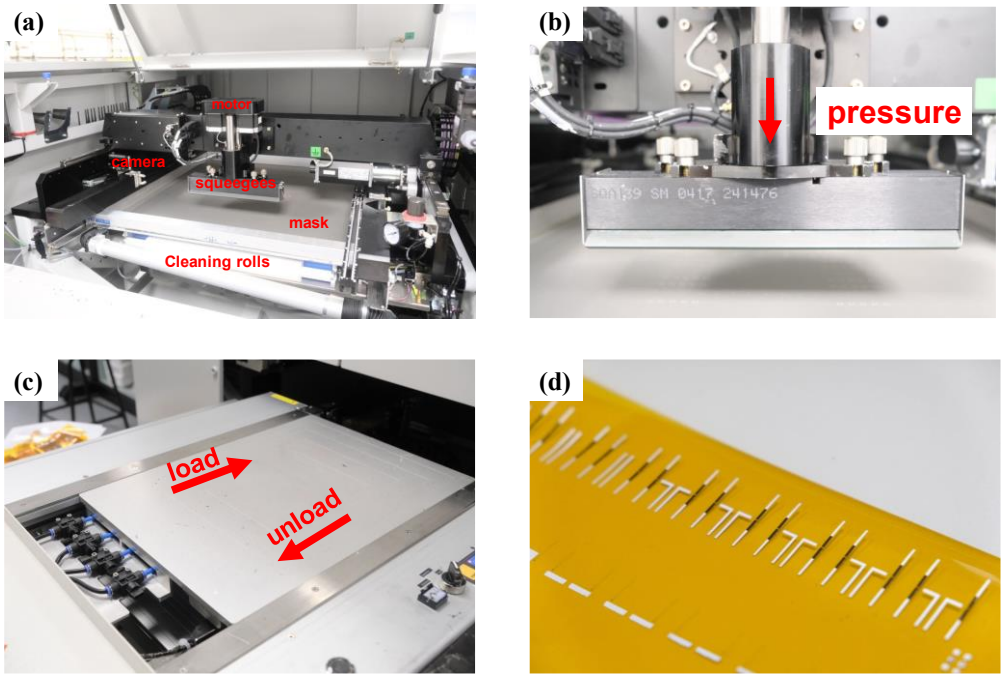

Figure 4.2 Critical components of screen printer. (a) Screen printer, (b)screen printing squeegees, (c) board loading system, (d) screen-printed PI substrate.

4.2Development and optimization of screen printed OECT

As described in the previous chapter, in the screen-printing process, optimization of printing parameters to achieve high resolution, high uniformity, and desired thickness is required with different screen-printing paste, depending on the paste rheology. The printing parameters can be divided into 2 categories – print tools and print settings. Print tools include screen types (e.g. metal, polyester, silk), mesh count, squeegee tensile strength, mask bias angle, squeegee angle, squeegee hardness, etc. Print settings include printing pressure, printing velocity, printing gap, printing layers, and separation speed. These factors affect the pattern resolution and uniformity. In this thesis, key factors (printing pressure, printing gap, printing layer) that contribute most to the printed pattern will be considered.

The device schematic of an all-printed OECTs with carbon side gate is shown in Figure 4.3. For the printed OECTs, there are 5 layers in total. Silver is used as lead lines connecting to the source, drain and gate electrodes. An organic semiconducting material PEDOT: PSS forms p-type channel which operates in depletion mode. The carbon source-drain electrodes and side gate are printed subsequently. The separation distance between the carbon source-drain electrode defines the channel length of OECT and protects the underlying silver lead lines from degradation caused by a faradaic reaction between Ag and halide electrolytes when a negative

gate voltage is applied[95]. The insulating layer is printed to reduce the leakage current from gate to source and hence increases the on/off ratio of the transistor. The electrolyte was later deposited both on the channel and carbon side gate by various printing methods including spin coating, blade coating, and screen printing to provide ions to dope and de-dope the channel.

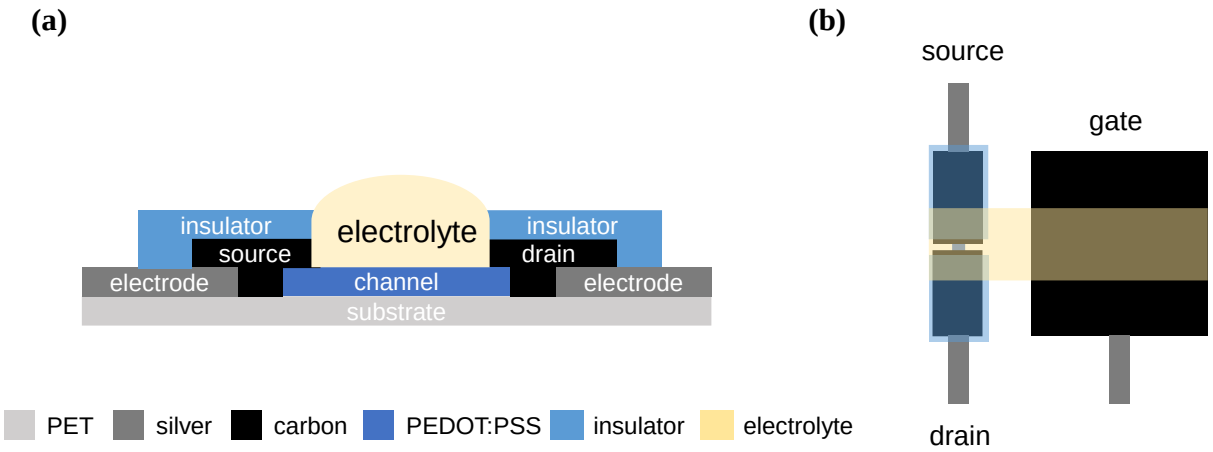

Figure 4.3 Schematic of the printed OECT, (a) cross-sectional view (b) top view.

For the printed OECTs, there are a total of 5 layers printed in the following sequence: silver electrode, PEDOT: PSS channel, carbon electrode, insulator, and electrolyte (as shown in Figure 4.4). Since the pastes have different viscosities, the print parameters for each layer needs to be separately improved to obtain an effective printed pattern. The printing paramters of different layers will be discussed below.

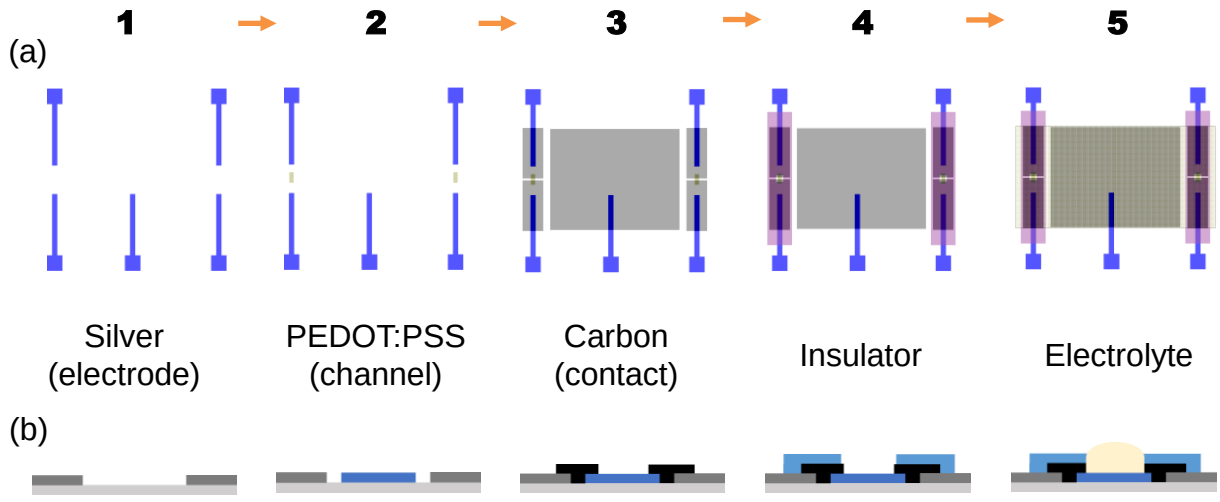

Figure 4.4 Schematic of the printing sequence of OECTs, (a) top view (b) cross-sectional view.

4.2.1 Silver electrodes

The silver electrodes are printed to connect the source, drain and gate electrodes. Before the tuning the printing parameters(3mm printing gap and 3kg), the silver pattern was discontinuous and not conductive (Figure 4.5). Hence, the printing pressure was increased from 3kg to 5kg and 2 layers instead of 1 layer were printed. The printing gap, referring to the distance between the screen and substrate during the printing process, will also affect the pattern resolution. If the printing gap is increased, the printing pressure should be increased correspondingly to obtain a continuous pattern. Here, the gap is fixed at 1mm.

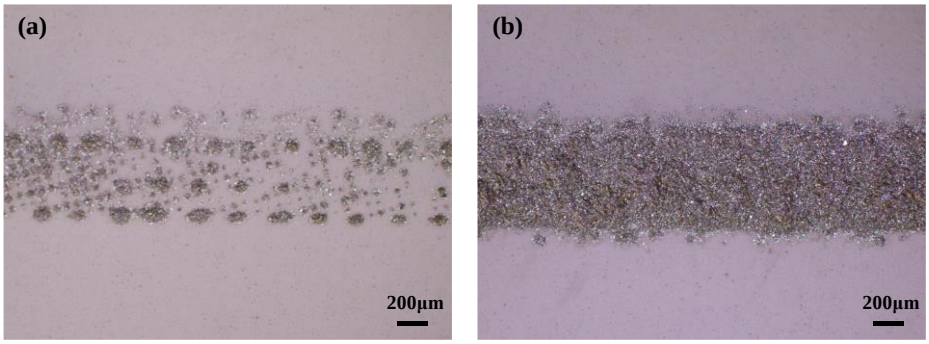

Figure 4.5 Printed silver electrode with (a) high printing gap(3mm), low printing pressure(3kg) and (b) optimized low printing gap(1mm), high printing pressure(5kg) .

Finally, the sheet resistance of the most uniformly printed silver electrodes were measured to be 7.3×10^{-2} ohm/square for a film thickness of 13.14µm, with a conductivity of 1.05×10^{7}S/m.

Table 4.1 Optimized printing parameters for silver electrode

Printing parameters	**Value**
Printing pressure	5 kg
Printing gap	1 mm
Printing layers	2
Printing velocity	20 mm/s
Separation speed	1 mm/s

4.2.2 PEDOT:PSS channel

The width of the PEDOT: PSS channel is critical in the printed OECTs. It is also important to ensure the film is as smooth and uniform as possible. Compared to the silver or carbon paste used, PEDOT: PSS paste has a lower viscosity but higher surface tension and hence tends to bleed or smear – this phenomenon will be more obvious when the screen opening area is too big (> few mm). During the printing PEDOT: PSS, vastly different opened pattern areas affect the uniformity. The bigger area ~5mm×10mm (Figure 4.6(a-b)) has poor uniformity compared to the targeted PEDOT: PSS channel size ~ 800μm×1000μm (Figure 4.6(c)) as some of the paste within the big pattern was trapped in the screen mesh instead of being transferred to the substrate, thus resulting in holes on the channel surface. As shown in Figure 4.6(d), the channel length and width will be further defined by the carbon electrodes and insulator, respectively in the following printing steps (4.2.3 and 4.2.4), the final printed channel dimension is around 400μm×800μm. Besides tuning the printing pressure and gap, the separation speed (i.e. the descent speed of the substrate from the screen after printing) was also varied. Higher separation speed ensures dimensional accuracy and avoids smudging on the substrate.

Finally, uniformly printed PEDOT: PSS channels were obtained with a thickness of approximately 500nm using the printing parameters in Table 4.2. The sheet resistance of the

screen printed PEDOT:PSS channel is 384.6 ohm/square.

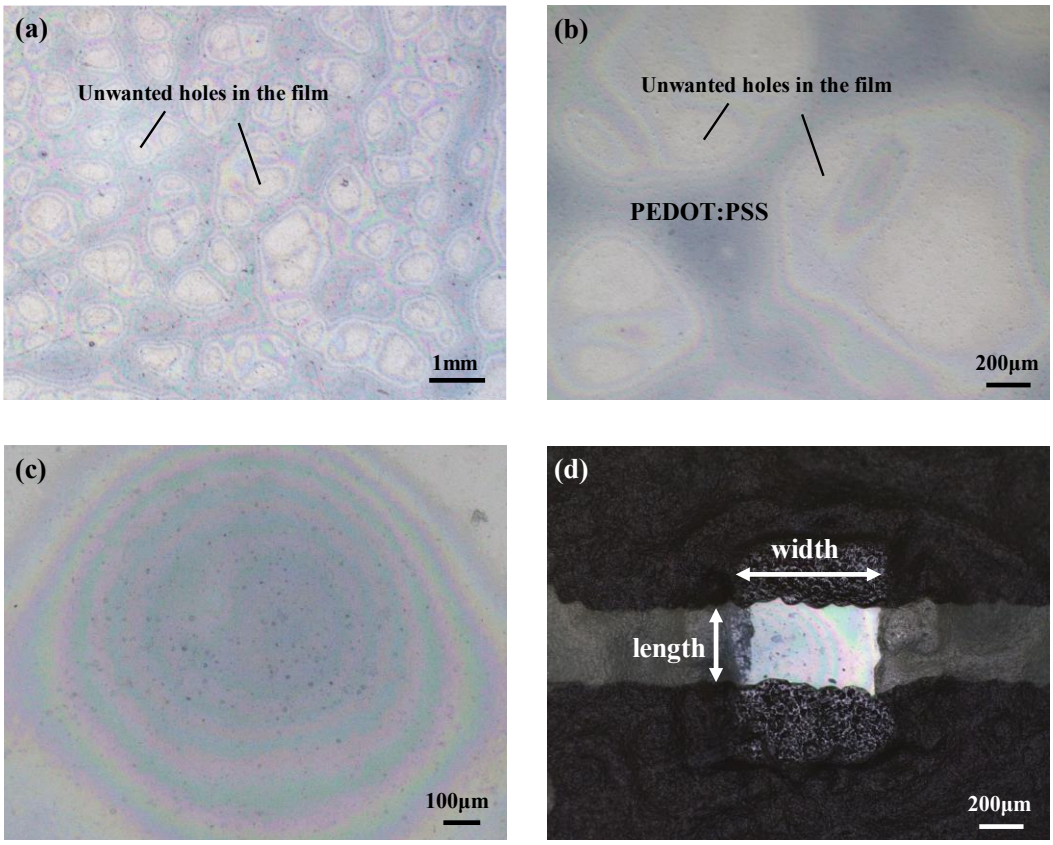

Figure 4.6 Printed PEDOT: PSS channel for (a) (b) pattern areas of 5mm×10mm, (c) 800µm×1000µm, (d) the channel dimension defined by carbon, PEDOT: PSS and insulator.

Table 4.2 Optimized printing parameters for PEDOT: PSS channel

Printing parameters	**Value**
Printing pressure	5 kg
Printing gap	2 mm
Printing layers	4
Printing velocity	20 mm/s
Separation speed	2 mm/s

4.2.3 Carbon electrodes

The carbon electrodes were printed subsequently and defines the channel length of OECT. The additional carbon electrode, instead of the silver electrode, was used to protect the silver from degradation caused by a faradaic reaction between Ag and the halide electrolyte when the negative gate voltage is applied[92]. Since the channel length is defined by the gap between source and drain electrodes (see Figure 4.4 above), having control of the gap between the carbon electrodes is very important for good device performance. Therefore, the printing parameter should be tuned carefully to avoid excessive smearing and to obtain the desired channel length. The same printing parameters as silver are employed here since the carbon 7102 and silver 5000 have similar viscosity, the carbon electrodes were printed with a thickness of 15.62μm, the sheet resistance of 21.84 ohm/square, and conductivity of 2.94×10^3 S/m.

Table 4.3 Optimized printing parameters for carbon electrode

Printing parameters	**Value**
Printing pressure	5 kg
Printing gap	1 mm
Printing layers	2
Printing velocity	20 mm/s
Separation speed	1 mm/s

4.2.4 Insulator

The insulator that isolated the gate from source and drain is important to prevent large leakage currents from gate to source. Zabihipour et al. [81] has compared the printed OECTs with different exposed areas between the carbon source-drain electrodes and the electrolyte – larger exposed area increases the leakage current and results in lowered on/off ratio of the device. Therefore, it is crucial to reduce the exposed area to obtain good device performance.

Some issues were found during the printing of the UV curable insulator – one of the components (2-Hydroxy-2-methylpropiophenone, dibutyltin dilaurate, or 2-[(3a,4,5,6,7,7a-Hexahydro-4,7-methano-1Hinden-6-yl)oxy]ethyl acrylate) in the insulator could possibly react with the PEDOT: PSS channel as the channel's resistance is approximately doubled after printing the insulator. Limiting the print area of the insulator to prevent overlap with the

PEDOT:PSS channel was found to circumvent this issue. Overlap occurs due to bleeding or smearing of the insulator layer and thus should be avoided to ensure stability of the device. Moreover during the UV-curing of the insulator, the PEDOT: PSS channel is also exposed to UV and degrades, resulting in reduced ON current of the OECTs.

Compared to the other conductive pastes which have higher viscosity, e.g. viscosity of silver and carbon are around 20 Pa·s and 60 Pa·s respectively, the insulator has a lower viscosity and is more likely to bleed or smear and reduce the accuracy during the printing process. A bigger printing gap (2mm) is used here to get a better resolution and form the targeted print area and dimensions (Figure 4.7(c)). However, the big gap will also cause an uneven surface of the insulator, as shown in Figure 4.7(a), leading to poor insulating and increased leakage current. On the other hand, by reducing the printing gap to 1 mm as shown in Figure 4.6(b), the printed insulator film becomes more uniform but smeared. This results in a complete coverage of the PEDOT:PSS channel (Figure 4,6(d)) by the insulator(Figure4.7(d)); hence, ions from the electrolyte cannot penetrate through the insulator to dope and dedope the channel. Therefore, there is a trade-off between film uniformity, resolution and diffusivity that depends on the printing gap. In the following devices, the 2mm gap is employed to form the insulator with 8.76 μm thickness to ensure that ions from the electrolyte is able to enter and exit channel properly.[49]

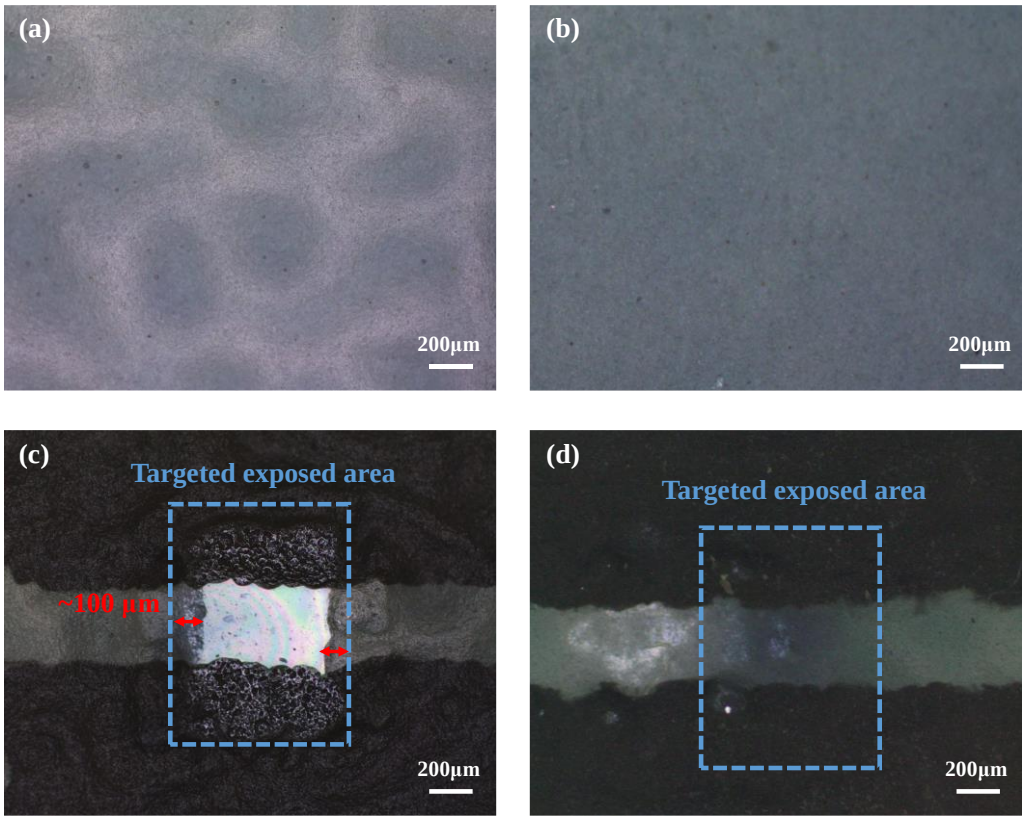

Figure 4.7 Printed insulating layer with (a) 2mm printing gap (b) 1mm gap. The corresponding channel with (c) 2mm printing gap and (d) 1mm printing gap.

Table 4.4 Optimized printing parameters for insulator

Printing parameters	Value
Printing pressure	5 kg
Printing gap	2 mm
Printing layers	4
Printing velocity	20 mm/s
Separation speed	1 mm/s

4.2.5 Electrolyte

For traditional OECTs, a liquid electrolyte such as aqueous NaCl, is often employed to provide ions for the channel. However, there are many problems with the liquid state OECTs. For instance, it is challenging to integrate the OECTs based on a liquid electrolyte with solid

devices. Long-term device stability will also be affected due to the volatile electrolyte, which quickly evaporates or dries. In this thesis, different printable electrolytes that can meet the requirement for device performance will be tested and served as electrolytes for printed OECTs. The different printing methods of different electrolytes, including spin coating, blade coating, drop-casting, and screen printing are also compared in subsequent section 5.2.

4.3All printed OECT array

After optimization of all the layers, the screen-printed OECT devices with a channel size defined by the carbon electrodes and PEDOT: PSS pattern were printed successfully, as shown in Figure 4.8 (a), (b). The entire OECTs array made of 10 devices, where two neighboring devices share one carbon side gate, is shown in Figure 4.8 (c).

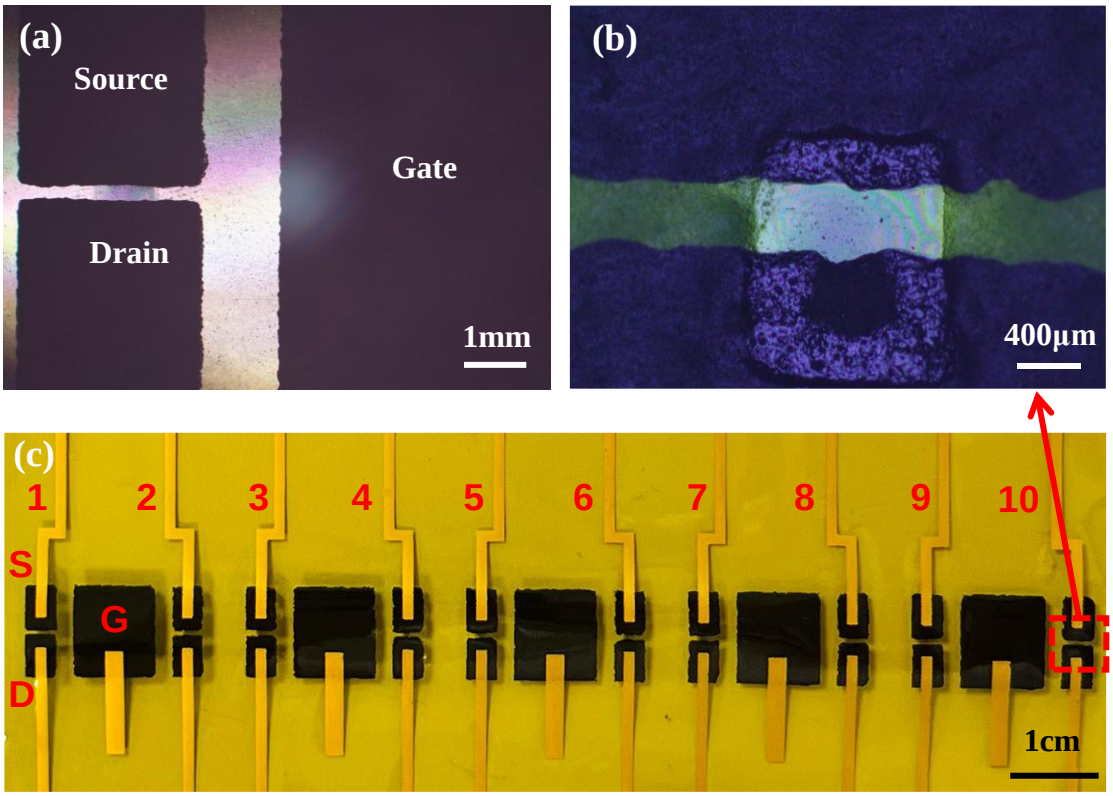

Figure 4.8 Screen printed OECT array. Optical microscope photo of (a) a single OECT, (b) OECT channel, and (c) photo of the printed OECTs array consisting of 10 OECT devices.

The printed OECTs consist of a side gate and the channel dimension is approximately 400µm/800µm (channel length/channel width) with thickness approximately 500nm. The variation in channel dimensions of the 10 OECTs arrays is shown in Figure 4.9 and presents high printing uniformity. The printing uniformity can be further improved by re-designing the pattern position on screen mask: when all the channel layers and carbon contacts pattern are aligned on the central area of mask, the uniform printing pressure distribution can be obtained, achieving smaller variations on channel dimensions.

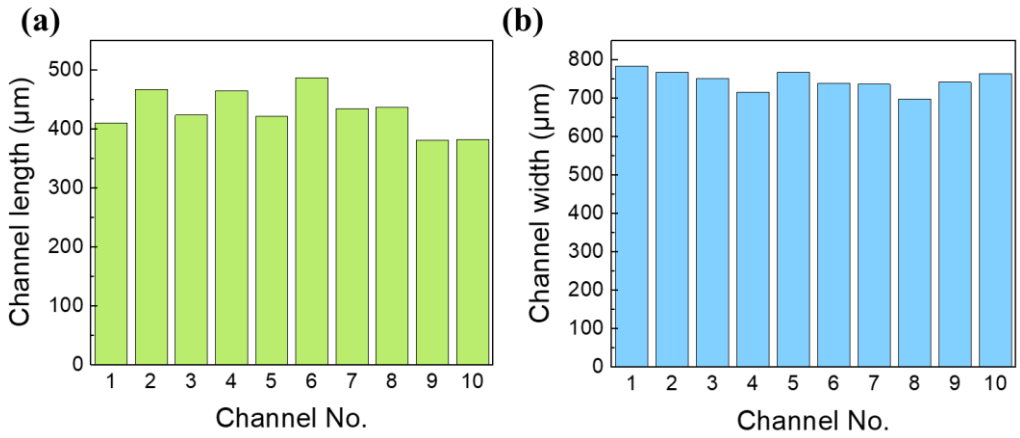

Figure 4.9 Channel dimension of printed OECT arrays (a) channel length of each channel, the average length is 430µm, (b) channel width of each channel, the average width is 731µm.

In the following section, the effect of the printed OECTs with different electrolytes will be discussed and compared. The electrolytes play an important role in the OECT structure, providing the ions for doping and de-doping. The ion concentration, polymer host matrix, thickness, and liquid or solid state electrolytes will influence the device's performance, including transfer properties and transient response.

4.4 Summary

In this chapter, an OECT structure has been designed under the consideration of device performance, printability, and high-volume production. Printing parameters including printing pressure, printing gap, the number of printing layers, and separation process for various layers: silver electrode, PEDOT: PSS channel, carbon electrodes, and insulating layer have been

optimized. Screen-printed OECT array with high uniformity were fabricated successfully on flexible substrates.

5. Study of OECT device performance with printable electrolytes

In this chapter, different electrolytes (both solid and liquid state) were used and tested with the screen-printed OECTs that were in the previous chapter. OECTs with various electrolytes were fabricated by different printing methods including blade coating, spin coating, and screen printing. The device performances including on/off ratio, leakage current, threshold voltage, and transient response with different electrolytes were measured and compared. The transient response and long-term stability of the printed OECTs have been improved using various electrolytes. Finally, a high on/off ratio, low threshold voltage, and fast transient response have been observed under a small threshold voltage with a blended PSSNa(Poly(sodium 4-styrenesulfonate))-based solid electrolyte system.

2 Device performance of OECTs with NaCl liquid electrolyte

For traditional OECTs, a liquid electrolyte NaCl solution is usually used in conjunction with a Ag/AgCl pellet as gate electrode. Here, a comparison of the effectiveness of the printed carbon gate electrodes (Figure 5.1(a)) versus Ag/AgCl (Figure 5.1(b)) is made.

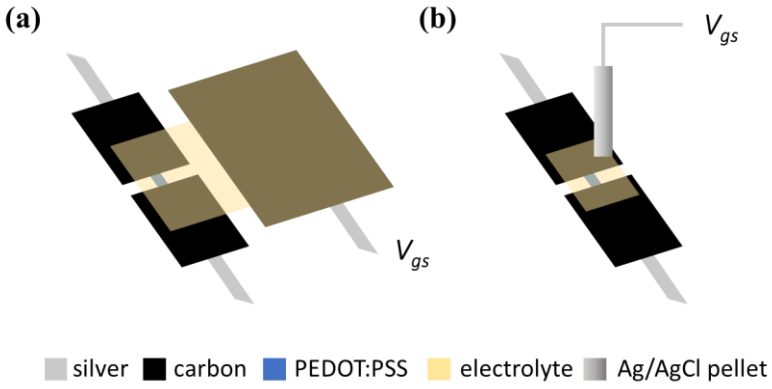

Figure 5.1 Printed OECT device with (a) printed carbon side gate structure, and (b) Ag/AgCl pellet gate.

0.1M NaCl aqueous solution is drop-casted onto the printed OECTs. As shown in Figure 5.2(a), the printed OECT with carbon side-gate reaches an ON current around 1.5 mA at V_{gs}= -0.2V and has a threshold voltage (V_T) +0.8V and on/off ratio of 10^2 with high leakage current (I_{gs}) ~30 µA. In contrast, the Ag/AgCl pellet is a much more effective gate electrode (Figure 5.2(b)). A much lower leakage current (I_{gs} around 1µA) was observed and a much higher on/off ratio and transconductance (g_m) of 5000 and 6mS respectively were obtained.

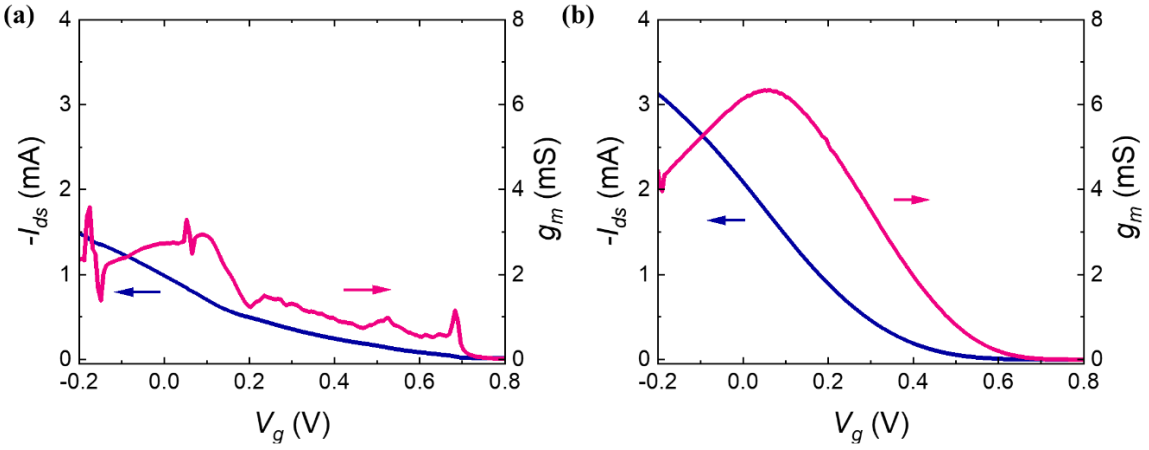

Figure 5.2 OECT transfer performance with NaCl liquid electrolyte under (a) carbon side gate and (b) Ag/AgCl top gate. V_{ds} was fixed at -0.5V.

The poor performance of the carbon side-gate with 0.1M NaCl could be attributed to a large drop in gate voltage across the electric double layer formed at the carbon-electrolyte interface due to the non-faradaic carbon electrode [91]. On the other hand, Ag/AgCl acts as a faradaic gate electrode [92] in the electrochemical reaction where AgCl is oxidized in the NaCl solution and thus a negligible voltage drop across the gate electrode/electrolyte interface[58] and more efficient drain current modulation[79].

Although OECTs based on a liquid electrolyte can be used for various sensing applications, including light sensing[96], bio-sensing[97], and chemical sensing[98], it is challenging to integrate liquid electrolytes with commonly used solid-state circuit. It also tends to suffer from poor device long-term stability due to its volatile behavior. To resolve this issue associated with liquid electrolytes, the solid-state electrolyte-based OECTs have attracted much attention from researchers and have been used for many different applications like printable and wearable electronics [63,64].

5.2Device performance of OECTs with solid electrolyte

In this part, the different solid electrolytes were developed and employed for printed OECTs array with a carbon side gate. These solid electrolytes are printable. However, to evaluate the suitability of these solid electrolytes, the conventional coating methods such as spin-coating and blade coating are first employed. The device performance with different solid electrolytes, including transfer curve and transient response, will be compared and discussed.

5.2.1 PVDF-HFP/EMIM:BF_4 electrolyte

Poly(vinylidene fluoride-hexafluoropropylene) (PVDF-HFP) and ionic liquid blend is a commonly used solid electrolytes for OECTs[7,99]. Here, the PVDF-HFP-based solid electrolyte with ionic liquid 1-ethyl-3-methylimidazolium tetrafluoroborate (EMIM:BF_4) is deposited directly by spin-coating on the channel. The chemical structure of the polymer and ionic liquid is shown in Figure 5.3(a),(b).

The transfer characteristics with solid electrolyte is shown in Figure 5.3(c). The printed OECT reaches an ON current around 3 mA at V_{gs}= -0.2V, V_T =1.2V, and on/off ratio of 2×10^3 with a leakage current of ~2uA. Compared to the liquid electrolyte, the leakage current is reduced

significantly by the solid-state electrolyte; hence, an increment in the on/off ratio was observed. However, the PVDF-HFP-based solid electrolyte suffered from slow transient response, as shown in Figure 5.3 (d), in which the response time was longer than 5s during the switching between ON and OFF states.

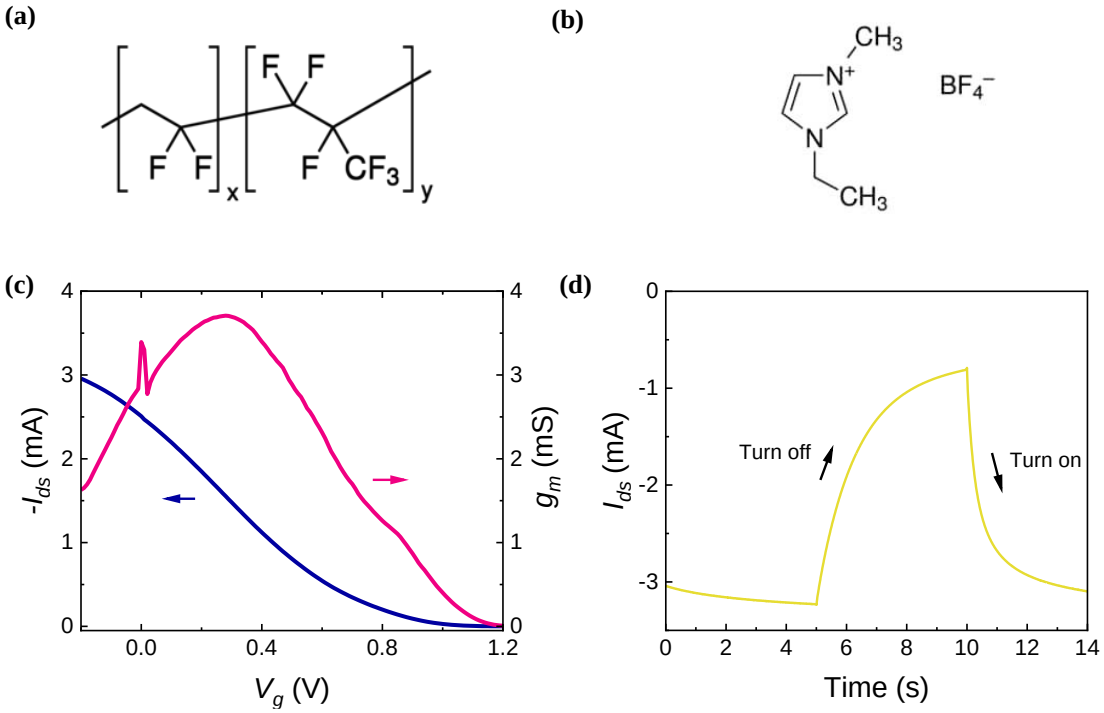

Figure 5.3 Chemical structures of (a) PVDF-HFP and (b) EMIM:BF4.Performance of OECT with PVDF-HFP/EMIM:BF_4 solid electrolyte. (a) transfer performance at V_{ds}= -0.5V and (b) transient response with V_{gs} pulse from -0.5V to 1V at 0.2Hz.

Although PVDF-HFP-based solid electrolyte has better transfer characteristics than the liquid electrolyte NaCl, there are still some problems for the OECTs. For example, the leakage current (2.73μA) is still higher than that of other electrolytes (<1 μA) with the same insulator thereby limiting the ON/OFF ratio of the OECT. Moreover, PVDF-HFP with EMIM:BF_4 system is not bio-compatible due to its toxicity[100].

Therefore, search for a new solid electrolyte with a faster transient response, low leakage currents, and high ON/OFF ratio is necessary to obtain better OECT performance for widespread applications with these printed OECTs.

5.2.2 PVA/NaCl electrolyte

Polyvinyl alcohol (PVA) is a printable polymer commonly used in biological and medical fields. There are no mobile ions in the PVA structure; however, PVA can serve as a polymer matrix of ions for fabricating printable solid electrolytes. The chemical structure of PVA is shown in Figure 5.4(a). Here PVA: water: NaCl were blended at a weight ratio of 10:40:1 and (Figure 5.4.(b)) blade-coated onto the screen-printed OECTs.

The devices were measured immediately after the electrolyte is deposited. The printed OECT can reach an ON current ~ 2.5 mA at -0.2 V_{gs} and can be turned off at +1.0 V with around 5000 ON/OFF ratio as shown in Figure 5.4(a), which is comparable with the NaCl with Ag/AgCl gate. The leakage current of PVA/NaCl system (0.76 μA) is also much lower compared to the other electrolytes mentioned.

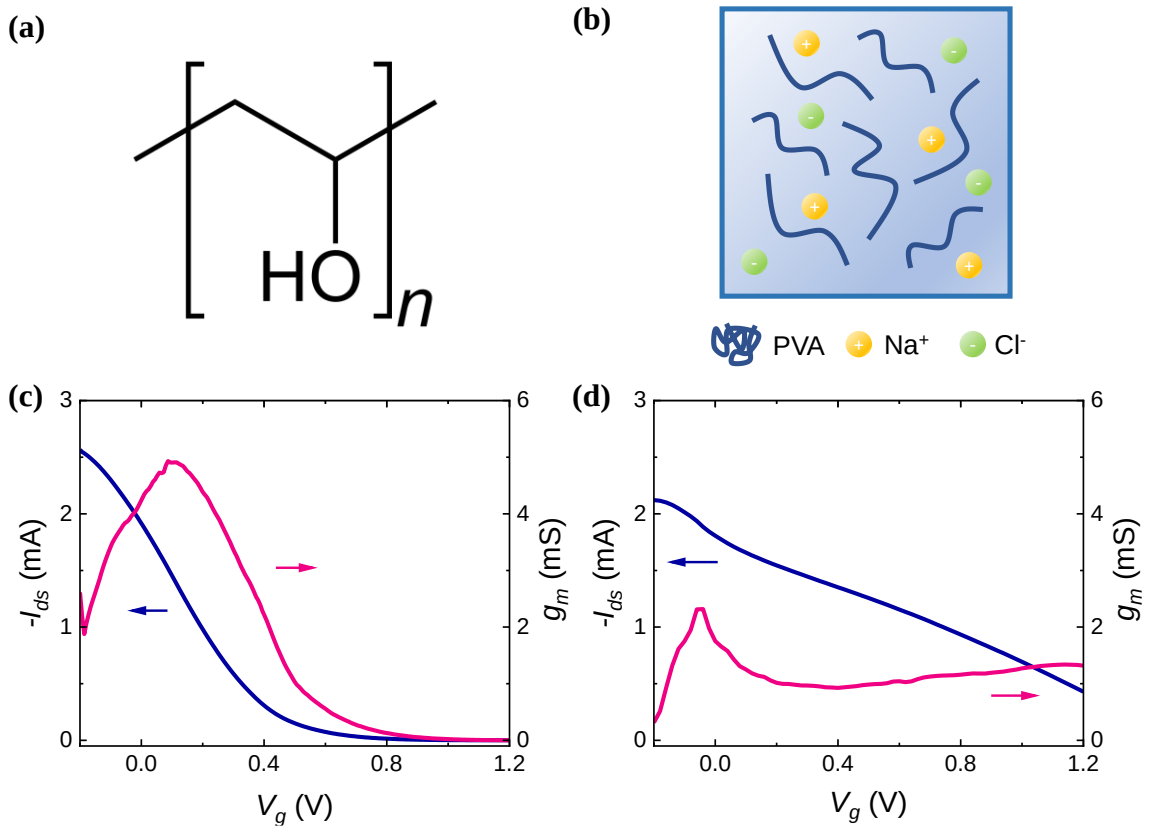

Figure 5.4 (a)Chemical structure of PVA. (b) PVA as ion holder of NaCl.OECT transfer performance with (a) PVA-NaCl solid electrolyte and (b) the re-drop-casting PVA-NaCl solid electrolyte after 16 hours at V_{ds}= -0.5V.

Despite PVA being hydrophilic due to the presence of hydroxyl group, most of the water present in the electrolyte evaporates over time in air to give a dried film. The dried PVA

electrolyte cannot act as an effective ionic reservoir anymore because the ions were 'frozen' in the dried PVA matrix which significantly deteriorate the ionic penetration into the PEDOT:PSS channel. After re-wetting the dried PVA electrolyte (dried by leaving the device in air for 16 hours) with aqueous NaCl (Figure 5.4(b)), the device is still unable to operate as well as its freshly-prepared initial state. This poor long-term stability presents a deadly drawback of the PVA/NaCl system.

5.2.3 PAAMPSA/NaCl electrolyte

The following part investigates a more hydrophilic polymer, poly(2-acrylamide-2-methyl-1-propane sulfonic acid) (PAAMPSA), as a polymer matrix for ionic storage. The abundant oxygen groups in PAAMPSA (chemical structure shown in Figure 5.5(a)) forms strong hydrogen bond with water in the environment[66], keeping the electrolyte moist and solving the 'frozen' ion issue observed in PVA/NaCl system. Similar to PVA, there are no mobile ions in PAAMPSA, but the external ionic species NaCl can be introduced to the PAAMPSA polymer host to provide free mobile ions. The transfer curve with PAAMPSA and NaCl system is demonstrated in Figure 5.5(b). Here the PAAMPSA/NaCl electrolyte is blade coated on the top of the channel and side gate. The printed OECT can be turned off at +1.5V gate voltage with around 1000 ON/OFF ratio. The leakage current is around 400nA. Compared to PVA/NaCl system and liquid NaCl electrolyte, the PAAMPSA/NaCl system has good long-term stability and repeatability, as shown in Figure 5.5(c-d). The device can function well even after a few days in the room environment. Besides, the current level can also remain stable (>93%) after 100 operating cycles.

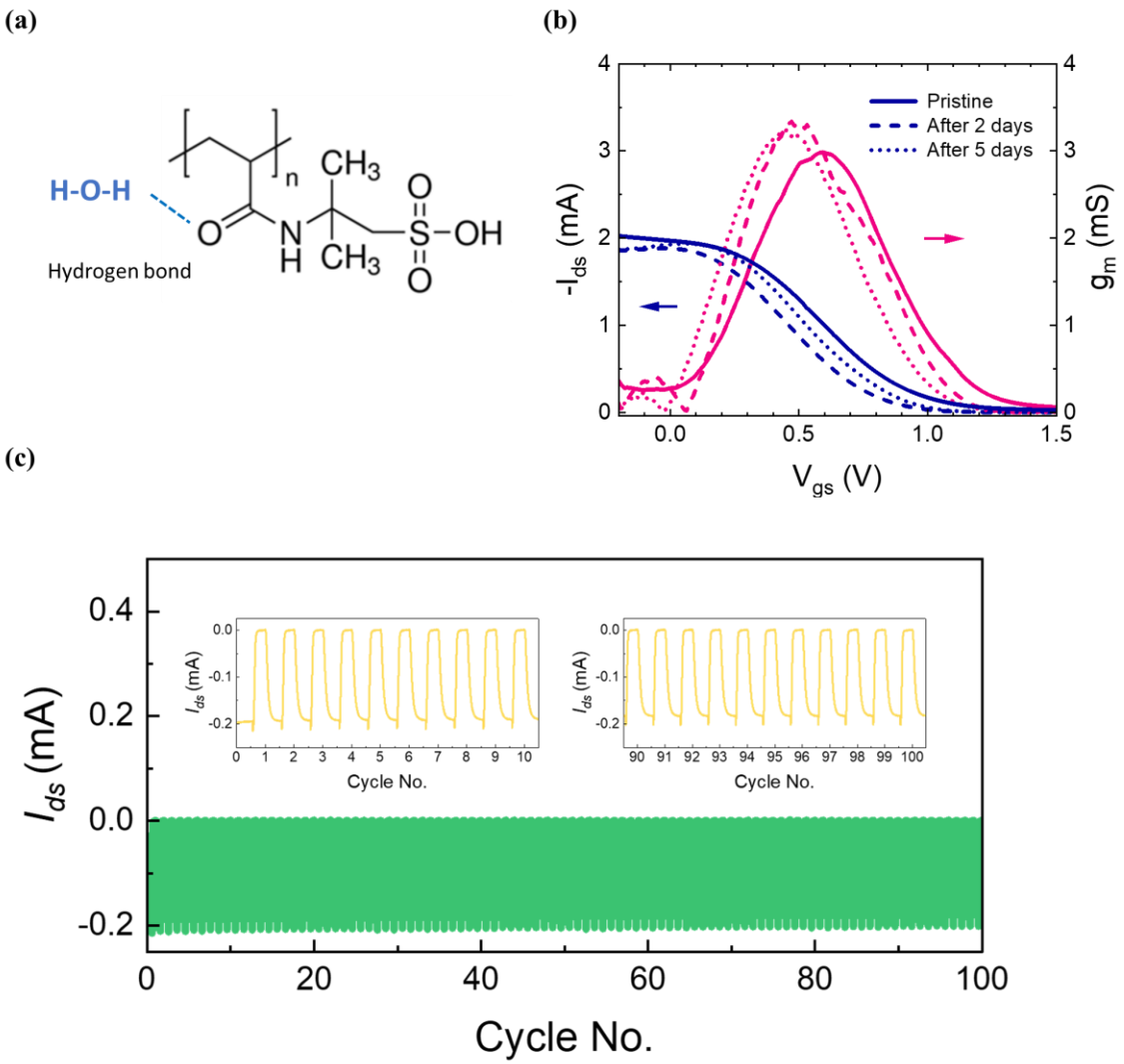

Figure 5.5 (a) Chemical structure, (b) long-term stability of OECT transfer performance at Vds=-0.5V, and (c) long-term stability of PAAMPSA-system after 100 cycles.

However, the transient response time of PAAMPSA/NaCl is very slow (>5s) and cannot be used for high frequency applications. Besides, since the V_T of the PAAMPSA was high (around +1.5V), the electrolysis of water may happen in the PAAMPSA-NaCl aqueous solution, which will also cause the device degradation.

5.2.4 PSSNa/D-sorbitol/glycerol electrolyte

Another type of electrolyte was developed to enhance the transient response for printed OECTs compared to PAAMPSA-system, as well as good long-term stability. Poly (sodium 4-styrene sulfonate) (PSSNa) is a type of screen-printable gel electrolyte that can provide cations for the

p-type channel. By mixing a high and low molecule weight PSSNa, the viscosity can be altered depending on the ratio of two materials to form a viscous solution for screen-printing.[67] Here, two different molecular weights PSSNa were blended with D-sorbitol and glycerol to alter the plasticity of PSSNa-blend solution[64]. The chemical structures of these polymers are demonstrated in Figure 5.6(a)-(c).PSSNa-blend electrolytes were fabricated by spin-coating and screen-printing methods in order to compare their device characteristics. The thickness of the spin-coated PSSNa-blend film (spun at a low spin speed) is expected to be thicker(around 200μm) due to the high viscosity of solution. In contrast, the screen-printed film is much thinner(around 30μm). The as-cast PSSNa-blend electrolytes remain semi-hydrated in air over time to form a sticky-gel-like film.

A lower V_T was achieved for OECT with spin-coated PSSNa-blend electrolyte (Figure 5.6(d)), as compared to OECT with screen-printed PSSNa-blend electrolyte (Figure 5.6(e). This could be due to insufficient ions in thinner screen-printed electrolyte compared to the spin-coated film. Moreover, the ON/OFF ratio of OECT with screen-printed electrolyte is also poor. The spin-coated PSSNa-blend electrolyte demonstrated a high ON/OFF ratio (around 10^4) and extremely low leakage current (around 120 nA) which made PSSNa-blend the best performing solid-state electrolyte for printed OECT among what have been tested. A more detailed study to improve the device performance with the screen-printed electrolyte will be performed in subsequent work.

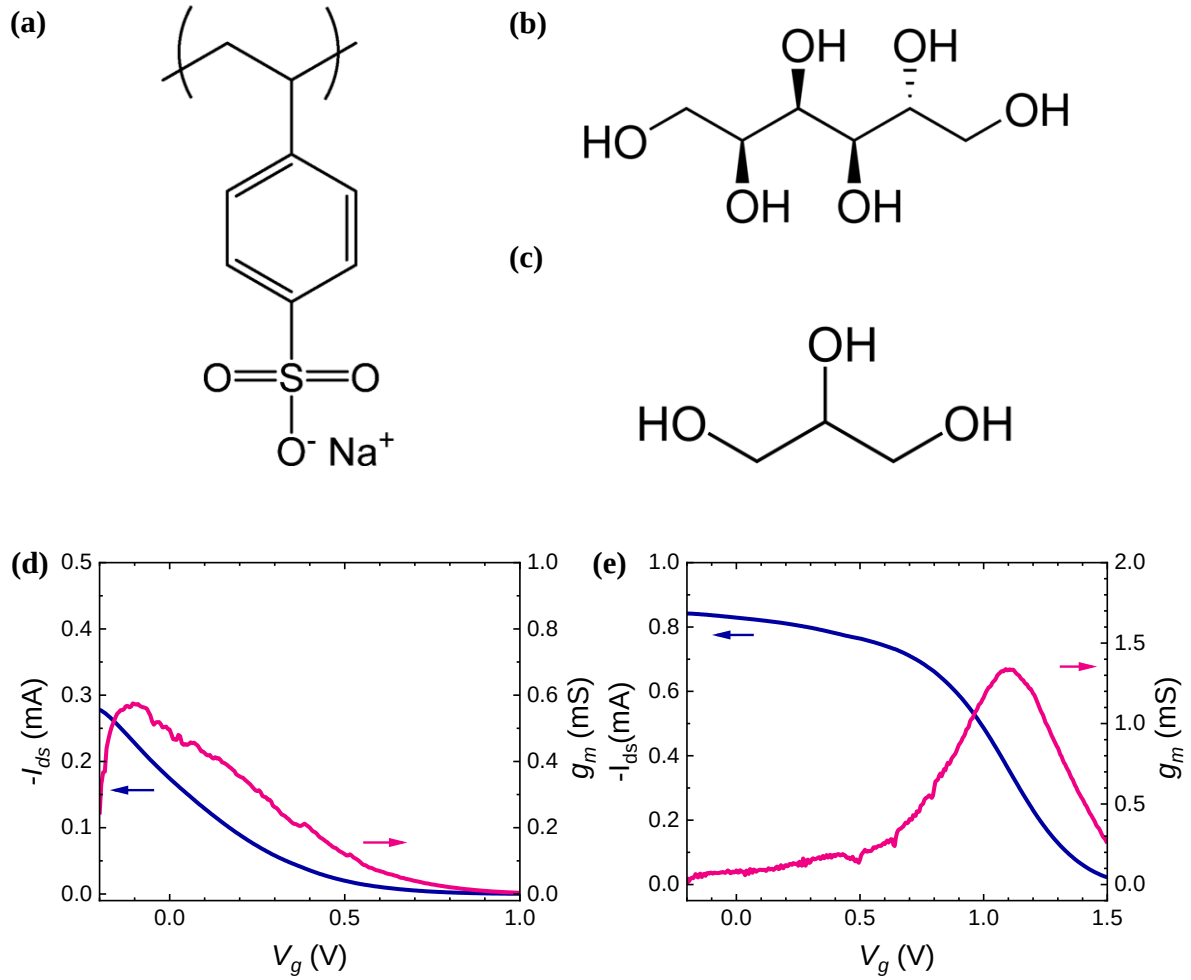

Figure 5.6 Chemical structure of (a) PSSNa, (b) S-sorbitol, and (c) glycerol.Transfer curves at V_{ds}= -0.5V for OECTs with (d) spin-coated and (e) screen printed PSSNa-based electrolyte.

The transient response of OECT with spin-coated PSSNa-blend electrolyte is much faster (Figure 5.7) than previous electrolytes with the same device structure – the transient response from on-to-off is around 69ms while off-to-on is much slower (around 480ms). This phenomenon has been reported previously[101,102] and is attributed to the channel material beneath the drain electrode: when a positive gate voltage as well as a negative drain voltage is applied, the front reduction edge in channel can extend beyond the electrolyte covered area and reach the bulk near the drain electrode, longer time is needed to re-oxidize the expanded electrochemically reduced channel volume beneath the drain electrode.

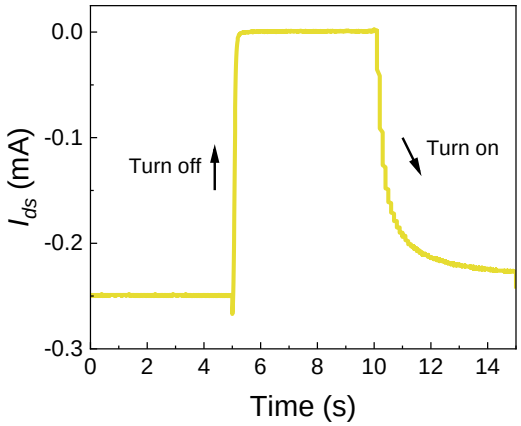

Figure 5.7 The transient response of the screen printed PSSNa-based electrolyte with V_{gs} pulse from -0.5V to 1V at 0.2Hz.

The printed PSSNa-based gel-like film works well for OECT mainly due to its strong hydrophilicity which keeps the film moist in air. The ionic conductivity of this gel-like PSSNa-based film may be sensitive to humidity and viscosity (i.e. temperature-dependent) and may be employed as a humidity and temperature sensors. The potential use of this unique behavior will be explored in future work. Annealing the film beyond 90°C will drive off moisture within the film, however, annealing treatment also leads to a more brittle film which cracks easily upon impact.

5.2.5 Comparison of solid electrolyte

Table 5.1 summarizes the device performance with different solid electrolytes. In conclusion, the PSSNa-blend film demonstrates a high on/off ratio, fast transient response, low leakage current and low threshold voltage. Compared to other electrolytes which are not screen printable due to their low viscosity solution and solvent causticity etc., the PSSNa-blended system is the most suitable electrolyte for an all screen-printed OECTs.

Table 5.1 Comparison of different solid electrolytes with carbon side gate

Electrolyte	Printing method	On/Off Ratio	Transient Time (off/on)	Leakage Current	Threshold Voltage
PVDF-HFP/ EMIM:BF_4	Spin coating	2209	>5s	2.73μA	1.2V
PVA/NaCl	Blade coating	4723	>5s	0.76μA	1V
PAAMPSA/ NaCl	Spin coating	1666	680ms/2.42s	0.9μA	1.5V
PSSNa/ D-sorbitiol/ glycerol	Spin coating	9462	69ms/480ms	0.21μA	1.2V
	Screen printing	1357	270ms/905ms	0.74μA	1.5V

5.3Summary

In this chapter, different electrolytes are deposited on the PEDOT:PSS channel by multiple printing methods. The different polymer matrixes and ion reservoirs in the composite electrolyte will affect the device performance both in steady-state and transient process of printed OECTs.

The PVDF-HFP/EMIM:BF_4 solid electrolyte system has a high on/off ratio and is most stable in air, while it suffers from high leakage current and significant slow transient response with the carbon side gate. The different gate structures and materials may influence the transient response of the OECT, and it will be the future scope to improve the device performance further.

The PVA/NaCl electrolyte has good initial device performance with a particularly high on/off ratio while it is very slow and failed to work after a few hours due to the mobile ions being ‘frozen’ in the film as the film dries over time in air.

The PAAMPSA/NaCl electrolyte has good device performance with exceptionally good long-term stability, functioning well even after 2 weeks. However, the PAAMPSA has a slow transient response, which is unsuitable for future application based on printed OECTs.

The PSSNa-blend electrolyte features a high on/off ratio, low operation voltage, quick response, and the compatibility of different printing methods, make this electrolyte the most promising

candidate amongst the others. In conclusion, the PSSNa based blended electrolyte will be used in the following experiments with different gate structures and materials to improve further the device performance, focusing particularly on the transient response for applications requiring a high-frequency operation.

6. Improvement of the transient response time by efficient gating

In this chapter, different gate materials were deposited on the printed OECT devices developed in previous chapter. Two gating mode of OECT, faradaic gate and non-faradaic gate were discussed and compared. Printed OECTs with two different gate structures, top gate and side gate, were compared. Ag/AgCl paste was employed as a top gate with the screen-printed OECTs. The transient performance of these printed OECT was improved when used with a faradaic top-gate. Finally, an all-printed OECTs with high on/off ratio, fast transient response, good long-term stability and stable resistance to bending cycles was demonstrated.

6.1 Faradaic and Non-faradaic Gate Materials

As discussed in the previous chapter, the PSSNa-blend electrolyte system will be used in the following experiments to further improve the device performance, especially the transient response for applications requiring a high-frequency operation.

The transient response of OECTs typically comprise of two stages – an initial quick (<1s) response is followed by slow change, which occurs over a longer timescale (>1s). The quick turn-off component refer to the formation of the double electrical layer and de-doped channel in the electrolyte-channel interface (surface doping/de-doping). While the slow component could be due to the redistribution of the ions and polymer chains in the electrolyte interface and the shift of the threshold voltage caused by bias stress or trap filling[100,101](bulk doping/de-doping).[103,104] The typical transient response is shown in Figure 6.1[101]. As a result, the overall transient response time will be dominated by the slow switching component. Since the slow component can be affect by the distribution of ions in the electrolyte-channel interface, it can be controlled by the concentration and ionic mobility in the electrolyte[102].[105] An electrolyte with high conductivity will reduces the influence of the slower response.

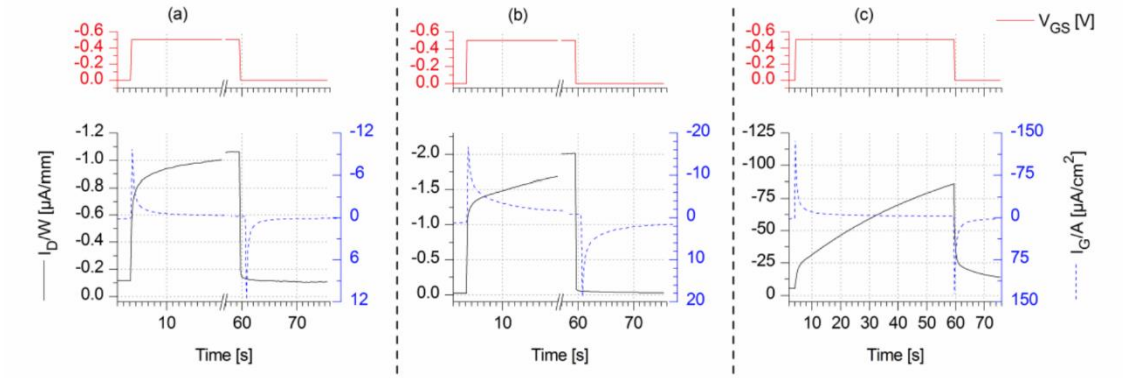

Figure 6.1 Typical turn-off transient response for PEDOT:PSS based OECT device.[101]

The total transient response time also depends on the gating mode which will affect the time constant of ionic circuit. There are two different working mechanisms of OECT gating – non-faradaic gate and faradaic gate. Faradaic gating typically yield more efficient channel modulation compared to non-faradaic gating. Hence, the OECT performance can depend on which gating mode dominates the channel modulation.

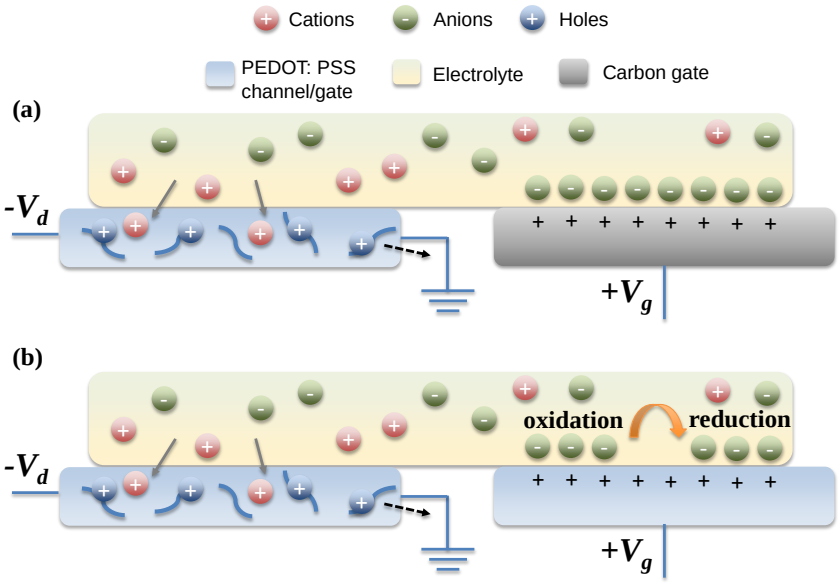

Figure 6.2 The gating mechanism for side gate OECTs with (a) captive gate mechanism and (b) faradaic gate.

In most reported printed OECTs, carbon is a commonly used gating material due to its stability and printability[54,106]. OECTs with a printed carbon side gate will be under capacitive gating (non-faradaic gating). In capacitive gating scenario, the gate is considered as ideal polarizable electrode, due to charge separation at the gate-electrolyte interface. Shown in Figure 6.2(a), an electric double layer will form near gate electrode when a positive gate voltage is applied. It will push the cations in electrolytes entering the channel and modulating the PEDOT: PSS channel doping state by compensation of the anions[107,108].

However, the bare carbon gate usually has low capacitance compared to the channel materials. As reported, the capacitance of bare printed carbon electrode is around 20-70 μF/cm^2 [109] without activation. While for the PEDOT: PSS, the volumetric capacitance is as high as 10-100 F/cm^3 [110] . Hence, to have the same capacitance as 1 mm^3 PEDOT: PSS channel, at least 0.5 cm^2 gate area is needed. Further more, to achieve efficient channel modulation, the gate capacitance should be far more large than channel capacitance. This will lead to a large gate area which is not ideal for high-density printed OECT arrays. To solve this issue, researchers have tried to modulate carbon gate by electrodepositing other materials including gold and platinum and obtaining a dual gate[107,111,112]. This method can lead to enhancement in device performance including higher current and lower threshold voltage, however, the voltage shifting is still high (>1.6V)[107]compared to the faradaic gate.

In contrast, the faradaic mode shown in Figure 6.2(b) can be more efficient due to the electrochemical process. In the operation of a faradaic dominated gate, the gate material will be reduced and oxidized when applying a negative and positive voltage respectively. Especially, the flow of electrons through the electronic circuit can be much more efficient in reducing the potential drop through the gate-electrolyte interface. This will substantially lead to a higher leakage current from gate to source (I_g) and potential drop in the electrolyte ϕE. The combined effect leads to enhanced channel conductivity, compared to the capacitive mode at the same gate voltage (V_g)[108,113].

Although capacitive mode is expected to avoid the generation of reactive species[93] in traditional transistors, the large potential drop in the electrolyte layer caused by capacitive response is not ideal for channel modulating in OECT device. Figure 6.3 shows ionic circuit of OECTs and the potential drop through the gate-electrolyte interface and electrolyte-channel interface. Undoubtedly, the high potential drop across the gate/electrolyte interface will lead to higher threshold voltage and thus higher power consumption. Besides, the higher threshold voltage may also cause electrolysis of water in the aqueous electrolyte solution, and affect ion mobility and channel doping state.

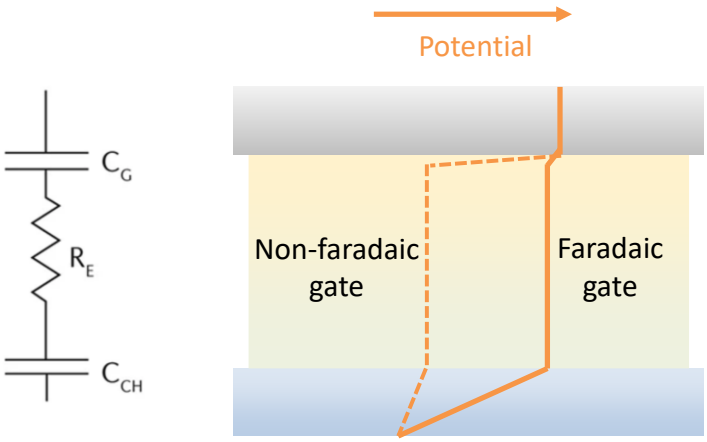

Figure 6.3(a) Ionic circuit of OECT and (b) potential drop through it with faradaic gate and non-faradaic gate.

To shed light on the behaviors of different gating modes, cyclic voltammetry (CV) study is performed here. In all experiments below, the counter electrode and reference electrode are shorted and connected to the blade-coated PEDOT: PSS film deposited on a patterned silver electrode with an area of 5mm × 10mm. The working electrode is connected to different gates in each CV scan. The CV scan is carried out under a scan rate of 0.025 V/s and scan step of 2mV. All the gate materials including carbon, PEDOT: PSS, and Ag/AgCl are blade-coated

onto a patterned silver electrode with an area of 5mm × 10mm. Finally, the PSSNa/D-sorbitol/glycerol electrolyte blend is coated over both the working and counter electrodes.

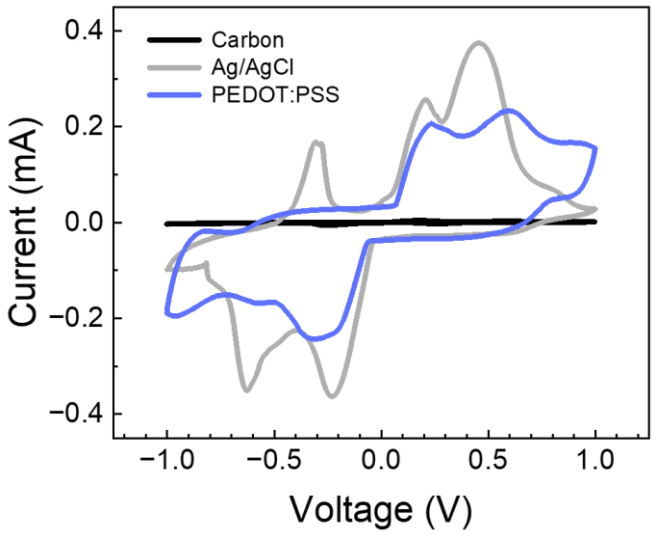

Figure 6.4 Cyclic voltammograms of 3 different working electrodes (WE) – blade-coated carbon, Ag/AgCl and PEDOT:PSS side gates. PSSNa/D-sorbitol/glycerol/water as electrolyte and PEDOT: PSS as the reference electrode (RE) and counter electrode(CE).

The shape of the CV curve for PEDOT:PSS is a typical Faradaic capacitor whereby reversible broad redox peaks are observed at -0.3V (reduction) and 0.2V, 0.5V (oxidation). With Ag/AgCl, additional reversible sharp redox peaks are observed at -0.6V (reduction) and -0.3V (oxidation) which might correspond to Ag/Ag^{+}. The electrochemical reaction can also be observed during the CV scan. The color of PEDOT:PSS working electrode turns dark blue when negative voltage is applied on the reference electrodes and becomes nearly colorless when positive voltage is applied.

The main advantage of faradaic gate can be reflected in the gate capacitance. As discussed in previous part, higher gate capacitance will lead to negligible potential drop in electrolyte and thus more efficient gate modulation. As reported, the volumetric capacitance of the gate can be calculated from the area under the CV curve,

$$C^{*} = \frac{1}{2V_{gate}\upsilon(V_c - V_a)} \int_{Va}^{Vc} I(V)dV$$

where V_{gate} refers to the volume of the electroactive materials in the electrodes, υ is the potential scan rate, I(V) is the response current density, V_a and V_c is the anodic potential and cathodic potential.

The capacitance of Ag/AgCl gate and PEDOT: PSS gate is around 2.24×10^{-4} F/cm^2 and 2.05×10^{-4} F/cm^2 which is much higher than the capacitance of the carbon gate (2.80×10^{-6} F/cm^2). This capacitance of the carbon gate corresponds fairly well to reported non-faradaic gate (1–10 μF/cm^2)[114]. Ag/AgCl has the largest capacitance amongst the three gate materials tested and should achieve the most efficient channel modulation in OECT.

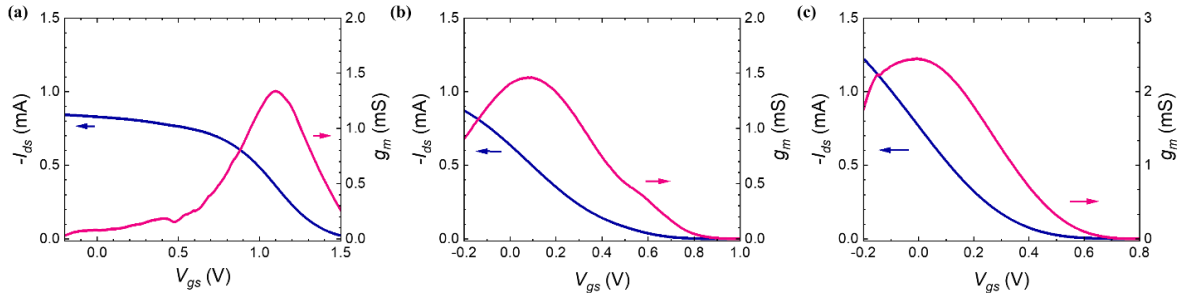

Figure 6.5 Transfer curves at V_{ds}= -0.5V for all printed OECTs with PSSNa-blended electrolyte system with (a) screen-printed carbon side gate, (b) blade-coated PEDOT: PSS side gate, and (c) dispenser-printed Ag/AgCl side gate.

Figure 6.5 shows the transfer curve of OECTs with carbon, PEDOT: PSS, and Ag/AgCl side gates, respectively. The OECTs reported in this Section 6 have a channel width of 400μm and channel length of 200μm to further reduce its transient response. The printed OECT with a non-faradaic carbon side-gate has an on/off ratio of 1×10^3 and high threshold voltage (V_T) larger than 1.5V. As discussed in previous chapter, this high threshold voltage may cause electrolysis of water in the water-based electrolyte (e.g. PSSNa-blended electrolyte used here). In contrast, the faradaic PEDOT: PSS side gate is a much more effective gate electrode. A much lower leakage current (I_{gs} around 130nA) was observed and a much higher on/off ratio of 8×10^3 and lower threshold voltage (V_T) of +1.0V respectively were obtained. The dispenser-printed Ag/AgCl paste also works well as a faradaic side gate to enhance the OECT performance. The printed OECT with the faradaic Ag/AgCl side gate can achieve on/off ratio of around 4×10^3. Besides, lower leakage current (I_{gs} around 220 nA) and lower threshold voltage (V_T) of +0.8V respectively were obtained.

Moreover, a faster transient response time (Figure 6.6) was achieved for OECT with PEDOT: PSS side gate, compared to the OECT with carbon side gate. The transient response for PEDOT: PSS side gate from on-to-off is around 6.5 ms while off-to-on is around 45.9ms. Here, the on-to-off and off-to-on time of PEDOT: PSS gate is more than 20 times faster than that of carbon side gate(270ms/905ms). An even faster transient response time is observed with the faradaic Ag/AgCl side gate. The transient response time from on to off and off to on is 5.6ms and 37.3 ms with the V_g pulse from 0V to 0.8V, respectively. An operation frequency of 250 Hz can be achieved by printed OECT.

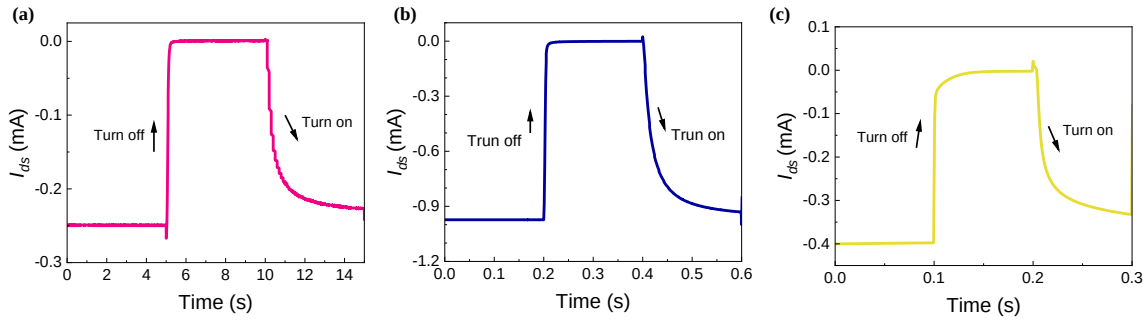

Figure 6.6 The transient response for OECTs with PSSNa blended electrolyte system with (a) screen printed carbon side gate and(b) blade coated PEDOT: PSS side gate. (c) dispensed Ag/AgCl side gate.

On the other hand, the repeatability and stability of the OECTs are also improved by the faradaic gate material. For the carbon side gate OECT, the ON current, and transconductance degrade significantly in the second scan (Figure 6.7(a),(b)). This decrement may be due to the lack of mobile anions in the PSSNa blended electrolyte. In PSSNa blended system, the anion PSS^- cannot move freely. When a high positive gate voltage is applied, the mobile cations Na^+ will be driven into the channel and de-dope it. When the gate voltage returns back to zero, it is insufficient to pull the mobile cations Na^+ out of the channel and hence the channel remains mostly de-doped. A higher negative gate potential (around -0.5V) is needed to pull the Na^+ otherwise the channel will remain in the de-doped state leading to a lower ON current. Another possible reason behind this phenomenon is the high threshold voltage of the carbon side gate structure. High threshold voltage around 1.5V is needed to turn off the device. The high threshold voltage may have caused irreversible side reactions on the PEDOT:PSS channel, destroying its conjugation leading to lowered conductivity, due to electrolysis of water present in the PSSNa blended system.

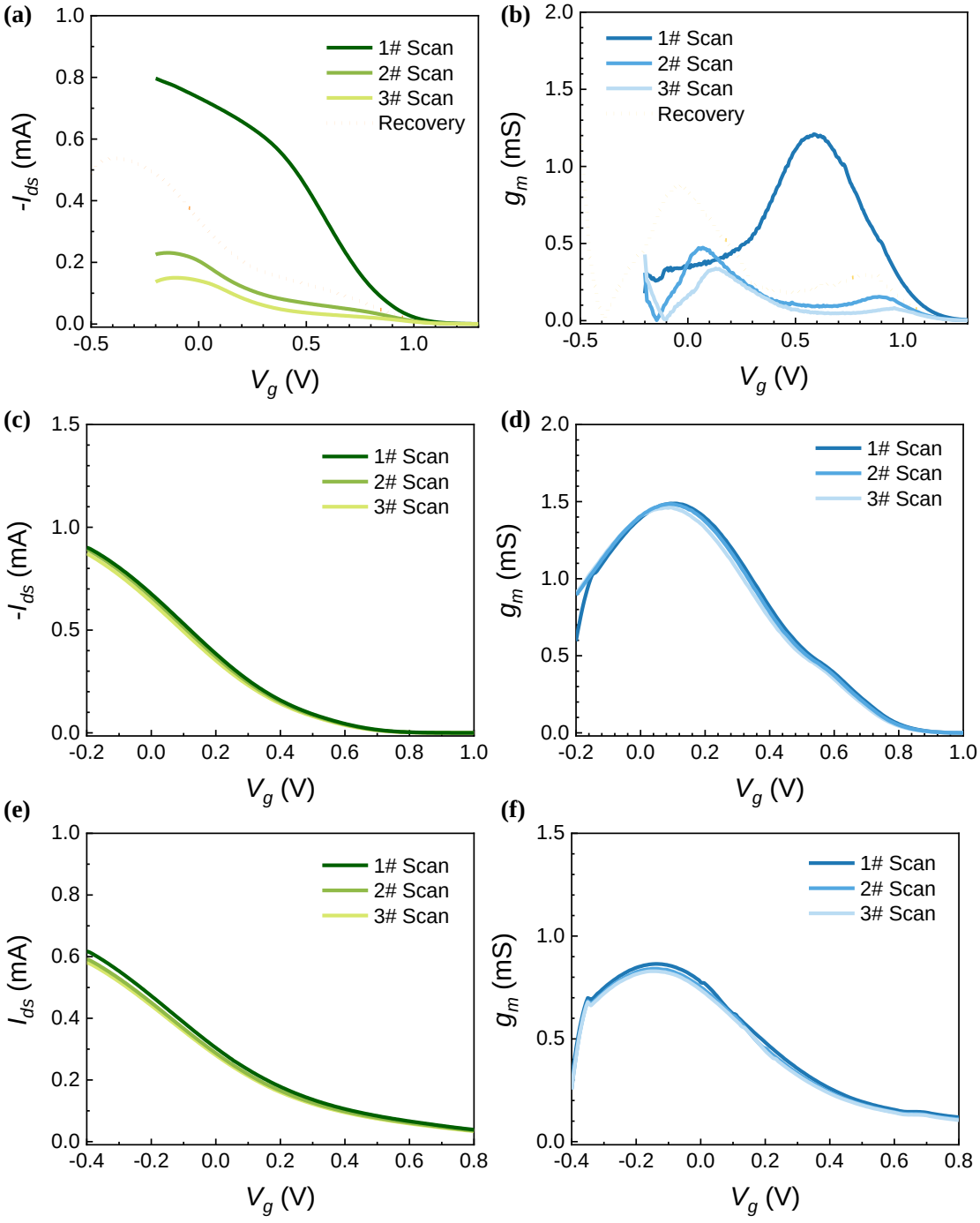

Figure 6.7 The stability of the transfer curve at V_{ds}= -0.5V for OECTs with (a),(b) screen printed carbon side gate, (c),(d) blade coated PEDOT: PSS side gate, and (e),(f) dispensed Ag/AgCl side gate.

In contrast, with the faradaic gate, electrochemical reactions occur at the gate-electrolyte interface upon applying a gate bias, e.g. $PEDOT^0/PEDOT^+$ or Ag^0/Ag^+ for the PEDOT:PSS and Ag/AgCl gate respectively. This leads to a small voltage drop across the gate-electrolyte

interface while most of the voltage drop occurs in the channel enhancing the doping/dedoping of the OECT channel, as suggested from their lowered threshold voltages. A significantly enhanced device stability upon repeated scans were observed with the Ag/AgCl and PEDOT/PSS side gate.

To investigate the universality of the faradaic gate effect, another electrolyte with both mobile cations and anions, PVDF-HFP/ EMIM:TFSI, was deposited on OECTs with carbon and PEDOT:PSS side gates. Similar trend of lowered threshold voltage with the faradaic gate, PEDOT:PSS, was observed. Figure 6.8 shows that the printed OECT with PVDF-HFP/ EMIM:TFSI electrolyte and PEDOT: PSS side gate can achieve on/off ratio of around 1×10^3 and a lower threshold voltage of around 1.1 V compared to the carbon side gate structure(See Figure 5.3). More importantly, the transient response has been significantly improved from more than 5 seconds to 138ms for switching off and 301ms for switching on.

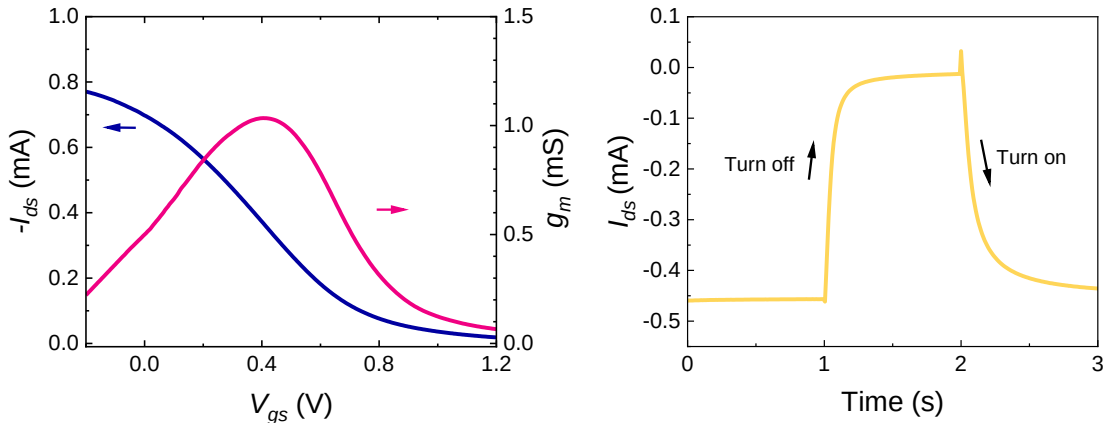

Figure 6.8 The device performance of all printed OECTs with PVDF-HFP/EMIM:TFSI electrolyte with blade coated PEDOT: PSS side gate. (a) The transfer curves at V_{ds}= -0.5V and (b) transient response from V_g= 0V to V_g= 1.2V

In conclusion, the device's performance (threshold voltage and transient response) can be improved by using an effective faradaic gate (PEDOT:PSS and Ag/AgCl). For the two faradaic gate materials used here, the Ag/AgCl gate is considered more efficient due to its high capacitance.

6.2 Ag/AgCl side-gate and top-gate structure

In previous section, the effect of different side-gate materials including carbon, PEDOT: PSS, and Ag/AgCl was discussed. Ag/AgCl was the best performing amongst the three materials. Besides gate material, the gate structure would also affect the device performance and particularly its transient response. For the following section, the OECT performance with Ag/AgCl as a top-gate, side-gate and pellet will be compared.

For the reported printed OECTs, to reduce the number of different printing layers and simplify the printing process, side gate structures are often used to modulate the channel conductivity and drain current [115]. As compared to top-gates, printed side-gates do not have the complication of considering orthogonal solvents with underlying layers. However, ions typically have to traverse a much longer distance from the side-gate to the OECT channel (~ few hundred μm to several mm) compared to top-gate structure (~up to tens of μm). According to Bernard's model, the transient behavior for a simplified OECT can be described as:

$$I(t, V_g) = I_{ss}(V_g) + \Delta I_{ss}(1 - \frac{\tau_h}{\tau_i})\exp(-t/\tau_i)$$

Here, $I_{ss}(V_g)$ is the drain current in steady-state with a applied gate voltage V_g and $\Delta I_{ss} = I_{ss}(V_g = 0) - I_{ss}(V_g)$. From this formula, the OECT's transient performance can be dominantly determined by two factors, τ_i and τ_h, where τ_i refers to the time constant of ion transportation in electrolyte, τ_h refers to the time constant of holes in channel materials. Applying theory for double layer capacitance with linear solution conductivity, the time constant for ion transportation in the electrolyte strongly depends on the electrical double layer by gate and channel capacitance and electrolyte resistance. [84,116]

$$\tau_i \sim l/C^{1/2}$$

where l is distance between the gate electrode and channel and C is the concentration of ions in electrolyte. Limited by the screen printing resolution and device structure, the distance between the channel and gate electrode in a side-gate structure is restricted to minimally few hundreds of micrometer which will lead to poor transient response due to the increased τ_i.

Although the above equation for τ_i is derived assuming a double-layer capacitance exist in the device, i.e. valid for non-faradaic gates only, the distance between the channel and faradaic gates would still influence the transient response. Increased distances can lead to higher overall electrolyte resistances and hence slower transient response. Distance between channel and top

gates can be reduced by approximately 10-1000 times compared to a side-gate design. This will lead to more efficient gating for both non-faradaic and faradaic gates. The device schematic for OECTs with side-gate and top-gate structure are shown in the Figure 6.9.

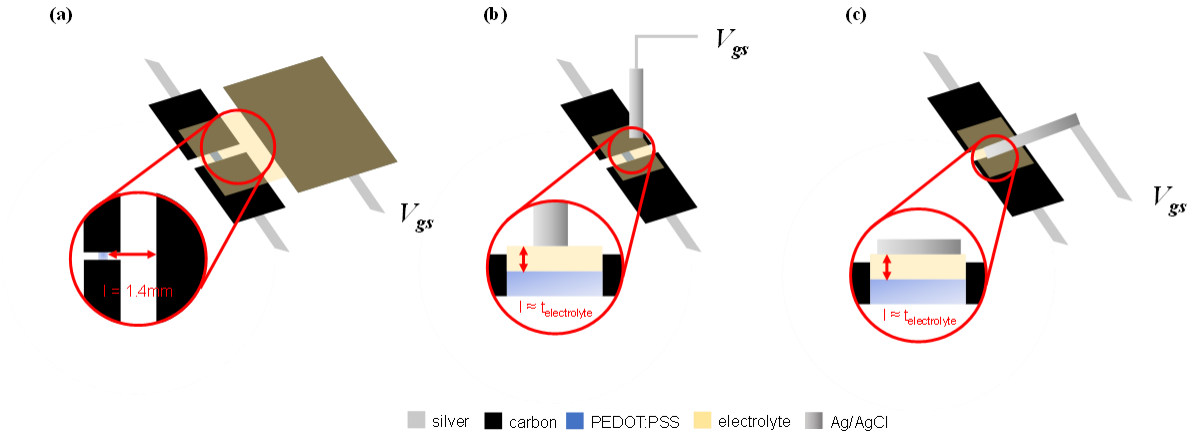

Figure 6.9 Device schematic with different gate and distance between gate and channel. (a) carbon side gate, (b)Ag/AgCl pellet as top gate, (c) Ag/AgCl paste as top gate.

6.2.1 Ag/AgCl pellet

Ag/AgCl pellet is a commonly used gate electrode for the electrolytes in liquid and gel states[117,118]. As a faradaic gate material, electrochemical reactions can occur in the gate and electrolyte interface, leading to a powerful channel modulating. The Ag/AgCl pellet can form a proper contact with the PSSNa-blended electrolyte as it is in gel-like state. The Ag/AgCl pellet is carefully lowered and immsersed into the gel electrolyte with a micro-manipulator, bringing it close to the OECT channel.

As expected, the high on/off ratio (3×10^3) and lower threshold voltage (0.6V) were observed in Ag/AgCl pellet top gate structure (Figure 6.10(a)) compared to side gate structure with the same material. Besides, the total transient response time was also improved slightly, the switching time from on to off and off to on is around 3.4 ms and 33.6 ms respectively (Figure 6.10(b)). This improvement is caused by the reduced distance between channel and gate electrode[84,119]. Working as a faradaic side gate structure, the Ag/AgCl pellet system also shows good repeatability (Figure 6.10(c),(d)).

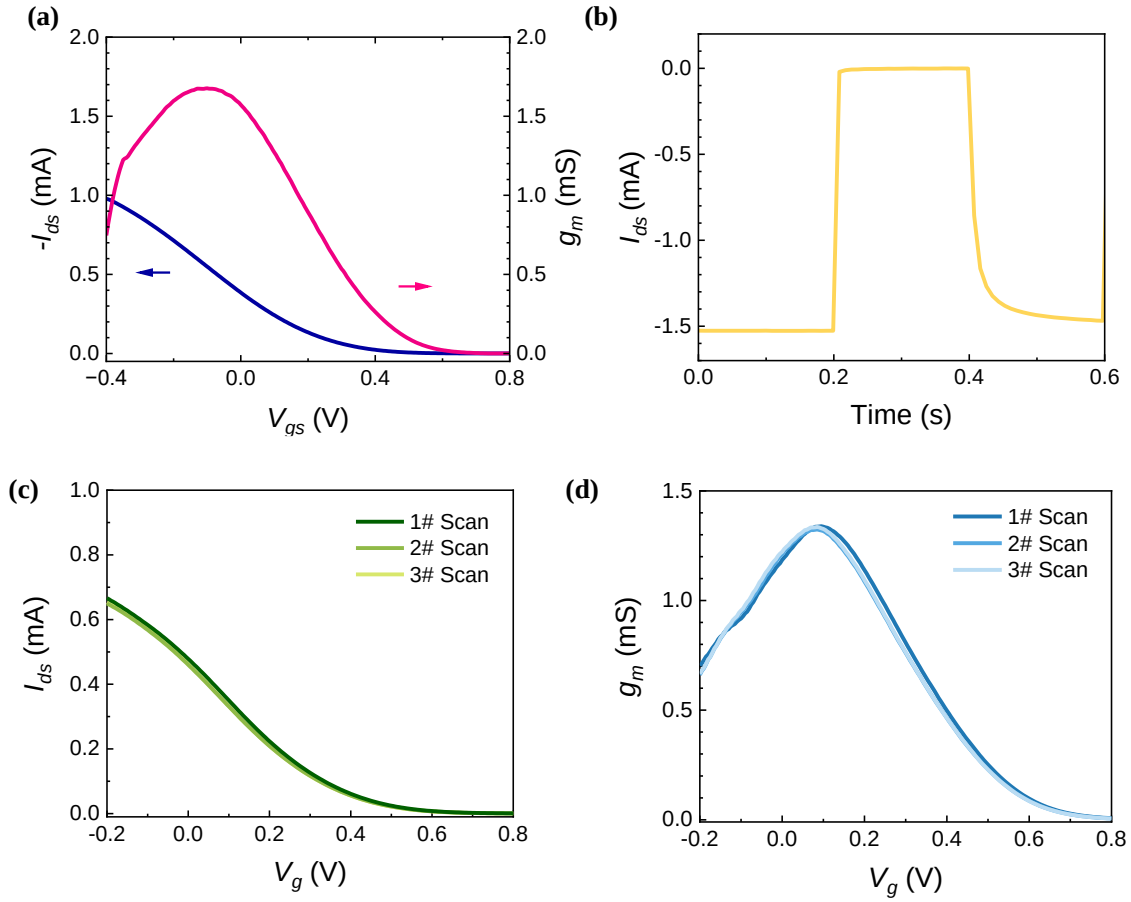

Figure 6.10 The device performance of all printed OECTs with PSSNa based blended electrolyte with Ag/AgCl pellet top gate. (a) Transfer curves at V_{ds}= -0.5V and (b) transient response from V_g= 0V to V_g= 0.8V. The stability of (c) drain current and (d) transconductance.

6.2.2 Ag/AgCl paste

Although Ag/AgCl pellet gate shows good device performance both in steady state and transient response, it is impractical to use with a large array of OECTs or for printed circuits. Ag/AgCl printed top gate could be a potentially better alternative. However, as discussed in section 5.2.4, the PSSNa based blended electrolyte is in a sticky-gel-like state. Therefore Ag/AgCl paste cannot be printed directly on this sticky-gel electrolyte.

To overcome this issue and fabricate printable top gates, the PSSNa-blended electrolyte were annealed at 80°C for 10 minutes to dry the film. Ag/AgCl paste is then dispensed on the dried PSSNa-blend film, above the channel region, to form a top gate. The device structure of this Ag/AgCl top gate is inserted Figure 6.11(a). The freshly prepared devices can achieve high on/off ratio around 1×10^4 at low threshold voltage around 0.8V (Figure 6.11(a)). The on/off ratio and high transconductance is repeatable (see Figure 6.11(c), (d)). These results indicate

that the cured film does not affect the device performance in steady state. However, slow transient response is observed in the cured system(29ms for turning off and 559ms for turning on), particularly for turn on time. (Figure 6.11(b)).

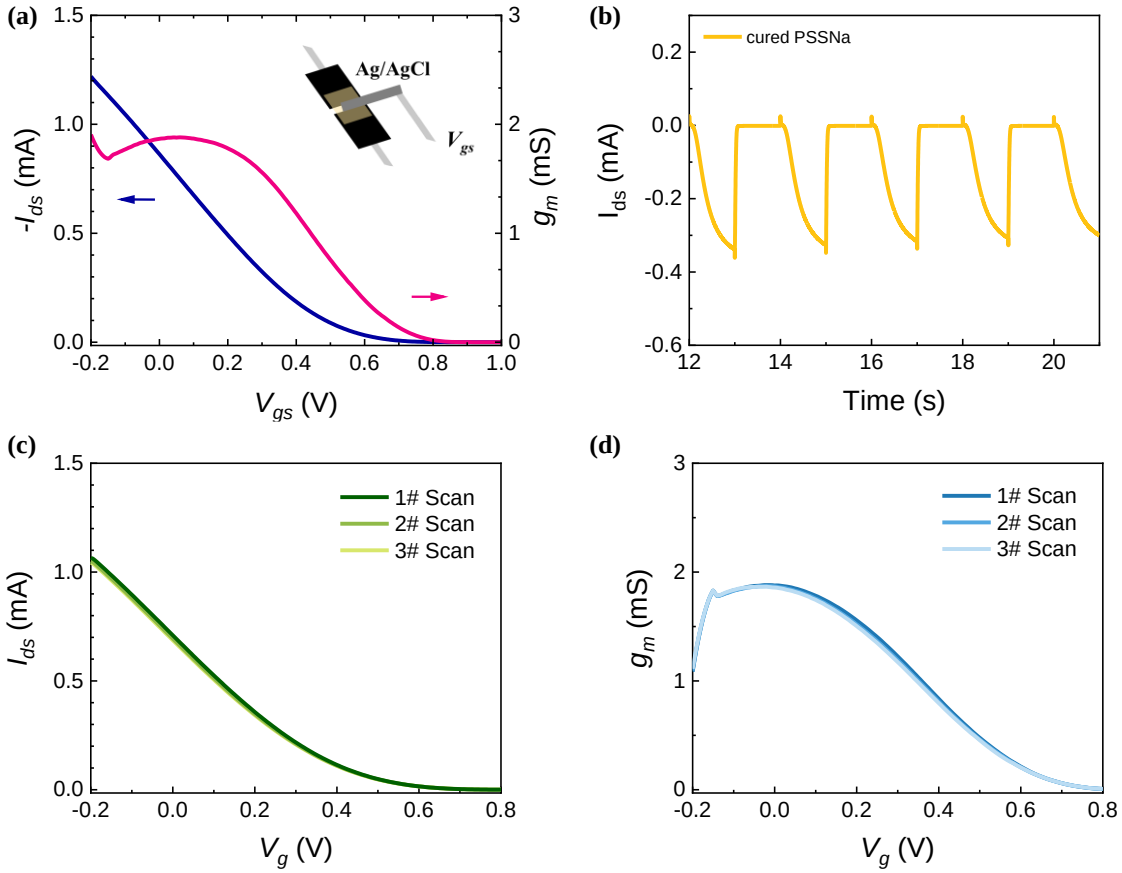

Figure 6.11 The device performance of all printed OECTs with PSSNa based blended electrolyte with Ag/AgCl pellet top gate. (a) The transfer curves at V_{ds}= -0.5V and (b) transient response from V_g= 0V to V_g= 1V. The stability of (c) drain current and (d) transconductance.

This poor transient response may be due to reduced ion conductivity in the dried film. To investigate the relationship between the ion conductivity of a dried vs moist electrolyte film, Electrochemical Impedance Spectroscopy (EIS) measurements were carried out. Two stainless steel plates are placed close to each other with a small separation gap of approximately 1mm and connected by PSSNa-blend electrolyte. The stainless steel – electrolyte – stainless steel structure is then annealing at 80 ℃ for 10 minutes, and store at room temperature (24.5℃) and humidity (61.8%) for 24 hours. At high frequencies, the real impedance *Z'* can be considered as the resistance of the electrolyte system. The ion conductivity σ can be calculated according to this equation,

$$\sigma = \frac{1}{R_0} \cdot \frac{t}{A}$$

where R_0 is the absolute value of Z' when at a high frequency, t is the thickness of the electrolyte layer and A is the area of electrolyte layer. In this measurement setup, the thickness and area of PSSNa is poorly defined. However, assuming that A remains unchanged while t reduces by approximately half (water content in the electrolyte blend is 40%), then R_0 can be used to give a good estimation of ion conductivity before and after curing.

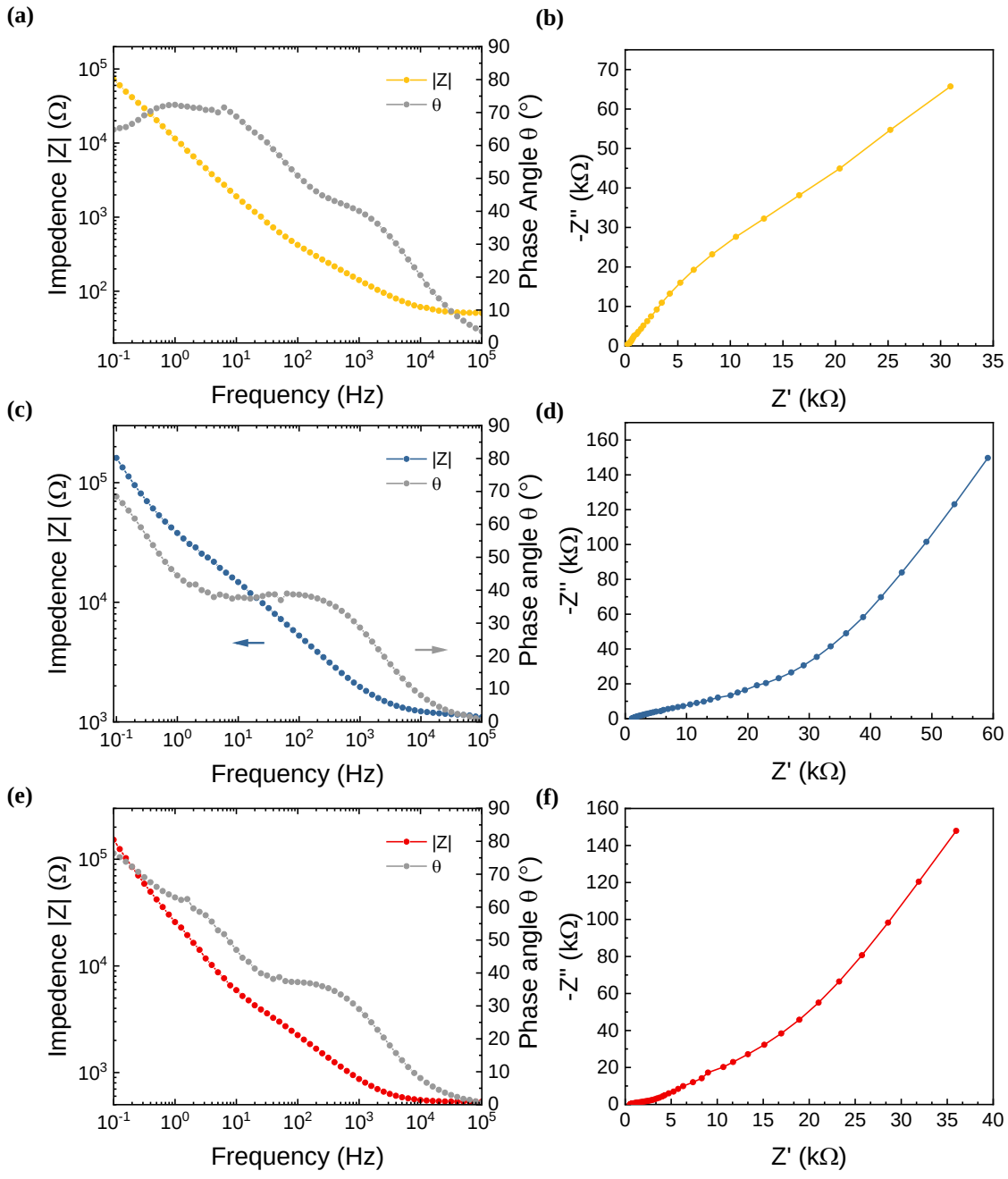

Figure 6.12 (a)Frequency dependent impedance and phase angle, (d) Nyquist plot of pristine PSSNa based blended electrolyte. (c)Frequency dependent impedance and phase angle, (d) Nyquist plot of

cured PSSNa based blended electrolyte. (e)Frequency dependent impedance and phase angle, (f) Nyquist plot of cured PSSNa based blended electrolyte exposed to room condition for 24 hours.

The frequency dependent impedance and phase angle plots, and Nyquist plots of three state of PSSNa based blended electrolyte (pristine, cured, 24 hours after curing) is demonstrated in Figure 6.12. As shown in the Nyquist plots, the R_0 of PSSNa based blended electrolyte increased significantly after annealing (from 55 Ω to 1121 Ω), and then drop back to around 213 Ω after exposing to the room condition for 24 hours. These results indicate that the ion conductivity of PSSNa-blend electrolyte is highly-dependent on the water content in the film.

In the pristine state, the weight ratio of all the components in PSSNa based blended electrolyte is: PSSNa: water: D-sorbitol: glycerol = 4:4:1:1, so the initial water content is 40%. After annealing, the measured mass loss of the electrolyte indicates most of the water in the film is driven off (Figure 6.13). The boiling point of other components are much higher and is not expected to evaporate at 80℃. Water uptake occurs almost immediately in air after the film has cooled down. The increased mass of electrolyte suggest that re-absorbed water content equilibrates at around 30%. This ability of PSSNa-blended electrolyte to absorb moisture may be due to the hygroscopic nature of both glycerol[120] and D-sorbitol[121] .

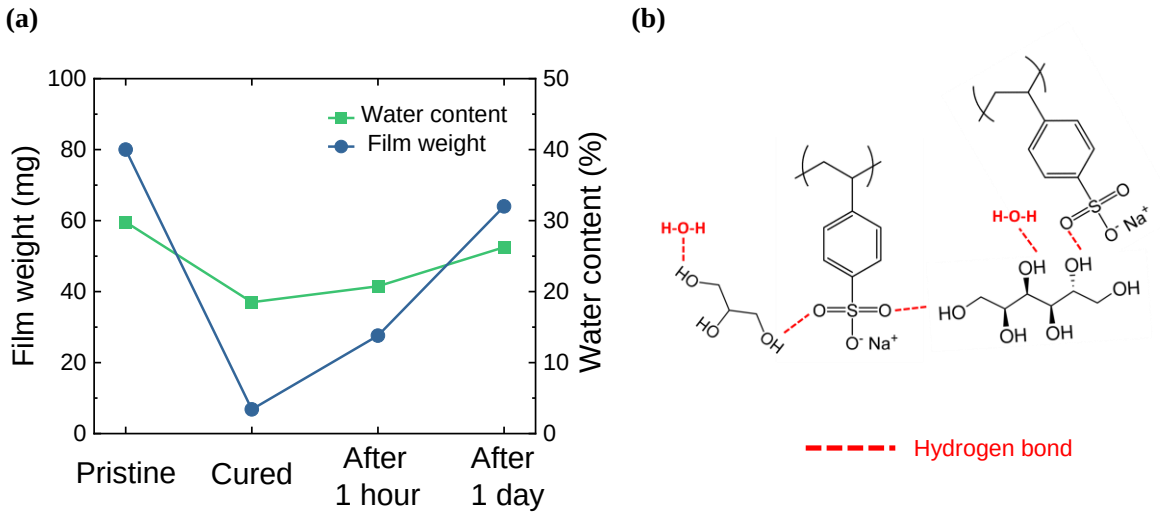

Figure 6.13 The water re-absorption process of PSSNa-blend electrolyte (a) The film weight and water content of PSSNa based blended electrolyte in 3 different states. (b) Chemical structure of PSSNa

As higher water content in the electrolyte leads to higher ionic conductivity[122], device performance of OECT is also expected to improve for the annealed film left in air to re-absorb water. Figure 6.14(a) shows the steady state performance of device including on/off ratio and threshold voltage is similar to the cured one. As expected, the transient response of device with the annealed PSSNa-blended electrolyte and printed Ag/AgCl top-gate significantly improved after 1 hour and finally reach a stable state after a few days (Figure 6.14(b)). The transient response of the top-gate devices after 3 days is 1.9 ms from on-to-off and 28 ms from off-to-on. This is the fastest transient response, to the best of our knowledge, for screen-printed OECTs [41,81,101].

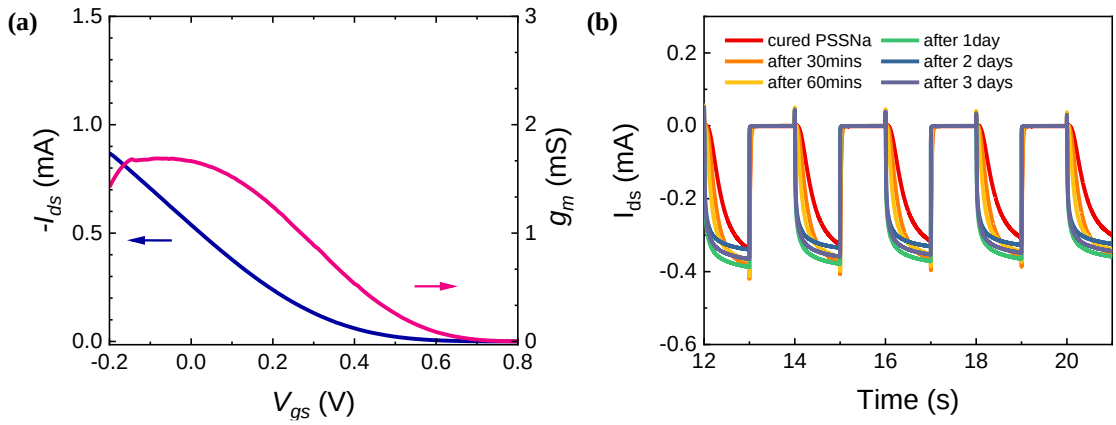

Figure 6.14 The device performance of all printed OECTs with PSSNa based blended electrolyte with Ag/AgCl pellet top gate for 3 days. (a) The transfer curves at V_{ds}= -0.5V and (b) transient response from V_g= 0V to V_g= 1V.

The device also shows good long-term stability after the measurement, maintaining 95% of the initial magnitude of current after 300 cycles (Figure 6.15) of gate pulsing, which shows good reversibility of the electrochemical reactions. It also shows that the printed Ag/AgCl top gate is an effective gate for channel modulation and OECT operations.

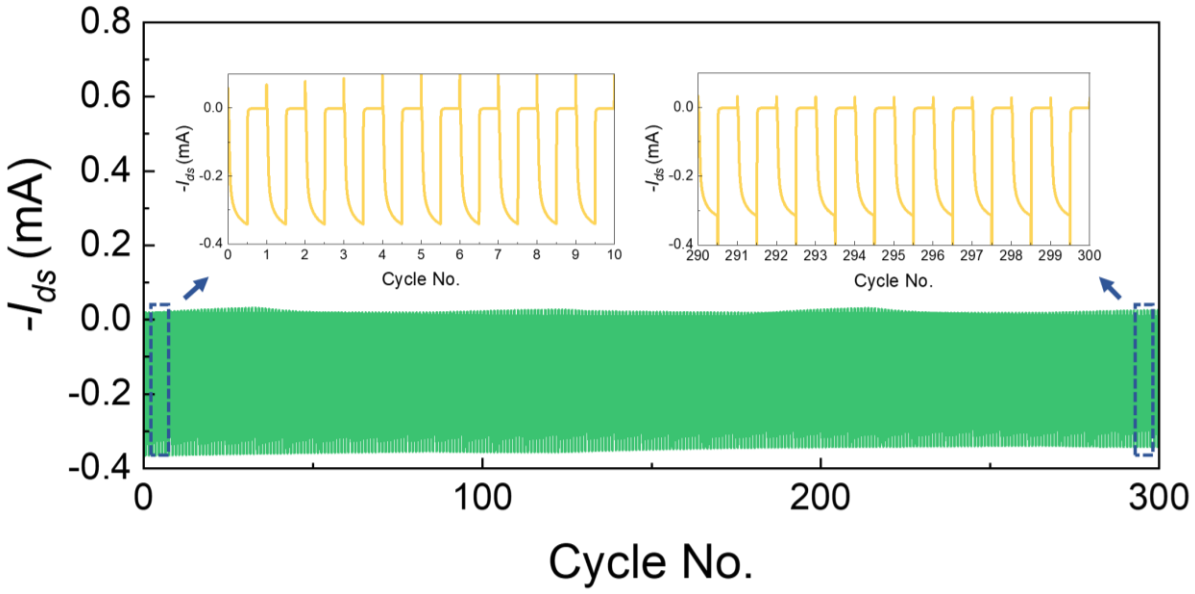

Figure 6.15 Long-term stability measurement with V_G from 0 to 1 V and constant V_D = −0.5 V and a pulse width of 0.1 s after 300 cycling with cured PSSNa based blended electrolyte after 3 days.

6.3Mechanical performance of printed OECTs

The mechanical performance is crucial to the flexible and wearable electronics. To achieve a good compatibility with soft interface, the devices are expected to keep stable under multiple exogenic process including bending, twisting and strain. Here, the device performance under different bending angle is measured.

To test the device performance under repeated bending cycles, the flexible devices with PSSNa blended electrolyte and Ag/AgCl side were printed on the PI substrate and attached to the metal fixture (Figure 6.16(a)). The channel area was placed on the center of fixture to sustain the bending process. The fixture was then connected to the gear, as the gear rotate along clockwise, the bending angle of substrate can be tune from 0° to 180°as shown in Figure 6.16(b).

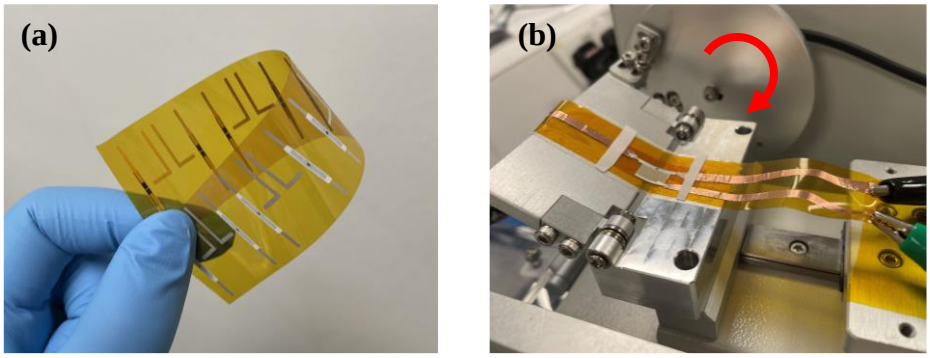

Figure 6.16 (a) flexible printed device on PI substrate (b) bending testing setup when the bending angle is equal to 30°.

Figure 6.17(a) demonstrate the transfer curves of printed OECT under different bending angle. The drain current drops slightly (<5%) until the bending angle reach to 150°, indicating the good flexibility in this bending range. The drain current continues to drop from 0.15mA to 0.13mA when the substrate is totally folded with bending angle of 180°. The minor degradation sustains when the bending process is released (dash line). This reduced conductivity may be due to the irreversible small cracks on the silver electrode and carbon contact caused by the severe bending. The small recovery on drain current and transconductance after relaxation may introduced by the physical contacts of cracks.

The transient performance under bending processing is shown in Figure 6.17(b). Though there is a small current degradation, the turn off/on time at initial state and 180° bending angle is 5.78ms/35ms and 5.75ms/36ms respectively. These results indicate that the bending state didn't affect the properties of channel/electrolyte interface, show good bending stability and flexibility of printed device.

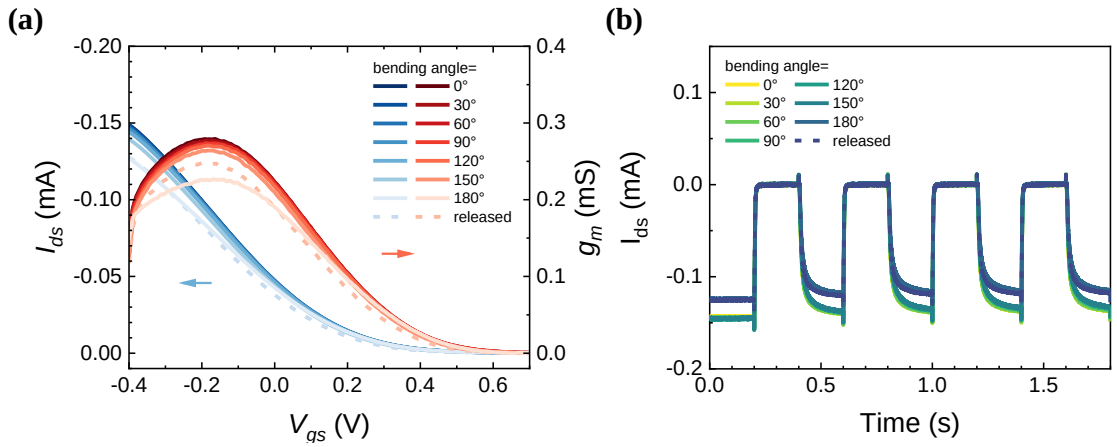

Figure 6.17 The device performance under different bending angle. (a) Transfer curves at V_{ds}= -0.5V (b) Transient response from V_g= -0.2V to V_g= 0.8V.

To further investigate the device stability under bending, the repeated bending test has been carried out for the device. The device has been bent from 0° to 120° to ensure the stability with the bending speed at 30° per second for 100 and 1000 cycles. After 100 times bending cycles, both the transfer performance and transient response stay the same (see Figure 6.18.). When the number of cycles increases to 1000, the drain current(0.13mA), ON/OFF ratio (~3×10^3) and threshold voltage(0.6V) stay very similar to the initial state. While for the transient response, the turn off/on time is 5.75ms/36ms, 5.85ms/36ms and 12.15ms/60ms at initial state, 100 cycles and 1000 cycles respectively. These results indicate that the printed device can sustain the good static performance under repeated bending cycles of 1000 times, while the transient response degrade a bit after 1000 cycles.

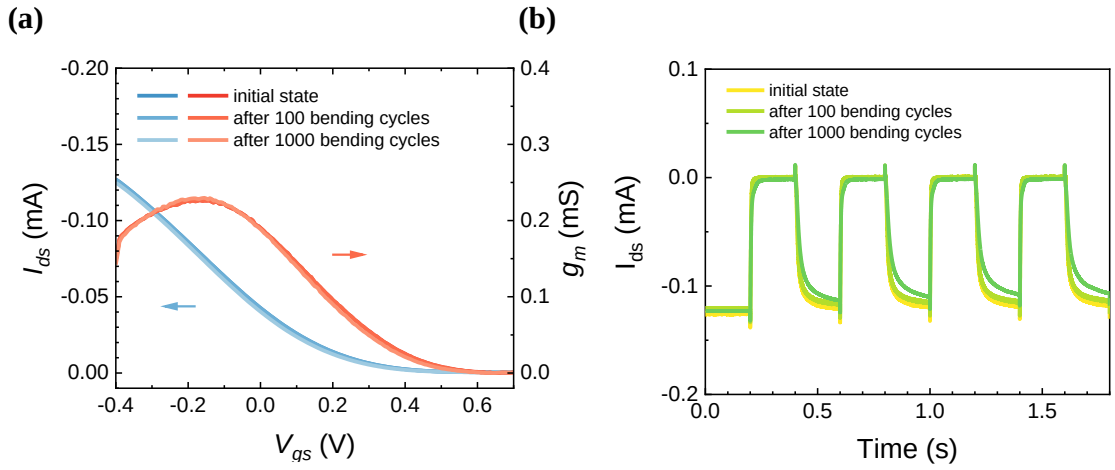

Figure 6.18 The device performance after repeated bending cycles. (a) Transfer curves at V_{ds}= -0.5V (b) Transient response from V_g= -0.2V to V_g= 0.8V.

6.4Comparison of different gate materials and structures

Table 6.1 summarized the OECT performance with PSSNa-blended electrolyte and different gate materials and structures used in this chapter. In conclusion, the printed OECT with PSSNa-blended electrolyte can obtain best transient performance and good steady state performance with printed Ag/AgCl top gate.

Table 6.1 OECT performance with different gate materials and structures

Gate materials	Gate structures	On/Off Ratio	Transient Time (off/on)	Leakage Current	Threshold Voltage

Carbon	Side gate	1357	270ms/905ms	0.74µA	1.5V
PEDOT: PSS	Side gate	7909	6.5ms/45.9ms	0.13µA	1V
Ag/AgCl (paste)	Side gate	4188	5.6ms/37.3s	0.22µA	0.8V
Ag/AgCl (paste)	Top gate	17285	1.9ms/28ms	0.09µA	0.8V
Ag/AgCl (pellet)	Top gate	2956	3.4ms/33.6ms	0.31µA	0.6V

6.5Summary

In this part, firstly, the printed OECTs with different gate materials including carbon, PEDOT: PSS, and Ag/AgCl are developed. The channel modulation modes of these gates are divided into non-faradaic gating (carbon) and faradaic gating (PEDOT: PSS and Ag/AgCl). The faradaic gating is proven to be more efficient due to its high capacitance and negligible voltage drop via electrolyte-gate interface. High on/off ratio, low threshold voltage and fast transient response is observed in printed OECTs under faradaic gating.

Secondly, the printed OECTs with different gate structure are compared and discussed. The Ag/AgCl pellet and printed Ag/AgCl paste worked as top gate for channel modulation. Both types of Ag/AgCl top gate can achieve better device performance compared to the printed Ag/AgCl side gate. Between them, the Ag/AgCl paste is versatile due to its printability. The initial slow transient response caused by poor ion conductivity of annealed electrolyte is resolved by allowing the hygroscopic film to reabsorb moisture in air. This system with PSSNa-blended electrolyte and printed Ag/AgCl top gate can obtain a fast switching which is comparable and even faster than reported screen printed devices.

Thirdly, the mechanical performance of printed are investigated by repeated bending testing. The device shows good flexibility at bending angle of 150°, although the current degraded a bit at bending angle 180°, the transient response stays fast. For the repeated bending testing, the static performance stays stable even after 1000 cycles.

Table 6.2 summarises the state-of-the-art screen-printed OECT compared against our best performing PSSNa-blended electrolyte and Ag/AgCl OECT. The OECT developed and reported in this thesis is the fastest device especially for de-doping process (switch from on to off). The efficient faradaic top gate Ag/AgCl and high ion concentration of PSSNa-blended electrolyte accounts for this improvement.

Table 6.2 Comparison of performance of reported screen printed PEDOT: PSS based OECTs and this work.

Channel dimension (W/L) (µm/ µm)	**Gate**	**Electrolyte**	**I_{ds}(mA)**	**V_{th}(V)**	**t_{on-off} / t_{off-on} (ms)**
200/200 (Ref.[69])	PEDOT: PSS top gate	AFI VV009 (Commercial)	0.45	1.3V	20/225
150/100 (Ref.[41])	PEDOT: PSS top gate	AFI VV009 (Commercial)	0.8	1.2V	20/30
200/25 (Ref.[123])	PEDOT: PSS top gate	E009 (Commercial)	1.5	1.2V	34/88
150/100 (Ref.[124])	PEDOT: PSS top gate	AFI VV009 (Commercial)	1.3	1.2V	10/40
400/200 (this work)	Ag/AgCl top gate	PSSNa	1.2	0.8V	1.9/28

7. Conclusion and Recommendations

A summary of this study and conclusions drawn from the experiments are presented in this chapter. Challenges for printing and degradation issue of PEDOT: PSS are discussed in detail. Suggestions regarding future work related to this study are presented. Extension of printed OECT with pressure sensor, logic circuit, and further transient performance improvement on device structure as well as materials is proposed.

7.1 Conclusion

This study successfully demonstrates the viability of screen-printing technique for the fabrication of flexible organic electrochemical transistors which can operate at a high frequency and sustain repeated bending cycles.

Screen printing is a large-scale electronics fabrication technology that is commonly used in industry. Compared to traditional silicon-based photolithology methods and other printing technologies, screen printing enables high volume and uniform deposition of flexible materials on flexible substrates. The screen printing system typically consists of a pair of squeegees to move towards the set printing direction, a screen mask with designed pattern open, a transfer platform to load and unload the production and fix the flexible substrate, camera system for fiducial identification and alignment, and the pastes with different viscosity. Various parameters including the hardness and angle of squeegees, mesh number, materials and emulsion thickness of the mask, the viscosity and surface tension of paste will affect the printing resolution, thickness, and uniformity.

The printing quality also depends on the printing parameters including printing pressure, printing gap, printing velocity and the number of printing layers. These printing parameters should be tuned regarding the different paste with different viscosity and rheology.

A total of 4 paste and their printing parameters were optimized and deposited on the flexible substrate respectively. The OECT array has been printed successfully with high uniformity and close channel dimension as designed.

To overcome the limitations of OECT devices imposed by liquid electrolytes, alternative solid electrolytes based on various polymer matrixes with addictive ions were tested. The device performance in both steady state and transient state is measured and compared. The screen printable PSSNa-blended electrolyte has the best performance with high on/off ratio, low threshold voltage, fast transient response and is finally chosen for the further improvement.

In order to further improve the transient response of OECTs, another important component – gate was discussed too. The non-faradaic and faradaic mode of OECT gating are discussed and compared. Device with top gate structure take place of side gate to reduce the distance between channel and gate electrode and hence reduce the time constants of ionic circuit, finally leads to the fast transient response which is comparable and even fast than the reported screen printed OECT.

7.2 Recommendations for Future Work

7.2.1 Optimization of channel dimension

Current study about screen printed OECTs are focusing on the improvement of device transient performance by optimizing the electrolyte and gate. However, the transient response of the transistor also depends on the channel dimension and device structure. Restricted by the printing resolution, the limitation channel dimension of screen printed OECT are around 100μm in width and length, and 500nA in thickness. To overcome this issue, people combined the screen printing technology with other fabrication technology including, aerosol printing[83], vapor phase polymerization [125] and laser ablation[126] . However, it is a palliative method and complicate the fabrication process, thus defending the purpose of screen printing.

During OECT operation process, the whole bulk of channel layer is doped and de-doped. In this work, the total area of PEDOT:PSS is 3 times larger than the area used in the OECT channel. The overlapping area between the excess PEDOT:PSS and the carbon electrodes should be reduced to improve the device performance[127,128]. An optimization study on this is recommended.

Besides, to further reduce the transient time of screen printed device, the device structure can be modulated in the future. For example, instead of an in-plane source-drain connection to the channel, the channel length can be significant reduced using the vertical structures[129,130].

7.2.2 Development of printable electrolyte

Another major issue with current research is the lack of screen printable electrolyte. Although the PSSNa based blended electrolyte is screen printable after mixing two molecule weight powder together, the uniformity of the screen printed electrolyte is still not as good as spin-coating.

Another issue for the all screen printed device is the top gate issue. As discussed in the chapter 6, the top gate can only be deposited on the solid state electrolyte. However the solid state electrolytes usually have lower ion conductivity and poor doping ability compared to the gel or liquid electrolyte. The understanding of formulation of ionic liquid and their polymer matrices will help in developing the screen printable electrolytes which has good device performance and long-term stability.

Reference

1. Liu, Q. *et al.* A High-Performances Flexible Temperature Sensor Composed of Polyethyleneimine/Reduced Graphene Oxide Bilayer for Real-Time Monitoring. *Adv Mater Technol* **4**, 1800594 (2019).

2. Ren, X. *et al.* A Low-Operating-Power and Flexible Active-Matrix Organic-Transistor Temperature-Sensor Array. *Advanced Materials* **28**, 4832–4838 (2016).

3. Turkani, V. S. *et al.* A highly sensitive printed humidity sensor based on a functionalized MWCNT/HEC composite for flexible electronics application. *Nanoscale Adv* **1**, 2311–2322 (2019).

4. Ma, L. *et al.* Full-Textile Wireless Flexible Humidity Sensor for Human Physiological Monitoring. *Adv Funct Mater* **29**, 1904549 (2019).

5. Wu, J. *et al.* Carbon Nanocoil-Based Fast-Response and Flexible Humidity Sensor for Multifunctional Applications. *ACS Appl Mater Interfaces* **11**, 4242–4251 (2019).

6. Yu, Z., Cai, G., Liu, X. & Tang, D. Pressure-Based Biosensor Integrated with a Flexible Pressure Sensor and an Electrochromic Device for Visual Detection. *Anal Chem* **93**, 2916–2925 (2021).

7. Chen, S. *et al.* Contact Modulated Ionic Transfer Doping in All-Solid-State Organic Electrochemical Transistor for Ultra-High Sensitive Tactile Perception at Low Operating Voltage. *Adv Funct Mater* **30**, 2006186 (2020).

8. Tao, L. Q. *et al.* Graphene-Paper Pressure Sensor for Detecting Human Motions. *ACS Nano* **11**, 8790–8795 (2017).

9. Lee, S. *et al.* A transparent bending-insensitive pressure sensor. *Nature Nanotechnology 2016 11:5* **11**, 472–478 (2016).

10. Lo, L. W. *et al.* Inkjet-Printed Soft Resistive Pressure Sensor Patch for Wearable Electronics Applications. *Adv Mater Technol* **5**, 1900717 (2020).

11. Yang, W. *et al.* A Breathable and Screen-Printed Pressure Sensor Based on Nanofiber Membranes for Electronic Skins. *Adv Mater Technol* **3**, 1700241 (2018).

12. Zhang, Y. *et al.* Performance Enhancement of Flexible Piezoelectric Nanogenerator via Doping and Rational 3D Structure Design For Self-Powered Mechanosensational System. *Adv Funct Mater* **29**, 1904259 (2019).

13. Bharti, D. K., Gupta, M. K., Kumar, R., Sathish, N. & Srivastava, A. K. Non-centrosymmetric zinc silicate-graphene based transparent flexible piezoelectric nanogenerator. *Nano Energy* **73**, 104821 (2020).

14. Tang, Y. *et al.* Triboelectric Touch-Free Screen Sensor for Noncontact Gesture Recognizing. *Adv Funct Mater* **30**, 1907893 (2020).

15. Friedlein, J. T. *et al.* Microsecond Response in Organic Electrochemical Transistors: Exceeding the Ionic Speed Limit. *Advanced Materials* **28**, 8398–8404 (2016).

16. Rivnay, J. *et al.* Organic electrochemical transistors. *Nature Reviews Materials 2018 3:2* **3**, 1–14 (2018).

17. Yang, C.-Y. *et al.* Low-Power/High-Gain Flexible Complementary Circuits Based on Printed Organic Electrochemical Transistors. *Adv Electron Mater* **8**, 2100907 (2022).

18. Galliani, M. *et al.* Flexible Printed Organic Electrochemical Transistors for the Detection of Uric Acid in Artificial Wound Exudate. *Adv Mater Interfaces* **7**, 2001218 (2020).

19. Mangoma, T. N., Yamamoto, S., Malliaras, G. G. & Daly, R. Hybrid 3D/Inkjet-Printed Organic Neuromorphic Transistors. *Adv Mater Technol* **7**, 2000798 (2022).

20. Tortorich, R. P., Shamkhalichenar, H. & Choi, J. W. Inkjet-Printed and Paper-Based Electrochemical Sensors. *Applied Sciences 2018, Vol. 8, Page 288* **8**, 288 (2018).

21. Su, R., Hyun Park, S., Ouyang, X., Ih Ahn, S. & McAlpine, M. C. 3D-printed flexible organic light-emitting diode displays. *Sci. Adv* **8**, 8798 (2022).

22. Sun, J. *et al.* Fully R2R-Printed Carbon-Nanotube-Based Limitless Length of Flexible Active-Matrix for Electrophoretic Display Application. *Adv Electron Mater* **6**, 1901431 (2020).

23. Kim, J. *et al.* Ultrathin Quantum Dot Display Integrated with Wearable Electronics. *Advanced Materials* **29**, 1700217 (2017).

24. Tang, Y. *et al.* Triboelectric Touch-Free Screen Sensor for Noncontact Gesture Recognizing. *Adv Funct Mater* **30**, 1907893 (2020).

25. Chen, K. *et al.* Dynamic Photomask-Assisted Direct Ink Writing Multimaterial for Multilevel Triboelectric Nanogenerator. *Adv Funct Mater* **29**, 1903568 (2019).

26. Wang, P. *et al.* The Evolution of Flexible Electronics: From Nature, Beyond Nature, and To Nature. *Advanced Science* **7**, 2001116 (2020).

27. Nomura, K. I. *et al.* Fine pattern formation with solder paste using screen printing with stainless steel mesh-cut screen mask. *Journal of Micromechanics and Microengineering* **30**, 115023 (2020).

28. Wan, Z. *et al.* Screen printing process control for coating high throughput titanium dioxide films toward printable mesoscopic perovskite solar cells. doi:10.1007/s12200-019-0904-7.

29. Li, S. *et al.* Rheological characterization and jet printing performance of Sn–58Bi solder pastes. *Journal of Materials Science: Materials in Electronics 2017 29:6* **29**, 4575–4582 (2017).

30. Wan, X., Luo, L., Liu, Y. & Leng, J. Direct Ink Writing Based 4D Printing of Materials and Their Applications. *Advanced Science* **7**, 2001000 (2020).

31. Raut, N. C. & Al-Shamery, K. Inkjet printing metals on flexible materials for plastic and paper electronics. *J Mater Chem C Mater* **6**, 1618–1641 (2018).

32. Fully Printed PEDOT:PSS-based Temperature Sensor with High Humidity Stabili...: EBSCOhost. https://web.s.ebscohost.com.remotexs.ntu.edu.sg/ehost/pdfviewer/pdfviewer?vid=0&sid=666e889e-83cb-466d-a648-c8879cf48be3%40redis.

33. Park, H. J., Yoon, J. H., Lee, K. G. & Choi, B. G. Potentiometric performance of flexible pH sensor based on polyaniline nanofiber arrays. *Nano Converg* **6**, NA-NA (2019).

34. Andersson Ersman, P., Lassnig, R., Strandberg, J. & Dyreklev, P. Flexible Active Matrix Addressed Displays Manufactured by Screen Printing. *Adv Eng Mater* **23**, 2000771 (2021).

35. Janczak, D. *et al.* Stretchable and Washable Electroluminescent Display Screen-Printed on Textile. *Nanomaterials 2019, Vol. 9, Page 1276* **9**, 1276 (2019).

36. Mathies, F. *et al.* Inkjet-Printed Triple Cation Perovskite Solar Cells. *ACS Appl Energy Mater* **1**, 1834–1839 (2018).

37. Lin, Y. *et al.* Printable Fabrication of a Fully Integrated and Self-Powered Sensor System on Plastic Substrates. *Advanced Materials* **31**, 1804285 (2019).

38. Yoon, Y. *et al.* Four Degrees-of-Freedom Direct Writing of Liquid Metal Patterns on Uneven Surfaces. *Adv Mater Technol* **4**, 1800379 (2019).

39. Xiang, S. *et al.* Liquid-Metal-Based Dynamic Thermoregulating and Self-Powered Electronic Skin. *Adv Funct Mater* **31**, 2100940 (2021).

40. Fan, J., Montemagno, C. & Gupta, M. 3D printed high transconductance organic electrochemical transistors on flexible substrates. *Org Electron* **73**, 122–129 (2019).

41. Andersson Ersman, P. *et al.* All-printed large-scale integrated circuits based on organic electrochemical transistors. doi:10.1038/s41467-019-13079-4.

42. Li, Z. *et al.* Ink Engineering of Inkjet Printing Perovskite. *ACS Appl Mater Interfaces* **12**, 39082–39091 (2020).

43. Sajedi-Moghaddam, A., Rahmanian, E. & Naseri, N. Inkjet-printing technology for supercapacitor application: Current state and perspectives. *ACS Appl Mater Interfaces* **12**, 34487–34504 (2020).

44. Liou, T. M., Chan, C. Y. & Shih, K. C. Effects of actuating waveform, ink property, and nozzle size on piezoelectrically driven inkjet droplets. *Microfluid Nanofluidics* **8**, 575–586 (2010).

45. Gao, M., Li, L. & Song, Y. Inkjet printing wearable electronic devices. *J Mater Chem C Mater* **5**, 2971–2993 (2017).

46. Beedasy, V. & Smith, P. J. Printed Electronics as Prepared by Inkjet Printing. *Materials 2020, Vol. 13, Page 704* **13**, 704 (2020).

47. Khan, S., Ali, S., Khan, A. & Bermak, A. Developing pressure sensors from impregnated textile sandwiched in inkjet-printed electrodes. *Journal of Materials Science: Materials in Electronics* **33**, 541–553 (2022).

48. S R Saadi, M. A. *et al.* Direct Ink Writing: A 3D Printing Technology for Diverse Materials. *Advanced Materials* 2108855 (2022) doi:10.1002/ADMA.202108855.

49. Kim, F. *et al.* Direct ink writing of three-dimensional thermoelectric microarchitectures. *Nature Electronics 2021 4:8* **4**, 579–587 (2021).

50. Zhao, J. *et al.* Direct Ink Writing of Adjustable Electrochemical Energy Storage Device with High Gravimetric Energy Densities. *Adv Funct Mater* **29**, 1900809 (2019).

51. Shi, G. *et al.* A versatile PDMS submicrobead/graphene oxide nanocomposite ink for the direct ink writing of wearable micron-scale tactile sensors. *Appl Mater Today* **16**, 482–492 (2019).

52. Chen, B., Jiang, Y., Tang, X., Pan, Y. & Hu, S. Fully Packaged Carbon Nanotube Supercapacitors by Direct Ink Writing on Flexible Substrates. *ACS Appl Mater Interfaces* **9**, 28433–28440 (2017).

53. Sitanurak, J. *et al.* T-shirt ink for one-step screen-printing of hydrophobic barriers for 2D- and 3D-microfluidic paper-based analytical devices. *Talanta* **205**, 120113 (2019).

54. Cao, X. *et al.* Screen printing as a scalable and low-cost approach for rigid and flexible thin-film transistors using separated carbon nanotubes. *ACS Nano* **8**, 12769–12776 (2014).

55. Aleeva, Y. & Pignataro, B. Recent advances in upscalable wet methods and ink formulations for printed electronics. *J Mater Chem C Mater* **2**, 6436–6453 (2014).

56. Yakoh, A., Álvarez-Diduk, R., Chailapakul, O. & Merkoçi, A. Screen-Printed Electroluminescent Lamp Modified with Graphene Oxide as a Sensing Device. *ACS Appl Mater Interfaces* **10**, 20775–20782 (2018).

57. Duan, S. *et al.* Scalable Fabrication of Highly Crystalline Organic Semiconductor Thin Film by Channel-Restricted Screen Printing toward the Low-Cost Fabrication of High-Performance Transistor Arrays. *Advanced Materials* **31**, 1807975 (2019).

58. Han, D. *et al.* Emission Area Patterning of Organic Light-Emitting Diodes (OLEDs) via Printed Dielectrics. *Adv Funct Mater* **28**, 1802986 (2018).

59. Wang, K. *et al.* Wettability-Guided Screen Printing of Perovskite Microlaser Arrays for Current-Driven Displays. *Advanced Materials* **32**, 2001999 (2020).

60. Ferri, J., Fuster, C. P., Llopis, R. L., Moreno, J. & Garcia-Breijo, E. Integration of a 2D Touch Sensor with an Electroluminescent Display by Using a Screen-Printing Technology on Textile Substrate. *Sensors 2018, Vol. 18, Page 3313* **18**, 3313 (2018).

61. Nguty, T. A. & Ekere, N. N. The rheological properties of solder and solar pastes and the effect on stencil printing. *Rheologica Acta 2000 39:6* **39**, 607–612 (2000).

62. The Basics of Screen Mesh Printing | ASADA MESH CO.,LTD. https://asadamesh-global.com/en/product-introduction/screen_printing_basics/.

63. The Basics of Screen Mesh Printing | ASADA MESH CO.,LTD. https://asadamesh-global.com/en/product-introduction/screen_printing_basics/.

64. Matsuhisa, N. *et al.* High-frequency and intrinsically stretchable polymer diodes. *Nature 2021 600:7888* **600**, 246–252 (2021).

65. Wang, T. *et al.* Printable and Highly Stretchable Viscoelastic Conductors with Kinematically Reconstructed Conductive Pathways. *Advanced Materials* **34**, 2202418 (2022).

66. Lin, M., Gai, Y., Xiao, D., Tan, H. & Zhao, Y. Preparation of pristine graphene paste for screen printing patterns with high conductivity. *Chem Phys Lett* **713**, 98–104 (2018).

67. Zhao, C. *et al.* Fully Screen-Printed, Multicolor, and Stretchable Electroluminescent Displays for Epidermal Electronics. *ACS Appl Mater Interfaces* **12**, 47902–47910 (2020).

68. Chen, C. *et al.* Perovskite solar cells based on screen-printed thin films. *Nature 2022 612:7939* **612**, 266–271 (2022).

69. Zabihipour, M. *et al.* ARTICLE High yield manufacturing of fully screen-printed organic electrochemical transistors. doi:10.1038/s41528-020-0078-9.

70. Zabihipour, M. *et al.* Designing Inverters Based on Screen Printed Organic Electrochemical Transistors Targeting Low-Voltage and High-Frequency Operation. *Adv Mater Technol* **6**, 2100555 (2021).

71. Huang, Y. *et al.* ARTICLE A self-healable and highly stretchable supercapacitor based on a dual crosslinked polyelectrolyte. (2015) doi:10.1038/ncomms10310.

72. Zhang, Z. *et al.* Nitrogen-Doped Core-Sheath Carbon Nanotube Array for Highly Stretchable Supercapacitor. *Adv Energy Mater* **7**, 1601814 (2017).

73. Mangoma, T. N., Yamamoto, S., Malliaras, G. G. & Daly, R. Hybrid 3D/Inkjet-Printed Organic Neuromorphic Transistors. *Adv Mater Technol* **7**, 2000798 (2022).

74. Ji, J. *et al.* Dual-liquid-gated electrochemical transistor and its neuromorphic behaviors. *Nano Energy* **87**, 106116 (2021).

75. Wustoni, S. *et al.* Membrane-Free Detection of Metal Cations with an Organic Electrochemical Transistor. *Adv Funct Mater* **29**, 1904403 (2019).

76. Pierre, A. *et al.* Monolithic Integration of Ion-Selective Organic Electrochemical Transistors with Thin Film Transistors on Flexible Substrates. *Adv Mater Technol* **4**, 1800577 (2019).

77. Wearable Sensor System for Detection of Lactate in Sweat.: EBSCOhost. https://web.p.ebscohost.com.remotexs.ntu.edu.sg/ehost/pdfviewer/pdfviewer?vid=0&sid=bdd33647-f092-49ec-a915-d2ee267256c6%40redis.

78. Bernards, D. A. *et al.* Enzymatic sensing with organic electrochemical transistors. *J Mater Chem* **18**, 116–120 (2007).

79. Han, S., Polyravas, A. G., Wustoni, S., Inal, S. & Malliaras, G. G. Integration of Organic Electrochemical Transistors with Implantable Probes. *Adv Mater Technol* **6**, 2100763 (2021).

80. Inal, S. *et al.* Organic electrochemical transistors based on PEDOT with different anionic polyelectrolyte dopants. *J Polym Sci B Polym Phys* **54**, 147–151 (2016).

81. Zabihipour, M. *et al.* ARTICLE High yield manufacturing of fully screen-printed organic electrochemical transistors. doi:10.1038/s41528-020-0078-9.

82. Ersman, P. A. *et al.* Screen printed digital circuits based on vertical organic electrochemical transistors. *Flexible and Printed Electronics* **2**, 045008 (2017).

83. Makhinia, A., Hübscher, K., Beni, V. & Ersman, P. A. High Performance Organic Electrochemical Transistors and Logic Circuits Manufactured via a Combination of Screen and Aerosol Jet Printing Techniques. *Adv Mater Technol* 2200153 (2022) doi:10.1002/ADMT.202200153.

84. Bernards, D. A. & Malliaras, G. G. Steady-state and transient behavior of organic electrochemical transistors. *Adv Funct Mater* **17**, 3538–3544 (2007).

85. Flagg, L. Q., Giridharagopal, R., Guo, J. & Ginger, D. S. Anion-Dependent Doping and Charge Transport in Organic Electrochemical Transistors. *Chemistry of Materials* **30**, 5380–5389 (2018).

86. Wu, X. *et al.* Ionic-Liquid Induced Morphology Tuning of PEDOT:PSS for High-Performance Organic Electrochemical Transistors. *Adv Funct Mater* **32**, 2108510 (2022).

87. Cendra, C. *et al.* Role of the Anion on the Transport and Structure of Organic Mixed Conductors. *Adv Funct Mater* **29**, 1807034 (2019).

88. Athanasiou, V., Pecqueur, S., Vuillaume, D. & Konkoli, Z. On a generic theory of the organic electrochemical transistor dynamics. *Org Electron* **72**, 39–49 (2019).

89. Friedlein, J. T. *et al.* Optical Measurements Revealing Nonuniform Hole Mobility in Organic Electrochemical Transistors. *Adv Electron Mater* **1**, 1500189 (2015).

90. Rivnay, J. *et al.* High-performance transistors for bioelectronics through tuning of channel thickness. *Sci Adv* **1**, (2015).

91. Sensi, M. *et al.* Modulating the Faradic Operation of All-Printed Organic Electrochemical Transistors by Facile in Situ Modification of the Gate Electrode. (2019) doi:10.1021/acsomega.8b03319.

92. Rae Cho, K. *et al.* Investigation of the AgCl Formation Mechanism on the Ag Wire Surface for the Fabrication of a Marine Low-Frequency-Electric-Field-Detection Ag/AgCl Sensor Electrode. doi:10.1021/acsomega.2c01481.

93. Berggren, M. & Malliaras, G. G. How conducting polymer electrodes operate. *Science (1979)* **364**, 233–234 (2019).

94. The Basics of Screen Mesh Printing | ASADA MESH CO.,LTD. https://asadamesh-global.com/en/product-introduction/screen_printing_basics/.

95. Zabihipour, M. *et al.* ARTICLE High yield manufacturing of fully screen-printed organic electrochemical transistors. doi:10.1038/s41528-020-0078-9.

96. Kolodziejczyk, B., Ng, C. H., Strakosas, X., Malliaras, G. G. & Winther-Jensen, B. Light sensors and opto-logic gates based on organic electrochemical transistors. *Mater Horiz* **5**, 93–98 (2018).

97. Decataldo, F. *et al.* Organic Electrochemical Transistors: Smart Devices for Real-Time Monitoring of Cellular Vitality. *Adv Mater Technol* **4**, 1900207 (2019).

98. Yazza, A. A., Blondeau, P. & Andrade, F. J. Simple Approach for Building High Transconductance Paper-Based Organic Electrochemical Transistor (OECT) for Chemical Sensing. *Cite This: ACS Appl. Electron. Mater* **2021**, 1886–1895 (2021).

99. Bischak, C. G. *et al.* Ion Exchange Gels Allow Organic Electrochemical Transistor Operation with Hydrophobic Polymers in Aqueous Solution. *Advanced Materials* **32**, 2002610 (2020).

100. Bhattacharya, G. *et al.* Structural changes in cellular membranes induced by ionic liquids: From model to bacterial membranes. *Chem Phys Lipids* **215**, 1–10 (2018).

101. Screen printed digital circuits based on vertical organic electrochemical transistors. (2017) doi:10.1088/2058-8585/aa903a.

102. Shirinskaya, A., Horowitz, G., Rivnay, J., Malliaras, G. G. & Bonnassieux, Y. Numerical Modeling of an Organic Electrochemical Transistor. *Biosensors (Basel)* **8**, (2018).

103. Paudel, P. R., Skowrons, M., Dahal, D., Radha Krishnan, R. K. & Lüssem, B. The Transient Response of Organic Electrochemical Transistors. *Adv Theory Simul* **5**, 2100563 (2022).

104. Toss, H. *et al.* On the mode of operation in electrolyte-gated thin film transistors based on different substituted polythiophenes. *Org Electron* **15**, 2420–2427 (2014).

105. Friedlein, J. T., McLeod, R. R. & Rivnay, J. Device physics of organic electrochemical transistors. *Org Electron* **63**, 398–414 (2018).

106. Tang, H. *et al.* Conducting polymer transistors making use of activated carbon gate electrodes. *ACS Appl Mater Interfaces* **7**, 969–973 (2015).

107. Sensi, M. *et al.* Modulating the Faradic Operation of All-Printed Organic Electrochemical Transistors by Facile in Situ Modification of the Gate Electrode. *ACS Omega* **4**, 5374–5381 (2019).

108. Tarabella, G., Santato, C., Yang, S. Y., Iannotta, S. & Malliaras, G. G. Effect of the gate electrode on the response of organic electrochemical transistors. *Citation: Appl. Phys. Lett* **97**, 123304 (2010).

109. Cui, G. *et al.* Effect of pre-treatment on the surface and electrochemical properties of screen-printed carbon paste electrodes. (2001) doi:10.1039/b102934g.

110. Rivnay, J. *et al.* High-performance transistors for bioelectronics through tuning of channel thickness. *Sci Adv* **1**, (2015).

111. Tang, H. *et al.* Conducting polymer transistors making use of activated carbon gate electrodes. *ACS Appl Mater Interfaces* **7**, 969–973 (2015).

112. Galliani, M. *et al.* Flexible Printed Organic Electrochemical Transistors for the Detection of Uric Acid in Artificial Wound Exudate. *Adv Mater Interfaces* (2020) doi:10.1002/admi.202001218.

113. Mabeck, J. T. *et al.* Microfluidic gating of an organic electrochemical transistor. *Appl Phys Lett* **87**, 013503 (2005).

114. Sensi, M. *et al.* Modulating the Faradic Operation of All-Printed Organic Electrochemical Transistors by Facile in Situ Modification of the Gate Electrode. (2019) doi:10.1021/acsomega.8b03319.

115. Andersson, P. *et al.* Fast-switching all-printed organic electrochemical transistors. *Org Electron* **5**, 1276–1280 (2013).

116. Toss, H. *et al.* On the mode of operation in electrolyte-gated thin film transistors based on different substituted polythiophenes. *Org Electron* **15**, 2420–2427 (2014).

117. He, R. X. *et al.* Detection of bacteria with organic electrochemical transistors. *J Mater Chem* **22**, 22072–22076 (2012).

118. Ting Melissa Tan, S. *et al*. High-Gain Chemically Gated Organic Electrochemical Transistor. *Adv Funct Mater* **31**, 2010868 (2021).

119. Paudel, P. R., Skowrons, M., Dahal, D., Radha Krishnan, R. K. & Lüssem, B. The Transient Response of Organic Electrochemical Transistors. *Adv Theory Simul* **5**, 2100563 (2022).

120. Müller, C. M. O., Yamashita, F. & Laurindo, J. B. Evaluation of the effects of glycerol and sorbitol concentration and water activity on the water barrier properties of cassava starch films through a solubility approach. *Carbohydr Polym* **72**, 82–87 (2008).

121. Peng, C., Chow, A. H. L. & Chan, C. K. Aerosol Science & Technology Hygroscopic Study of Glucose, Citric Acid, and Sorbitol Using an Electrodynamic Balance: Comparison with UNIFAC Predictions. (2010) doi:10.1080/02786820152546798.

122. Jiao, F. *et al.* Ionic thermoelectric paper. *J Mater Chem A Mater* **5**, 16883–16888 (2017).

123. Zabihipour, M. *et al.* Organic electrochemical transistors manufactured by laser ablation and screen printing. *Flexible and Printed Electronics* **7**, 035018 (2022).

124. Brooke, R. *et al.* Combining Vapor Phase Polymerization and Screen Printing for Printed Electronics on Flexible Substrates. *Adv Mater Technol* **7**, 2101665 (2022).

125. Brooke, R. *et al.* Combining Vapor Phase Polymerization and Screen Printing for Printed Electronics on Flexible Substrates. *Adv Mater Technol* **7**, 2101665 (2022).

126. Zabihipour, M. *et al.* Organic electrochemical transistors manufactured by laser ablation and screen printing. *Flexible and Printed Electronics* **7**, 035018 (2022).

127. Polyravas, A. G. *et al.* Effect of channel thickness on noise in organic electrochemical transistors. *Appl Phys Lett* **117**, 073302 (2020).

128. Rivnay, J. *et al.* High-performance transistors for bioelectronics through tuning of channel thickness. *Sci Adv* **1**, (2015).

129. Yan, Y. *et al.* High-Performance Organic Electrochemical Transistors with Nanoscale Channel Length and Their Application to Artificial Synapse. *ACS Appl Mater Interfaces* **12**, 49925 (2020).

130. Donahue, M. J. *et al.* Article type: Communication High Performance Vertical Organic Electrochemical Transistors. doi:10.1002/((please).